UNIVERSITÀ degli STUDI di CATANIA
Dipartimento di Agricoltura, Alimentazione e Ambiente
Di3A

UNIVERSITÀ DEGLI STUDI DI CATANIA

AGRICULTURAL, FOOD AND ENVIRONMENTAL SCIENCE

XXXIII CYCLE

Applications of Nanocellulose from Wastes and By-Products as Sustainable High-Performing Food Packaging Material

Luana Amoroso

Advisor:
Giuseppe Muratore

Coordinator:
Cherubino Leonardi

Ph. D. attended during 2017/2020

"The Brain is wider than the Sky
For put them side by side
The one the other will contain
With ease and You beside.

The Brain is deeper than the sea
For hold them Blue to Blue
The one the other will absorb
As Sponges Buckets do.

The Brain is just the weight of God
For Heft them Pound for Pound
And they will differ if they do
As Syllable from Sound."

(Emily Dickinson)

Acknowledgements

Above all, I would like to express my sincere gratitude to my mentors, Prof. Giuseppe Muratore and Prof. Luciano Piergiovanni, for the precious support throughout my PhD study and related research, for the outstanding help, motivation and for always being by my side when I needed them. Without their immense knowledge my PhD thesis would be far from what it is today. I will always be grateful to have had the privilege of having met them on my journey.

I want to thank Prof. Sara Limbo for the perseverance to excellence which definitely is reflected in the scientific work. Her guidance helped me in all the time of research.

My sincere thanks also go to Dr. Gustav Nyström, from Empa Institute, who provided me an opportunity to join its team as intern, and who gave access to the laboratory and research facilities. I am grateful also to Dr. Gilberto Siqueira and Dr. Kevin De France for enlightening me at the first glance of research. I thank all of them for trusting me and always supporting my ideas.

I thank my fellow labmates, from Milan University, in particular Begüm Akgün, Ghislain Fotie, Serena Gobbi and Rafael Cavalieri Marchi, for the stimulating discussions, for the sleepless nights, and for all the fun we have had in the last three years. I could not have imagined having a better labmates for my PhD study. I will always remember my friends from the “Cellulose & Wood Materials” group of

Empa: Electra D'Emilio, Alberto Giubilini, Ting Ting Wu, above all.

During my PhD study, I received help from brilliant students, Martina Scarpignato, Mariapaola Crisafi, Lidia Gemelli, Valeria Mascarello and Jessica Circelli, who endured my ideas, spent time accomplishing them with dedication and hard work and which eventually resulted in the successful accomplishment of them. A particular thank also to Chiara Galli who will always remain in my thoughts.

I want to thank also Valeria Rizzo for trusting me at first sight.

Last but not the least, I would like to thank Matteo and my family, for supporting me spiritually throughout writing this thesis and my life in general.

Table of Contents

Preface

The present thesis describes the study and research activities carried out during the PhD course *Agricultural, Food and Environmental Science* - XXXIII cycle attended in 2017-2020 at the Department of *Agriculture, Food and Environment* (*Di3A)* of University of Catania.
The thesis is framed within the original experimental work accomplished by the author under the supervision of Professor Giuseppe Muratore, from Di3A, and the co-supervision of Professor Luciano Piergiovanni, from the *Food Packaging Labs (*PackLAB*)* of the Department of *Food, Environmental and Nutritional Science (DeFENS)* of University of Milan. Where use is made of the co-work of others, it has been clearly stated in the text.

Abstract

In this PhD thesis, an in-depth experimental work was carried out to investigate the potentiality of waste and by-products as alternative raw materials to achieve eco-sustainable and biodegradable biopolymer, namely cellulose nanocrystal (CNC) and nanofiber (CNF). The targeted supplied agricultural and industrial materials in the form of waste or by-products, such soy hull and cotton powder or carrots or other waste products were chosen among the different biomass feedstock as alternative source of CNC and CNF. The final goal was the acquisition of scientific and technological knowledge regarding multifunctional cellulose-based materials characterized by improved performance and low cost, which are suitably in line with the actual trend and environmental need of reducing synthetic polymers and improve the global environmental impact of the packaged food products.

The dissertation consists of five chapters and an executive summary, which altogether cover the development of extraction processes, the optimization attempts with respect to conventional methodologies, along with the characterization and applications of the ensuing nanomaterials. After discussing the general background of the project, highlighting the shortcomings still existing to a widespread exploitation of nanocellulose in the food packaging field, in the first chapter the objective is pursued of identifying the most suitable raw materials for the recovery of their valuable cellulosic nanocomponents, in terms of technological and economic feasibility, and output quality. Over the following chapters, the most promising matrices are broken down into cellulose nanofibers or further

disintegrated into the smaller nanocrystals, by developing laboratory-scale deconstructing strategies, which provide, albeit building on previous investigations, innovative and more sustainable approaches entirely customized to the specific raw material. These activities are complemented by an in-depth investigation and comparison of the morphological and physico-chemical features of the nanomaterials produced, also determining how these features can affect the physical, mechanical, and diffusional performance of the nanomaterials once used in applications intended for food packaging.

Sommario

In questa tesi di dottorato è stato svolto un approfondito lavoro sperimentale per indagare le potenzialità di scarti e sottoprodotti come materie prime alternative per ottenere biopolimeri ecosostenibili e biodegradabili, noti come nanocristalli (CNC) e nanofibre (CNF) di cellulosa. I materiali agricoli e industriali oggetto di studio, in forma di rifiuti o sottoprodotti, come le bucce di soia e la polvere di cotone, la sansa di carote o altri prodotti di scarto, sono stati scelti tra le diverse biomasse come fonte alternativa di CNC e CNF. L' obiettivo finale è stato l'acquisizione di conoscenze scientifiche e tecnologiche su materiali multifunzionali avanzati a base di cellulosa, caratterizzati da prestazioni migliorate e basso costo, opportunamente in linea con l'effettivo trend e la necessità ambientale di ridurre i polimeri sintetici e migliorare l'impatto ambientale globale del confezionamento alimentare.

La tesi si compone di cinque capitoli e un sommario esecutivo, che complessivamente coprono aspetti legati allo sviluppo dei processi di estrazione, ai tentativi di ottimizzazione rispetto alle metodologie convenzionali, nonché alla caratterizzazione e alle applicazioni dei nanomateriali risultanti. Dopo un'introduzione generale al contesto del progetto, evidenziando i limiti ancora esistenti ad uno sfruttamento diffuso della nanocellulosa nel settore del confezionamento alimentare, nel primo capitolo l'obiettivo perseguito è stato individuare le materie prime più idonee al recupero dei loro preziosi nano-componenti cellulosici, in termini di fattibilità tecnologica ed economica, e di qualità dell'output. Nel corso dei successivi capitoli, le matrici più promettenti sono scomposte in nanofibre di

cellulosa o ulteriormente disintegrate in nanocristalli, sviluppando strategie di decostruzione, in scala di laboratorio, che, seppur basate su precedenti indagini procedurali, propongono soluzioni estrattive completamente personalizzate e ottimizzate sulle materie prime, coinvolgendo approcci innovativi e più sostenibili. Queste attività sono integrate da indagini approfondite che consentono di identificare e confrontare le caratteristiche morfologiche e fisico-chimiche specifiche dei nanomateriali prodotti e determinare come queste ne influenzino le prestazioni fisiche, meccaniche e diffusionali, una volta utilizzati in applicazioni di imballaggio alimentare.

1 Introduction

1.1 *Background*

Food supply chains often involve large distances and multiple intermediaries. Each stage in the food supply chain, including production, processing, retail, and any other stage that food needs before reaching our plates, drives a multitude of impacts on society and environment, generates waste and pollution (Reisch et al., 2013). Appropriate packaging helps to reduce food loss and waste at any stage along the supply chain. It can facilitate the safe transit of food, even where it would not otherwise be accessible, and thus plays a central role in the global food system. At the same time, packaging practices and the nature of supply chains are under enquiry due to rising concerns over waste generation and the overwhelming use of non-renewable resources (Varun et al., 2016). The origin, the recyclability of the material and its ecological qualities are increasingly important considerations both for brands and user experience. Besides, in the last two decades sustainability has been a priority aspect in the policies of European Union and of the most industrialized countries. These have led some industrial sectors to minimize the environmental impact of their products, especially those intended for short-lived applications, such as packaging, catering or hygiene. (European Commission, 2019; European Union, 2019; OECD, 2009; Timmermans & Katainen, 2019; UN General Assembly, 2015). Therefore, today more than in the past, the design and manufacture of packaging materials cannot afford to ignore a sustainable logic that must consider both the supply sources and the destiny of packaging at the end of its useful life cycle. In the last few years, this need,

due to concrete issues, such as petroleum costs and its limited availability, the huge volume of packaging waste and the difficulties linked to its disposal, has represent the driving force behind various research approaches that look into the way to find alternative packaging solutions more attentive to environmental sustainability (Han et al., 2018; Pauer et al., 2019). Recent findings are raising the prospects that renewable resources will be a major contributor to the production of industrial products, so that scientists and engineers successfully implement innovations and technologies that more and more bring down costs and optimize performances of bio-based products (Bastioli, 2020; Flieger et al., 2003; Peelman et al., 2013; Sun, 2005). Food packaging, especially flexible packaging, is a strategic market for bio-based materials: it is a highly competitive area with a wide spectrum of requests on performances and cost, and its dependence of petroleum-based plastics is still strong. In this context, novel forms of cellulose, known as nanocellulose, successfully meet market trends and needs, and their application in the food packaging area has been proposed as rational solution for these issues (Gómez et al., 2016; Hubbe et al., 2017; Khan et al., 2014; Li et al., 2015). Being cellulose widely available all over the world, more and more attention has been paid to its renewability along with its new functionalities. The global annual production of cellulose is valued to be more than 75 billion tons and it is possible to estimate that no more than 5 % of this quantity is successfully used (Xie et al., 2018). Therefore, this represents practically inexhaustible resource. In the form of fibers or derivatives, the use of cellulose could date back many thousands of years for several daily-usage items, including wrapping materials and containers, primary and secondary

packages, as well as for chemical and pharmaceutical applications. What is quite recent instead is the discovery that, if cellulose fibers are subjected to controlled cleavage processes, they yield different nano-size fragments collectively called now cellulose nanomaterials (CNMs), which are nowadays attracting enormous attention from the scientific community due to their interesting properties and several potential applications (Dufresne, 2017b). Cellulose nanomaterials, or nanocellulose, refer to cellulosic materials that have at least one dimension in the nanometer range (1-100 nm) (Dufresne, 2017a; Kargarzadeh et al., 2018). They can be prepared through either top-down approach, in which the natural fiber is resized to smaller particles (e.g., homogenization, hydrolysis, combined chemical-mechanical processes), or bottom-up approach, in which cellulose is synthesized by connecting glucose molecules (e.g., electrospinning, bacterial biosynthesis) (Chen et al., 2011; Habibi et al., 2010; Lee et al., 2017; Meyabadi & Dadashian, 2012; Moon et al., 2011; Siqueira et al., 2010). Cellulose nanomaterials encompass a wide spectrum of nano-scale cellulose-based particles having various, shapes, sizes, surface chemistries and properties, which in turn depend mainly on the cellulosic source and processing conditions (Foster et al., 2018). The International Organization for Standardization (ISO) classified two main categories of cellulose "nano-objects", namely cellulose nanocrystals (CNCs) and cellulose nanofibres (CNFs) (ISO, 2017). As per the ISO standard, cellulose nanocrystals, also termed as nanowhiskers or nanocrystalline cellulose, present a pure crystalline structure and dimensions of 3–50 nm in width and an aspect ratio (ratio of the largest to the smallest dimension) greater than 5 and usually less than 50. They should not

exhibit longitudinal splits, inter-particle entanglement, or network-like structures. CNCs are obtained by a chemical process, typically through an acidic or oxidative hydrolysis which remove the amorphous domains existing in cellulose fibers, releasing flawless crystalline regions (Siqueira et al., 2009). Unlike CNCs, cellulose nanofibers, also known as cellulose nanofibrils or nanofibrillated cellulose, are long and flexible nanofilaments which consist of alternating crystalline and amorphous domains. CNFs typically have 3-100 nm in cross-section and up to 100 μm in length, with an aspect ratio typically greater than 50 and entangled network-like structures. They are prepared by disintegrating cellulose fibers using mechanical methods, such as high-pressure homogenization, micro-fluidization, and micro-grinding.

Regardless of origin and production methods, when the particle size is reduced until nanoscale threshold, the resulting material exhibits physicochemical properties that significantly differ from those of the macroscale material with the same elemental composition (Dufresne, 2018). Nanocellulose thus combines the key properties of cellulose, such as high tensile strength and modulus and extensive ability for chemical modification, with specific features of nanoscale materials, mainly originating from their very large surface area and aspect ratio (Kargarzadeh et al., 2018; Klemm et al., 2011). Thanks to its unique properties and renewable nature, this novel family of nanomaterials has been shown to have application potential in a variety of material-related domains that rely on characteristics such as strength, lightweight, optical transparency, shear thinning behavior, and extremely low gas permeability (Dufresne, 2019; Li et al., 2015). In the last 10-15 years, these renewable nanomaterials generated an exceptional appeal throughout

the world: the international scientific literature has been dramatically enriched with articles reviewing recent advancements and the experiments carried out on nanocellulose, some of which pertain the patents registered worldwide on this subject (Azizi Samir et al., 2005; Charreau et al., 2020; De France et al., 2017; Dufresne, 2013, 2017b; Duran et al., 2012; Habibi, 2014; Kalia et al., 2011; Klemm et al., 2011; Lindström & Aulin, 2014; Rebouillat & Pla, 2013; Sharma et al., 2019). However, a limited number of articles concern applications involving food packaging materials (Azeredo et al., 2017; Fotie et al., 2017; Hubbe et al., 2017; Khan et al., 2014; Lee et al., 2017; Li et al., 2015; Rampazzo et al., 2017). Regarding food packaging applications, the nanometric forms of cellulose seem to be a promising resource, not entirely exploited so far, to enhance the mechanical, rheological, and gas barrier properties to such an extent as to presume a substantial reduction in the thickness and mass of the synthetic polymers used today. On the other hand, in the food packaging field, the use of nanocellulose, as well as other bio-based materials, is a difficult challenge due to the specific needs of food protection. As responsible for the quality and safety of food, packaging innovations always require truly conscious choices both on the food itself and on its packaging. Nevertheless, from the potential emerged to date, good reasons suggest that cellulose nanomaterials could be used for the design of novel advanced food packaging materials, able to improve conventional materials, introduce new useful functionalities, and lower their overall lifecycle impacts. The large and inexpensive availability of cellulose sources, the advanced knowledge on its chemistry and the excellent properties achievable with cellulose at the nanoscale are the

key factors that make actually predictable an ever-growing application of CNMs across many sectors and for different purposes.

1.2 *Project Motivation*

The cellulose materials market is undoubtedly going through a new phase: the recognition of the hidden potential in the nano-sized forms of cellulose and the widening end-use opportunities have given cellulose market a boost. However, the real and substantial exploit of nanocellulose-based materials is hindered by some drawbacks whose technological solutions still need to be tested and implemented.

Despite nanocellulose is already available on the market as a commercial product, cost performance and procedures for affordable scaling up of manufacturing processes remain the greatest challenges (Dufresne, 2019; Nechyporchuk et al., 2016). Further efforts need to be done for claiming nanocellulose as an economically viable, as well as environmentally sustainable, business option.

Beside to the mechanical and chemical treatments typically used to prepare CNFs and CNCs, respectively, other techniques as well as pre-treatment processes should be investigated to design an industrially, economically, and eco-friendly viable route for nanocellulose. Furthermore, the exploitation of agricultural and industrial waste to realize cellulose nanomaterials could become an added benefit to accelerate their future growth along with to reduce the dependence on foreign forest resources. Major challenges are also associated with the hydrophilic nature of nanocellulose, which makes it poorly dispersible in apolar polymeric

matrices and gives it inadequate resistance to water vapor and moisture. This behavior may be considered a bottleneck in terms of certain applications, like in the case of food packaging (Fotie et al., 2017; Lindström & Aulin, 2014; Ramos et al., 2016). Up to date, most of the efforts to overcome the problem are surface chemistry oriented, since the large number of hydroxyl groups on the nanocellulose surface provides a suitable platform for several kinds of modification, including coupling hydrophobic small molecules, grafting polymers and oligomers, and adsorbing hydrophobic compounds (Bendahou et al., 2015; Dufresne, 2017a, 2019; Eyley & Thielemans, 2014). Nevertheless, guaranteeing effective surface modification paths while preserving the integrity of the nanoparticles and their ecological qualities is very challenging (Kargarzadeh et al., 2018). The moisture sensitivity has also been addressed by sandwiching nanocellulose within high moisture-resistant polymers (Fotie et al., 2020). Instead, not much attention was paid on taking advantage of this feature of nanocellulose to suit specific target in the food packaging. Lastly, a key problem still needs to be urgently solved. Although nanocellulose offers numerous desirable properties for food packaging, it has not yet reached widespread application in this sector due to some toxicological concerns. Even if powdered cellulose and microcrystalline cellulose are generally recognized as safe (GRAS), so they can be used as food contact materials or even as food additives, the risk assessment of its nanosized counterparts has yet to be done to ensure the safe commercialization of nanocellulose-containing products (Azeredo et al., 2017; Dufresne, 2019; Kangas & Pitkänen, 2020). Note that this arises whether any

other nanomaterial is intended for food contact or to be directly ingested.
While accounting for the expected future production growth of nanocellulose, and of nanomaterials in general, this issue came into the agenda of scientific committees, regulatory agencies, and standardization bodies that aim to advance scientific knowledge of the potential impact of nano-enabled materials on environmental and human health, and to provide tools for risk assessment and management along the entire life cycle (Amenta et al., 2015; EFSA et al., 2018; EFSA et al., 2020; European Parliament & Council of European Union, 2013; Kangas & Pitkänen, 2020; Poças & Franz, 2018; Sharma et al., 2020). From a safety perspective, the main concern is that the nanoscale features may influence the toxicokinetic and hazardous properties of a nanomaterial, thus it may expose humans to new risks (EFSA and Emerging Risks Unit et al., 2020; Kangas & Pitkänen, 2020; Shatkin & Kim, 2017). However, the European Food Safety Authority reiterates that not all nanomaterials have new hazard properties compared with larger sized counterparts and that therefore a case-by-case assessment is necessary (EFSA et al., 2018). Data to date suggest that cellulose nanomaterials are similarly safe to those GRAS cellulose, but a few gaps in knowledge remain, thus further studies are required to avert any doubts (Azeredo et al., 2017; Endes et al., 2016; Kangas & Pitkänen, 2020; Shatkin & Kim, 2017).

1.3 Scope and Approach

The aforementioned contents have largely shaped the framework of this dissertation, which revolved around the attempt to overcome all the above shortcomings still existing

on the large-scale diffusion of nanocellulose and its successful application in the food packaging sector.
Overall, the objective of the PhD project was to provide sustainable and cost-effective ways to isolate cellulose nanomaterials that allow the reuse of waste and by-products resulting from different agricultural and industrial supply chains.
The final goal was to get lightweight, multifunctional nanocellulose-based materials, with advanced performances and low cost, which could replace the synthetic polymers nowadays used and improve the global environmental impact of the packaged food product.
To pursue these objectives, the initial raw materials, the extraction processes and some target properties and performances of the ensuing nanomaterials were extensively studied, following an interdisciplinary approach that integrated both technological and chemical-physical aspects. Specifically, the main research topics of the project can be summarised as follows:

- Suitability assessment of cellulosic feedstocks:

characterization and selection of the most suitable agricultural and industrial waste/by-products to obtain CNMs.

- Process optimization and adjustment:

development of laboratory scale approaches for a fast and effective production of CNMs, in an attempt to face the drawbacks in the conventional methodology, to reduce the cost and enlarge the production, while fitting the extraction method to the different raw materials.

- Application of CNMs and performance evaluation: characterization of the properties of CNMs from different feedstocks and evaluation of the effectiveness of nanocellulose films and coatings in various applications intended for food packaging.

Additionally, as a side part of the doctoral work, preliminary investigation on safety contents was also performed to generate data aimed at justifying the potential future application of nanocellulose as a food contact material and provide tools for its risk assessment.
The following chapters discuss in detail the experimental activities carried out on these topics, each of which preceded by a brief overview on the state of the art and the progress in knowledge found in the literature.

References

Amenta, V., Aschberger, K., Arena, M., Bouwmeester, H., Botelho Moniz, F., Brandhoff, P., Gottardo, S., Marvin, H. J. P., Mech, A., Quiros Pesudo, L., Rauscher, H., Schoonjans, R., Vettori, M. V., Weigel, S., & Peters, R. J. (2015). Regulatory aspects of nanotechnology in the agri/feed/food sector in EU and non-EU countries. *Regulatory Toxicology and Pharmacology*, *73*(1), 463-476.

Azeredo, H. M. C., Rosa, M. F., & Mattoso, L. H. C. (2017). Nanocellulose in bio-based food packaging applications. *Industrial Crops and Products*, *97*, 664-671.

Azizi Samir, M. A. S., Alloin, F., & Dufresne, A. (2005). Review of Recent Research into Cellulosic Whiskers, Their Properties and Their Application in Nanocomposite Field. *Biomacromolecules*, *6*(2), 612-626.

Bastioli, C. (2020). *Handbook of Biodegradable Polymers* (3rd ed.). De Gruyter.

Bendahou, A., Hajlane, A., Dufresne, A., Boufi, S., & Kaddami, H. (2015). Esterification and amidation for grafting long aliphatic chains on to cellulose nanocrystals: a comparative study. *Research on Chemical Intermediates*, *41*(7), 4293-4310.

Charreau, H., Cavallo, E., & Foresti, M. L. (2020). Patents involving nanocellulose: Analysis of their evolution since 2010. *Carbohydrate Polymers*, *237*, 116039.

Chen, W. S., Yu, H. P., Liu, Y. X., Chen, P., Zhang, M. X., & Hai, Y. F. (2011). Individualization of cellulose nanofibers from wood using high-intensity ultrasonication combined with chemical pretreatments. *Carbohydrate Polymers*, *83*(4), 1804-1811.

De France, K. J., Hoare, T., & Cranston, E. D. (2017). Review of Hydrogels and Aerogels Containing Nanocellulose. *Chemistry of Materials*, *29*(11), 4609-4631.

Dufresne, A. (2013). Nanocellulose: a new ageless bionanomaterial. *Materials Today*, *16*(6), 220-227.

Dufresne, A. (2017a). Cellulose nanomaterial reinforced polymer nanocomposites. *Current Opinion in Colloid & Interface Science*, *29*, 1-8.

Dufresne, A. (2017b). *Nanocellulose: From Nature to High Performance Tailored Materials* (2 ed.). Walter de Gruyter GmbH & Co KG.

Dufresne, A. (2018). Cellulose nanomaterials as green nanoreinforcements for polymer nanocomposites. *Philosophical Transactions of the Royal Society A: Mathematical, Physical and Engineering Sciences*, *376*(2112).

Dufresne, A. (2019). Nanocellulose Processing Properties and Potential Applications. *Current Forestry Reports*, *5*(2), 76-89.

Duran, N., Lemes, A. P., & Seabra, A. B. (2012). Review of Cellulose Nanocrystals Patents: Preparation, Composites and General Applications. *Recent Patents on Nanotechnology*, *6*(1), 16-28.

EFSA Scientific Committee, Hardy, A., Benford, D., Halldorsson, T., Jeger, M. J., Knutsen, H. K., More, S., Naegeli, H., Noteborn, H., Ockleford, C., Ricci, A., Rychen, G., Schlatter, J. R., Silano, V., Solecki, R., Turck, D., Younes, M., Chaudhry, Q., Cubadda, F., Gott, D., Oomen, A., Weigel, S., Karamitrou, M., Schoonjans, R., & Mortensen, A. (2018). Guidance on risk assessment of the application of nanoscience and nanotechnologies in the food and feed chain: Part 1, human and animal health. *EFSA Journal*, *16*(7).

EFSA Scientific Committee and Emerging Risks Unit, (Chair), J. T., Dorne, J. L., & Astuto, M. C. (2020). Minutes of the workshop on the NAMs Nanofibers/Nanocellulose case study. TELE-conference, 22 and 25 June 2020 Parma, Italy.

Endes, C., Camarero-Espinosa, S., Mueller, S., Foster, E. J., Petri-Fink, A., Rothen-Rutishauser, B., Weder, C., & Clift, M. J. D. (2016). A critical review of the current knowledge regarding the biological impact of nanocellulose. *Journal of Nanobiotechnology*, *14*(1), 78.

European Commission. (2019). The European Green Deal. (COM(2019) 640). Brussels, Belgium

European Food Safety Authority (EFSA), Schoonjans, R., & Tarazona, J. (2020). Annual report of the EFSA Scientific Network of Risk Assessment of Nanotechnologies in Food and Feed for 2019. *EFSA Supporting Publications 2020*, *17*(2), EN-1784.

European Parliament, & Council of European Union. (2013). Regulation (EU) No 1291/2013 of the European Parliament and of the Council of 11 December 2013 establishing Horizon 2020 - the Framework Programme for Research and Innovation (2014-2020) and repealing Decision No 1982/2006/EC (L 347/104). Bruxelles, Belgium: *Official Journal of the European Union*

European Union. (2019). Directive (EU) 2019/904 of the European Parliament and of the Council of 5 June 2019 on the reduction of the impact of certain plastic products on the environment. (L 155/1). Bruxelles, Belgium: *Official Journal of the European Union*

Eyley, S., & Thielemans, W. (2014). Surface modification of cellulose nanocrystals. *Nanoscale*, *6*(14), 7764-7779.

Flieger, M., Kantorová, M., Prell, A., Řezanka, T., & Votruba, J. (2003). Biodegradable plastics from renewable sources. *Folia Microbiologica*, *48*(1), 27-44.

Foster, E. J., Moon, R., Agarwal, U., Bortner, M., Bras, J., Camarero Espinosa, S., Chan, K., Clift, M., Cranston, E., Eichhorn, S., Fox, D., Hamad, W., Heux, L., Jean, B., Korey, M., Nieh, W., Ong, K., Reid, M., Renneckar, S., & Youngblood, J. (2018). Current characterization methods for cellulose nanomaterials. *47*, 2609-2679.

Fotie, G., Gazzotti, S., Ortenzi, M. A., & Piergiovanni, L. (2020). Implementation of High Gas Barrier Laminated Films Based on Cellulose Nanocrystals for Food Flexible Packaging. *Applied Sciences*, *10*(9), 3201.

Fotie, G., Rampazzo, R., Ortenzi, M., Checchia, S., Fessas, D., & Piergiovanni, L. (2017). The Effect of Moisture on Cellulose Nanocrystals Intended as a High Gas Barrier Coating on Flexible Packaging Materials. *Polymers*, *9*(9), 415.

Gómez H, C., Serpa, A., Velásquez-Cock, J., Gañán, P., Castro, C., Vélez, L., & Zuluaga, R. (2016). Vegetable nanocellulose in food science: A review. *Food Hydrocolloids*, *57*, 178-186.

Habibi, Y. (2014). Key advances in the chemical modification of nanocelluloses. *Chemical Society Reviews*, *43*(5), 1519-1542.

Habibi, Y., Lucia, L. A., & Rojas, O. J. (2010). Cellulose Nanocrystals: Chemistry, Self-Assembly, and Applications. *Chemical Reviews*, *110*(6), 3479-3500.

Han, J.-W., Ruiz-Garcia, L., Qian, J.-P., & Yang, X.-T. (2018). Food Packaging: A Comprehensive Review and Future Trends. *Comprehensive Reviews in Food Science and Food Safety*, *17*(4), 860-877.

Hubbe, M. A., Ferrer, A., Tyagi, P., Yin, Y., Salas, C., Pal, L., & Rojas, O. J. (2017). Nanocellulose in thin films, coatings, and plies for packaging applications: A review. *BioResources*, *12*(1), 2143-2233.

International Organization for Standardization – ISO. (2017). *Nanotechnologies — Standard terms and their definition for cellulose nanomaterial* (ISO/TS 20477:2017).

Kalia, S., Dufresne, A., Cherian, B. M., Kaith, B. S., Averous, L., Njuguna, J., & Nassiopoulos, E. (2011). Cellulose-Based Bio- and Nanocomposites: A Review. *International Journal of Polymer Science*.

Kangas, H., & Pitkänen, M. (2020). Chapter 12 - Environmental, Health, and Safety (EHS) Aspects of Cellulose Nanomaterials. In I. Filpponen, M. S. Peresin, & T. Nypelö (Eds.), *Lignocellulosics* (pp. 345-374). Elsevier.

Kargarzadeh, H., Mariano, M., Gopakumar, D., Ahmad, I., Thomas, S., Dufresne, A., Huang, J., & Lin, N. (2018). Advances in cellulose nanomaterials. *Cellulose*, *25*(4), 2151-2189.

Khan, A., Huq, T., Khan, R. A., Riedl, B., & Lacroix, M. (2014). Nanocellulose-Based Composites and Bioactive Agents for Food Packaging. *Critical Reviews in Food Science and Nutrition*, *54*(2), 163-174.

Klemm, D., Kramer, F., Moritz, S., Lindstrom, T., Ankerfors, M., Gray, D., & Dorris, A. (2011). Nanocelluloses: A New Family of Nature-Based Materials. *Angewandte Chemie-International Edition*, *50*(24), 5438-5466.

Lee, H., Sundara, J., & Mani, S. (2017). Production of Cellulose Nanofibrils and Their Application to Food: A Review. In R. Prasad, Kumar, Vivek, Kumar, Manoj (Ed.), *Nanotechnology: Food and Environmental Paradigm* (pp. 1-33). Springer.

Li, F., Mascheroni, E., & Piergiovanni, L. (2015). The Potential of NanoCellulose in the Packaging Field: A Review. *Packaging Technology and Science*, *28*(6), 475-508.

Lindström, T., & Aulin, C. (2014). Market and technical challenges and opportunities in the area of innovative new materials

and composites based on nanocellulosics. *Scandinavian Journal of Forest Research*, *29*(4), 345-351.

Meyabadi, T. F., & Dadashian, F. (2012). Optimization of Enzymatic Hydrolysis of Waste Cotton Fibers for Nanoparticles Production Using Response Surface Methodology. *Fibers and Polymers*, *13*(3), 313-321.

Moon, R. J., Martini, A., Nairn, J., Simonsen, J., & Youngblood, J. (2011). Cellulose nanomaterials review: structure, properties and nanocomposites. *Chemical Society Reviews*, *40*(7), 3941-3994.

Nechyporchuk, O., Belgacem, M. N., & Bras, J. (2016). Production of cellulose nanofibrils: A review of recent advances. *Industrial Crops and Products*, *93*, 2-25.

OECD. (2009). *The Bioeconomy to 2030: Designing a Policy Agenda*.

Pauer, E., Wohner, B., Heinrich, V., & Tacker, M. (2019). Assessing the Environmental Sustainability of Food Packaging: An Extended Life Cycle Assessment including Packaging-Related Food Losses and Waste and Circularity Assessment. *Sustainability*, *11*(3), 925.

Peelman, N., Ragaert, P., De Meulenaer, B., Adons, D., Peeters, R., Cardon, L., Van Impe, F., & Devlieghere, F. (2013). Application of bioplastics for food packaging. *Trends in Food Science & Technology*, *32*(2), 128-141.

Poças, F., & Franz, R. (2018). Chapter 10 - Overview on European Regulatory Issues, Legislation, and EFSA Evaluations of Nanomaterials. In M. Â. P. R. Cerqueira, J. M. Lagaron, L. M. Pastrana Castro, & A. A. M. de Oliveira Soares Vicente (Eds.), *Nanomaterials for Food Packaging* (pp. 277-300). Elsevier.

Ramos, M., Valdés, A., & Garrigós, M. C. (2016). Chapter 6 - Multifunctional Applications of Nanocellulose-Based Nanocomposites. In D. Puglia, E. Fortunati, & J. M. Kenny (Eds.), *Multifunctional Polymeric Nanocomposites Based*

on Cellulosic Reinforcements (pp. 177-204). William Andrew Publishing.

Rampazzo, R., Alkan, D., Gazzotti, S., Ortenzi, M. A., Piva, G., & Piergiovanni, L. (2017). Cellulose Nanocrystals from Lignocellulosic Raw Materials, for Oxygen Barrier Coatings on Food Packaging Films. *Packaging Technology and Science*, *30*(10), 645-661.

Rebouillat, S., & Pla, F. (2013). State of the Art Manufacturing and Engineering of Nanocellulose: A Review of Available Data and Industrial Applications. *Journal of Biomaterials and Nanobiotechnology*, *4*(2), 165-188.

Reisch, L., Eberle, U., & Lorek, S. (2013). Sustainable food consumption: an overview of contemporary issues and policies. *Sustainability: Science, Practice and Policy*, *9*(2), 7-25.

Sharma, A., Thakur, M., Bhattacharya, M., Mandal, T., & Goswami, S. (2019). Commercial application of cellulose nano-composites – A review. *Biotechnology Reports*, *21*, e00316.

Sharma, S., Rawat, N., Kumar, S., Mir, Z., & Gaikwad, K. (2020). Nanotechnology for Food: Regulatory Issues and Challenges. In T. R. Sharma, R. Deshmukh, & H. Sonah (Eds.), *Advances in Agri-Food Biotechnology* (pp. 367-389). Springer Singapore.

Shatkin, J. A., & Kim, B. (2017). Environmental Health and Safety of Cellulose Nanomaterials and Composites. In Kargarzadeh H. , Ahmad I., Thomas S., & Dufresne A. (Eds.), *Handbook of Nanocellulose and Cellulose Nanocomposites* (pp. 683-729). John Wiley & Sons.

Siqueira, G., Bras, J., & Dufresne, A. (2009). Cellulose Whiskers versus Microfibrils: Influence of the Nature of the Nanoparticle and its Surface Functionalization on the Thermal and Mechanical Properties of Nanocomposites. *Biomacromolecules*, *10*(2), 425-432.

Siqueira, G., Tapin-Lingua, S., Bras, J., Perez, D. D., & Dufresne, A. (2010). Morphological investigation of nanoparticles obtained from combined mechanical shearing, and enzymatic and acid hydrolysis of sisal fibers. *Cellulose*, *17*(6), 1147-1158.

Sun, X. S. (2005). 1 - Overview of plant polymers: resources, demands, and sustainability. In R. P. Wool & X. S. Sun (Eds.), *Bio-Based Polymers and Composites* (pp. 1-14). Academic Press.

Timmermans, F., & Katainen, J. (2019). Towards a Sustainable Europe by 2030. (978-92-79-98963-6). Bruxelles, Belgium: *European Commission - COM(2019)22 of 30 January 2019*

UN General Assembly. (2015). Transforming our world: the 2030 Agenda for Sustainable Development. (A/RES/70/1). New York, NY, USA: *United Nations*, 1-35.

Varun, Sharma, A., & Nautiyal, H. (2016). Environmental Impacts of Packaging Materials. In S. S. Muthu (Ed.), *Environmental Footprints of Packaging* (pp. 115-137). Springer Singapore.

Xie, H., Du, H., Yang, X., & Si, C. (2018). Recent Strategies in Preparation of Cellulose Nanocrystals and Cellulose Nanofibrils Derived from Raw Cellulose Materials. *International Journal of Polymer Science*, 2018, 7923068.

2 Enhancement of Agricultural and Industrial Wastes and By-products: New Openings for Nanocellulose Production

Abstract

Wood is the most important industrial source of cellulose fibers and therefore it is the main raw material to produce CNMs. However, interest in other sources such as agricultural crops and their by-products, or industrial waste streams is increasing. In this study, soy hulls and cotton powder were selected among the seven biomass feedstocks analyzed and transformed into CNCs and CNFs by developing tailored laboratory scale extractions. A controlled hydrolytic-oxidative treatment, with ammonium persulfate (APS), was applied to cellulosic fibers allowing dissolution of amorphous domains. Multiple mechanical shearing actions through a high-pressure homogenizer were applied to enzymatically pre-treated cellulose fibers, releasing more or less individually the nanofibrils. The CNCs were characterized through transmission electron microscopy, dynamic and electrophoretic light scattering, and infrared spectroscopy. The extraction yield was also estimated. Any changes in microstructural and morphological features of CNFs due to cleavage treatment were investigated after several homogenization steps by optical and scanning electron microscopy, and in terms of rheological properties. Lastly, hand-made paper sheets were produced by casting method, using the homogenates collected after suitable steps (3, 5, 7 and 10), and their mechanical and wettability properties were evaluated. The

two cellulose sources significantly differed in terms of extraction efficiency, geometry, morphology, and surface charge of CNCs, as well as in terms of morphology, viscosity, strength, and water absorption of CNFs. Adding an additive during the defibrillation provided benefits in process efficiency and productivity for cotton powder sample and improved the quality of both the nanofibers and the sheets made thereof.

Keywords: biomass feedstocks; oxidative-hydrolysis, high-pressure homogenization; cellulose nanocrystals; cellulose nanofibers.

2.1 Introduction

Cellulose is the most common and widespread polymer resource available in nature. It can be found in a variety of natural sources such as wood and plants, marine animal (tunicate), algae and fungi or certain bacteria (Acetobacter, Agrobacterium, Sarcina, etc.) (de Souza Lima & Borsali, 2004; Hirai et al., 2009; Siqueira et al., 2010). Although the main classification of cellulose sources depends on their origin in nature (vegetal, animal, or bacterial), in the context of sustainable development and bioeconomy, human activities turn into the most interesting categorizing criterion. In this sense, cellulose sources can be classified as:

- Primary: raw materials for cellulose fibre production purpose, like fibers for textile or paper, wood for building, industrial crops for bioethanol etc.).
- Secondary: non-processed by-products from agricultural, agri-food or forestry activities (branches, bark, straw, leaves, husks, hulls, etc.).

- Tertiary: wastes from conversion, processing, and recycling of biomass products (recollected textile waste, pulp mill residues, building demolition waste, food waste etc.) (García, 2016; Keijsers et al., 2013).

In the current stage of development, the world's leading commercial producers of nanocellulose generally use wood pulp as a raw material due to its large-scale availability and quality control (Nechyporchuk et al., 2016; Rajinipriya et al., 2018). However, wood pulp has several commercial uses and therefore other solutions such as the exploitation of lignocellulosic residues from agricultural and industrial processing side streams represents an intriguing alternative, especially in those countries where forest-based supplies are being scarce. Beside the ready availability at low-cost and the renewable nature, these alternative raw materials offer numerous environmental, technological, and economic benefits as a source for CNMs production. First, the exploitation of non-woody crops and industrial residues has the potential to simplify waste disposal and to turn end-of-life products into high value-added materials, in a "circular economy" vision (Brinchi et al., 2013). This would reduce the environmental impact of the processes while entail an additional economic profit. Finally, the use of bio-residues can have a positive impact on the manufacturing technologies in which they are involved. In fact, non-woody cellulose sources usually have a more open, less dense, and complex cell wall structure that encompass less lignin than wood. This leads to less chemically and energetically demanding processes to isolate cellulose nanomaterials, thereby making them more commercially competitive (Berglund et al., 2016; Nechyporchuk et al., 2016; Trache et al., 2017; Varanasi et al., 2018).

Therefore, despite to date mainly primary sources of cellulose have been studied and employed to produce cellulose nanocrystals and nanofibers, the investigation on these nanomaterials is gradually going towards the indirect use of lignocellulosic biomass from agricultural and industrial activities, i.e., the enhancement of secondary or tertiary sources (Rajinipriya et al., 2018). For instance, CNCs have been prepared from garlic straw (Kallel et al., 2016), corn husk (Smyth et al., 2017), walnut and groundnut shells (Bano & Negi, 2017; Hemmati et al., 2018), coconut fibres and branch-bark of mulberry (Duran et al., 2012), potato peels (Chen et al., 2012) and from chardonnay grape skins (Lu & Hsieh, 2012). Likewise, CNFs have been obtained from pineapple leaf (Cherian et al., 2010), swede root (Bruce et al., 2005), orange waste (Tsukamoto et al., 2013), sugar beet pulp (Li et al., 2014) and banana peels (Pelissari et al., 2014).

As agri-food and forestry activities are worldwide common, the resulting wastes could supply enough renewable feedstock for nanocellulose production (García, 2016). However, to ensure an adequate supply of lignocellulosic residues various aspects need to be considered, including locally available quantities and their accessibility, actual processability of the raw material and economies of scale, harvesting seasonality, environmental impact, and waste disposal costs, as well as potential competition within the bioenergy sector or with other recycling options. Also, the implementation of existing lignocellulosic biomass transformation processes with nanocellulose production steps (mechanically or chemically assisted) could be contemplated. It is known that different lignocellulosic feedstocks have, alongside a different chemical composition, different structure, and recalcitrance, i.e., different resistance of plant

cell walls to deconstruction. This is directly related to several factors, such as fiber strength and porosity, coarseness of the raw material as well as crystallinity and polymerization degree of cellulose, accessible surface area and protection of cellulose by the lignin and hemicelluloses sheathing (Lee et al., 2014). The variety of structure and recalcitrance of the different raw materials makes it mandatory to adjust the parameters involved in the extraction process and/or to perform some pre-treatments before the chemical or mechanical cleavage. Furthermore, a great heterogeneity in the characteristics of the CNMs is obtained from different native sources, influencing their functions in practical uses (Dufresne, 2017).

Motivated by above, the objective of the first phase of this PhD work corresponded to the identification of agricultural and industrial wastes and by-products most suitable to obtain CNMs in terms of technology, economy, availability, and environmental impact.

Cellulosic residues resulting from the processing and manufacturing of paper, cotton, cereals, and oilseeds were specifically discussed in this study, as they are among the productive sectors which contribute most to the generation of residual biomass ready for cellulose recovery operations.

Since each waste and by-product has a peculiar composition, depending on the starting material and the technologies adopted during its production, detailed analysis of the chemical composition was considered essential to establish its suitability for nanocellulose production and thus obtain a preliminary selection of raw materials.

Finally, the breakdown of selected lignocellulosic materials into their constitutive nano-sized components (nanocrystals and nanofibrils) has been carried out by multistep customized

procedures in order to investigate the effects of raw materials on production and properties of the cellulose nanomaterials.

2.1.1 Strategic Sectors for Cellulose Recovery

Currently, many of the EU's major agricultural and manufacturing industries generate wide waste streams with an increasing need for routes other than landfills and incineration at the end of life. As unexploited sources of cellulose, some of these waste streams could offer a strategic opportunity to turn production and processing left-over residues into valuable nanocellulose materials, ensuring sustainability, and minimizing environmental impacts.
The European production of agricultural residues is hugely dominated by cereal residues (Ronzon & Piotrowski, 2017). According to the JRC Science for Policy report (Camia et al., 2018), during the reference period 2011-2015, almost three-quarters (74%) of the total residue production of agricultural biomass in EU-28 originated from cereals (wheat, rye, barley, oats, grain maize, triticale, sorghum, and rice). This percentage corresponded to 329 million tonnes of dry matter per year (Mt/yr). Oilseed crops (rapeseed, sunflower, soya bean) was the second group of importance, contributing 17% (73 Mt/yr) to the total EU production. In both of these major crop groups, the biomass of residues is higher than economic production (i.e., the reason why the crop is cultivated) since the proportion of grain to total above ground biomass – also known as harvest index – in these crops typically ranges from 20% to 55%. The production of agricultural residues is concentrated in the major cereal-producing countries and is stable over time (Ronzon & Piotrowski, 2017). Among EU Member States, Italy ranked fifth in the total agricultural

residue production, with cereal crops contributing most and a substantial contribution from oilseed crops (Camia et al., 2018). In terms of average residue yield estimation in tonnes of dry matter per hectare (dry t/ha), the values were equal to 6.9 for rice, 5.9 for wheat, and 5.7 for soybean, among the main crops (García-Condado et al., 2019). It has been also estimated that approximately 37% of these residues are currently used in the agricultural sector and therefore the remaining 63% is potentially collectable for bio-based materials (Ronzon & Piotrowski, 2017). Their recovery would also be prompted by the fact that the main uses of these residues are low value-added, mostly meeting the needs in farming activities, soil fertilization and compensation or energetic requirements. These uses do not cover the real potential of this feedstocks from a technological and profitable point of view. Furthermore, owing to the predominance of cellulosic components, these primary agriculture residues constitute a valuable potential raw material for nanocellulose production (Camia et al., 2018; García, 2016; Ronzon & Piotrowski, 2017).

Concerning the manufacturing sector, pulp and paper industry has substantial climate change impacts, from its raw material sourcing in forests, through production, to the end of life of its products. It is counted among the most energy intensive sectors, hence the opportunities for reducing the left-over residues of the papermaking need to be urgently seized (Haggith et al., 2018). Different types of solid wastes and sludge are generated at different steps of the manufacturing process, mainly during pulping, deinking and wastewater treatment operations (Monte et al., 2009). European pulp and paper mills generate 11 million tonnes of waste yearly, of which 70% originates from deinking of

recycled paper (Nosek et al., 2017). The latter process is particularly common during tissue paper production, which generates up to 600 kg/t_{paper} of solid waste as dry content (Bajpai, 2015). In Italy alone, repulping of paper for recycling causes 280,000 tonnes of wastes every year, corresponding approximately to 32% of the total production. This waste has often no other recycling potential, so it is disposed of either by burning (34.7%) or dumping (22.4%) (Assocarta, 2019). In accordance with the European Commission Reference Report (BREF) on Best Available Techniques (BAT) for pulp and paper industry (Suhr et al., 2015), incineration combined with power and steam generation is regarded as best available technique, both in terms of energy saving and proper waste management, for paper mills processing paper for recycling. This preferential option, however, increasingly clashes with the impossibility for Italian companies to install this type of systems within their production sites and the concomitant lack, outside, of enough infrastructures to energetically recover the huge amount of waste produced. Besides, it should be noted that a part of the overall amount of waste collected in Italy for recycling is not employed locally but in substantial reports is preferably exported to Southeast Asia (Assocarta, 2019). As a result, the valuable resources (mostly cellulose) that are held within the waste of such a virtuous practice are currently being lost.

Lastly, in 2019 the European Commission identified textile sector as priority for a systemic change towards ‘circularity’, as all the environmental spheres as well as social aspects are seriously affected by textile manufacturing processes, from fiber production to waste management (European Commission, 2019; Uddin, 2019). Textile production accounts for 10% of the world’s carbon emissions and the

sector is reportedly the second most polluting in the world (ENTeR, 2018). Besides, most of the pressures and impacts related to the consumption of textiles in Europe occur in other regions of the world, where most of the production takes place. This is the case for 85% of the primary raw materials use, 92% of the water use, 93% of the land use and 76% of the greenhouse gas emissions (Manshoven et al., 2019). In addition to the unsustainable practices related to traditional materials used in textile products (critical sustainability issues particularly involve cotton farming), the environmental impact of the production and consumption of textiles reflects the high complexity of their value chain (FAO-ICAC, 2015; Manshoven et al., 2019). The textile industry is a highly diverse and heterogeneous sector which embraces a great variety of sub-sectors: next to apparel, so-called technical textiles can be found in various branches and application scenarios, e.g., automotive, aerospace, medicine and hygiene products, architecture, living, energy sector, logistics and many more (Manshoven et al., 2019; Rasheed, 2020). The flip side of this is that is a multitude of industrial processes, enterprises and market structures are involved which contribute massively to waste generation whose disposal represents an outlay cost for the companies and an environmental cost for the society. Textile products generate a problematic waste stream, and outside of well-established reuse markets and capacity limits for textile recycling processes, there remains a large proportion of low-value materials for which there is no market pull to utilise. Current treatment options for these unrecyclable textiles are incineration and landfill, where - at best - a miniscule fraction of the energy used in their production is recovered (Bell et al., 2018). However, even if complexity and variability of post-

consumer textile waste poses enormous challenges for recycling, pre-consumer textile waste, coming from textile production sites, is usually considered as “clean waste” (Euratex - European Apparel and Textile Confederetion, 2015; Ütebay et al., 2020). Therefore, nanocellulose production could potentially help to consume this share of valuable left-over textiles wastes for which technically efficient and economically sound revalorization options, beyond incineration, are lacking today.

2.2 Materials and Methods

2.2.1 Materials

Considering their wide availability, the high impact of their disposal and the concrete possibilities for their valorisation, the following biomass feedstocks from the above-mentioned target waste streams have been considered:

- Soy hulls (**Figure 2.1a**), residues of oil extraction from soybeans intended for animal feeds, were kindly supplied by Cereal Docks S.p.A. (Camisano Vicentino, Vicenza, Italy).
- Rice husk (**Figure 2.1b**), parboiled rice husk and parboiled rice straw (**Figure 2.1c**), agricultural residues generated as a by-product during the rice milling process, were kindly supplied by Riso Gallo S.p.A. (Robbio, Pavia, Italy).
- Wheat bran (**Figure 2.1d**), by-product of flour manufacture, was kindly supplied by Petra S.r.l. (Vighizzolo D'este, Padova, Italy).

- Buckwheat fine bran (**Figure 2.1e**), residual from the milling of buckwheat grains, was kindly provided by Molino Filippini S.r.l. (Sondrio, Italy).
- Tissue paper waste (**Figure 2.1f**), obtained from disposable tissue paper products for hygienic and domestic use, was kindly provided by Sofidel Group (Porcari, Lucca, Italy).
- Cotton powder (**Figure 2.1g**), kindly supplied by Sanitars S.p.A (Flero, Brescia, Italy), is a waste collected along production of cotton wool, coil, buds, pads, balls for personal care, hygiene, and cleaning purposes (cotton buds, rinse-off cosmetic pads, handkerchiefs, hygienic wipes, cleaning cloths, tablecloths, napkins etc.).

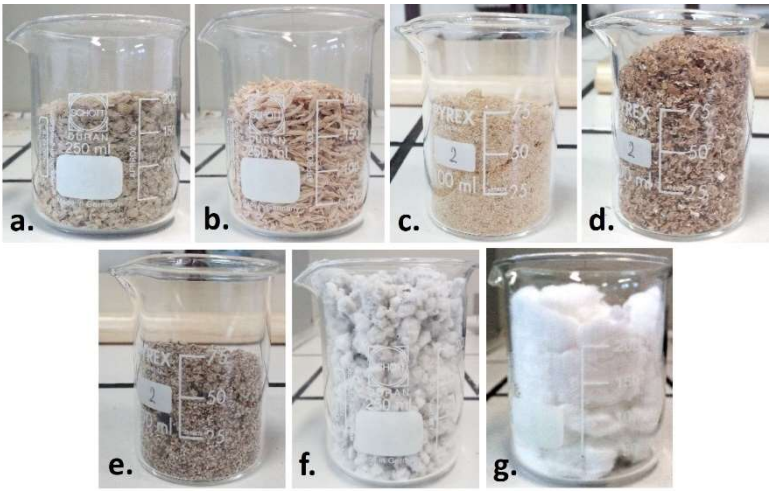

Figure 2.1 Biomass feedstocks from agricultural and industrial waste streams: **a.** soy hulls; **b.** rice husk; **c.** parboiled rice straw; **d.** wheat bran; **e.** buckwheat fine bran; **f.** tissue paper waste; **g.** cotton powder.

Henceforward, shortcuts will be used as follows: SH (soy hulls), RH (rice husk), PRH (parboiled rice husk), PRS (parboiled rice straw), WB (wheat bran), BFB (buckwheat fine bran), TW (tissue waste) and CP (cotton powder).
The chemicals and other materials used for production and characterization of nanocellulose materials were as follows: ethanol (96 %), sulfuric acid (95-98 %), sodium hydroxide pellets (97 %), calcium carbonate (≥ 99%), sodium chlorite (97 %), glacial acetic acid (≥ 99%), ammonium persulfate (98 %) all purchased from Sigma-Aldrich (Milan, Italy); D(+)glucose, D(+)xylose, D(+)galactose, L(+)arabinose, and D(+)mannose high purity standards (HPLC grade) obtained from Sigma-Aldrich (Milan, Italy); NCC®, supplied by CelluForce (Montreal, Quebec, Canada); cellulolytic enzyme multi-component mixture Viscozyme® L purchased from Novozymes A/S (Copenhagen, Denmark); Kemira FennoBond® EXP1080 dispersing agent provided by GEA (Parma, Italy).

2.2.2 Compositional Analysis of Biomass Feedstocks

Compositional analysis of the lignocellulosic feedstocks was carried out at Innovhub - Stazioni sperimentali per l'industria S.r.l. (Milano, Italy). Samples of each type of feedstocks were prepared according to NREL/TP-510-42620 (Hames et al., 2008) to standardize the materials in terms of particle size (20-80 mesh) and moisture content (< 10%) and minimize interferences in subsequent compositional analyses. Once prepared, the samples were subjected to the following characterizations.

2.2.2.1 Ash

Ash content of biomass feedstocks corresponds to inorganic matter bound into the physical structure of the biomass or derived from external additions such as surface fertilizer. (Sluiter et al., 2010). It was determined as per the NREL/TP-510-42622 technical report (Sluiter, Hames, et al., 2008) by transferring the samples into a muffle furnace set to 575 ± 25 °C till constant weight. Ash content (%) was calculated as the ratio of weights of ash and original sample on a dry weight basis.

2.2.2.2 Extractives

Sequential water and ethanol extractions was used to quantify extractives in biomass samples. They result from the non-structural components of biomass samples that include but are not limited to sucrose, nitrate/nitrites, protein, chlorophyll, and waxes, easily extractable with water or solvents (Sluiter, Ruiz, et al., 2008). Extractions were runned for 8 h in water then for 4 h in ethanol by using a Büchi Soxhlet extraction unit (Büchi Labortechnik, Switzerland), as described in the standard protocol NREL/TP-510-42619 (Sluiter, Ruiz, et al., 2008). The amount of extractives in the sample was calculate as percent on a dry weight basis.

2.2.2.3 α-cellulose

The percentage of α -cellulose was determined from the oven-dry holocellulose residue of biomass feedstocks. To obtain the holocellulose fraction, the extractives-free samples were subjected to an oxidative bleaching process using sodium

chlorite in acidic conditions (acetic acid), according to the procedure proposed by Rowell et al. (1996). The content of α-cellulose in the holocellulose was then determined by weighing the insoluble residue after subsequent reactions of the holocellulose with 17.5 wt% sodium hydroxide solution and with 10 wt% acetic acid solution at 20 ± 0.1 °C.

2.2.2.4 Structural Carbohydrates and Lignin

The skimmed off agricultural feedstocks from a first chemical characterization were further investigated by analysis of the structural carbohydrates and lignin content. According to NREL/TP-510-42618 (Sluiter et al., 2012), the biomass samples, after extractives removal, were subjected to two-step acid hydrolysis and subsequent analyses of acid soluble and acid insoluble portions. In the first step, 72 wt% H_2SO_4 was used at 30 ± 3 °C for 1h. The material was then diluted to 4 % H_2SO_4 with distilled water and autoclaved at 121 °C for 1h. The solution was filtered by using vacuum filtration system fitted with nylon membrane (pore 0.2μm). The resulting solid residue was washed three times with distilled water, dried (50 °C) to constant weight and reported as acid-insoluble lignin (AIL). The hydrolysis liquor was neutralized by addition of calcium carbonate, filtered, and subjected to sugars analysis by HPLC (Agilent Technologies, Inc., 1200 series, CA, USA) equipped with Biorad Aminex HPX-87P column, using water as mobile phase (0.6 mL min^{-1}, column temperature 75°C) and refractive index detector. Cellulose content was estimated from the glucose concentration by using correction factor of 0.9, while hemicellulose content was calculated from xylose, arabinose, mannose, and galactose concentrations by using correction factor 0.88 for

xylose and arabinose and 0.9 for mannose and galactose. Acid soluble lignin (ASL) was determined by taking absorbance of acid hydrolysis liquor at 240 nm using Cary 60 UV-vis spectrophotometer (Agilent Technologies, Inc., CA, USA). All measured constituents were reported as percentage values on a dry weight basis.

2.2.3 Extraction and Characterization of CNCs

Having emerged from the compositional analysis, cotton powder and soy hulls were selected as raw materials to isolate CNCs, specifically by the hydrolytic-oxidative method described by Leung and co-workes (2011; 2014). Before chemical hydrolysis, soy hulls were soaked in water for 6 h under stirring to partially remove the water-soluble contaminants. This pre-treatment step was necessary to soften the tight bond of polymeric constituents in the agricultural biomass and make it more accessible to the succeeding hydrolytic attack. On the other hand, the isolation of CNCs from cotton powder did not require any kind of pre-treatment, exept for the grinding of the starting material as it was received in a fully compacted form. The oxidative-hydrolysis of both raw materials made use of 1M ammonium persulfate (APS) solution (ratio between fibers and APS 10:1 g/L) heated onto a magnetic stirrer hotplate, equipped with a Vertex Digital thermoregulator (VELP Scientifica, Usmate, Italy). for 16 h at 75 °C. To remove excess acid, the suspension was centrifuged/washed at 8,000 rpm for 20 min, with distilled water repeatedly until the pH level increased from around 0.2 to 4 (correction at pH 8.0 ± 0.5 was then performed with sodium hydroxide to avoid aggregation of the

nanocrystals in acidic environment). An ultrasonic treatment (UP200St 200W, Hielscher Co., Germany) was carried out at 0.7 cycles of 20 min (70% output) to evenly distribute the CNCs in the suspension. The suspension was then vacuum filtered using Whatman glass microfiber filter (grade GF/F, 1-2 μm) to remove fibers that did not fully react with APS and other large cellulose agglomerates or contaminants that might have been introduced during the process. Finally, the purified CNCs suspensions were freeze dried for 3-4 days using LyoQuest -55/230V 50Hz freeze-dryer (Telstar, Spain), thus getting the white CNCs powders shown in **Figure 2.2**. Cellulose nanocrystals from soy hulls and cotton powder, (hereinafter SH-CNCs and CP-CNCs, respectively) were characterized through the following techniques.

Figure 2.2 Photographs of soy hulls (top row) and cotton powder (bottom row) and their ensuing freeze-dried cellulose nanocrystals (right side).

2.2.3.1 Gravimetric Yield

The yield (%) of CNCs production was calculated gravimetrically based on the weight of the dry sample (w_2, g) recovered after freeze-drying and the cellulosic content of the raw material (w_1, g) previously estimated by compositional analysis (Eq. (2.1)):

$$Yield\% = \left(\frac{w_2}{w_1}\right) \times 100 \qquad (2.1)$$

The yield was calculated on an average of four replicates.

2.2.3.2 Transmission Electron Microscopy (TEM)

The morphology of SH-CNCs and CP-CNCs were examined by TEM in a LEO 912AB transmission electron microscope equipped with Omega energy filter (Oberkochen, Germany). A drop of diluted nanocrystals aqueous suspension was deposited on a carbon-coated microscope grid and allowed to dry. The grid was negatively stained with a 3 wt% solution of uranyl acetate and dried at room temperature. The sample was observed at 120 kV. The dimensions of whiskers were determined using digital image analyses (iTEM, Olympus Soft Imaging Solutions GmbH, Germany). Fifty nanocrystals were randomly selected from eight representative TEM micrographs to determine the average length (L), diameter (D) and aspect ratio (L/D).

2.2.3.3 Dynamic Light Scattering (DLS)

DLS measurements were carried out after adjusting CNCs suspensions (0.1 wt%) to pH 8 by using Anton Paar Litesizer 500 (Graz, Austria) equipped with a 35mW laser diode light (λ = 658 nm) and collecting the scattered light at 15° and 90°. The suspensions were placed in a temperature-regulated cell at a temperature of 25.0 ± 0.1 °C. By applying correlation analysis and the Stokes–Einstein relation, the equivalent hydrodynamic diameters (D_{Hy}), polydispersity index (*PDI*) and size distributions of the scatters were calculated. Three runs were performed, withdrawing three different aliquots for each sample.

2.2.3.4 Electrophoretic Light Scattering (ELS)

Zeta potential (ζ) of CNCs in the diluted suspension at pH 8 was determined by electrophoretic light scattering (ELS), (mod. Litesizer 500, Anton Paar, Graz, Austria). Measures were replicated 3 times, at 25.0 ± 0.1 °C, by means of a 35-mW diode laser (λ= 658 nm) and at 15° detection angle.

2.2.3.5 Attenuated Total Reflectance-Fourier transform Infrared Spectroscopy (ATR-FTIR)

The IR-spectra of both type of CNCs produced were obtained and compared with that of CelluForce NCC®, regarded as commercial high-quality reference. A Perkin Elmer (Spectrum 100) infrared spectrophotometer was used, equipped with attenuated total reflectance (ATR) accessory and a spherical Ge crystal, and fixed at an incident angle of 45°. All spectra were collected over 180 scans with a

resolution of 4 cm^{-1} and recorded, in transmittance mode, in the wavenumber range of 4000-600 cm^{-1}.

2.2.4 Isolation and Characterization of CNFs

An enzyme-mediated homogenization was applied on CP and SH to isolate cellulose nanofibers. In order to increase the accessibility of the materials and make the fibers more susceptible to the fibrillation process, both materials were first ground (< 0.5mm) and then enzymatically pre-treated with Viscozyme® L multicomponent carbohydrase mixture and an enzyme dosage of 30 mg/g of biomass. The reaction was run in a 50 mM citrate buffer (pH 5) for 48 h at 50 ± 1 °C, ensuring constant stirring (40 rpm) through IKA® laboratory mixer RW16 (IKA-Werke GmbH & Co. KG, Staufen, Germany) equipped with a propeller stirrer. The suspensions (3% w/v) were heated (~ 90 °C) for 10 min to stop the enzymes activity, then treated with an Ultra Turrax® dispersing system at 10,000 rpm for approximately 5 min and immediately sent to mechanical homogenization. To obtain cellulose nanofibers from the enzyme-treated samples, successive homogenization passes were carried out using a high-pressure homogenizer (GEA - Very High Pressure, mod. NS3006L Panther, Parma, Italy), with a maximum flow rate of 50L/h. Based on the maximum pumpable concentration allowed by the machine, the pulps were homogenized with consistencies of 1.5% and 3% for CP and SH respectively. In addition, Kemira Fennobond® EXP1080 was added to part of the cotton sample as a dispersant additive for fibers, in a measure of 10% by weight on a dry basis, making the sample pumpable with a consistency of 2%. An

operating pressure of 800 bar was applied to soy hulls sample over 7 homogenization passes, compared to the 700 bar of the two cotton samples (with and without additive) which passed 10 times through the homogenizer. Three final CNFs suspensions were thus produced, which were named as SH-CNFs, CP-CNFs and CP_a-CNFs (where 'a' stands for 'additive'). Any changes in the microstructural and morphological features of the fibers due to cleavage treatment were investigated along the homogenization steps and on the final CNFs suspensions using the techniques described hereafter.

2.2.4.1 Optical and Scanning Electron Microscopy

Homogenates collected after 1, 3, 5, 7 and 10 (if any) passes were observed under optical microscope Nikon Eclipse H550L equipped with NIS-Elements Ar software (Nikon Instruments, Sesto Fiorentino, Italy). Scanning electron microscopy (SEM) images were also obtained from the final CNFs suspensions, i.e SH-CNFs, CP-CNFs and CP_a-CNFs. The images were acquired by LEO 1430-VP SEM (Carl Zeiss, Oberkochen, Germany) at accelerating voltage of 5kV and on gold-coated specimens (Sputtering Polaron E 5100). Fibril structure morphology was characterized using ImageJ software, performing around 30 measurements for each set of samples.

2.2.4.2 Viscosity Analysis

The evolution of the rheological behaviour of the samples along the homogenization process was investigated, under rotational strain, by Anton-Paar's Modular Compact

Rheometer (MCR 302, Anton Paar, Austria), equipped with cone/plate geometry (CP50-1/TG) and a thermostat set to 25 ± 0.05 °C. Measurements were performed for all samples with a solid content of 1.5% and a constant shear rate ($\dot{\gamma}$ 20 s^{-1}) along the radial direction. During measurements, a 100 μm cone/plate gap has been kept constant. The apparent viscosity (η, mPa·s) upon reaching the steady state plateau value was got for each set of samples in duplicate. As each individual sample could be measured within a short time, evaporation was considered negligible.

2.2.5 Fabrication and Testing of CNFs Sheets

To further characterize and compare the nanofibers, hand-made CNFs sheets were produced using the homogenates collected after 3, 5, 7 and 10 passes through the homogenizer. The CNFs sheets were made by vacuum filtration of 2 wt% CNFs suspensions (25 ± 0.5 g), using filter paper (Whatman, Grade 44) and Wigam DIP-402 vacuum pump (Wigam S.p.A, Castel San Niccolò, Arezzo). After oven-drying at 50°C for 24 h, CNFs sheets of 10.0 ± 0.5 cm in length and 2.5 ± 0.5 cm in width were shaped. All the sheets were conditioned at 30°C and 50% relative humidity for 48 h before testing.

2.2.5.1 Thickness

The average thickness of CNFs sheets was determined at 25 ± 1°C using Dialmatic DDI030M micrometer (Bowers Metrology, Bradford, UK), based on about twenty measurements randomnly taken across the specimen.

2.2.5.2 Surface Observation by Optical Microscopy

Top view images of the CNFs sheets were obtained by Nikon Eclipse ME600 optical microscope equipped with NIS-Elements Ar software (Nikon Instruments, Sesto Fiorentino, Italy).

2.2.5.3 Tensile Test

The mechanical properties of the CNFs sheets were evaluated by the tensile test according to ASTM D828-16 (2016). Measurements were made on 10.0 × 2.5 cm specimens, using an Instron® universal testing machine (Norwood, Massachusetts, USA), with a tensile speed of 10 mm/min, 2 cm of grips separation and a 0.1 kN load cell. The modulus of elasticity or Young's modulus (E) was calculated for each series of samples as the slope of the initial straight-line portion of the stress (σ) strain (ε) curve. For purposes of this calculation, the tensile stress was determined by dividing the load by the specimen's cross-sectional area, while the tensile strain by the change in length of the material divided by the material's original gauge length. Tensile strength was also calculated by dividing the load at break by the original cross-sectional area of test specimen. All tests were performed on at least ten specimens and the results averaged.

2.2.5.4 Surface wettability

The apparent water contact angle and the rate of change of contact angle as a function of time were measured on the sheets surface by the optical apparatus OCA 15 Plus (Data Physics Instruments GmbH, Filderstadt, Germany) with

SCA20 software (Data Physics Instruments), following the standard method (ASTM, 2009). Data acquisition was achieved, at 20 ± 5°C, with a video system equipped with a high-resolution CCD camera and a high-performance digitizing adapter. From each test unit of the sample, five 100 ± 1 x 5 ± 0.1 mm specimen strips were cut in such a way as to be thoroughly representative of the sample. A 1-mL glass micro-syringe was used as liquid delivery system. The tip of the needle was set at 3.2 mm from the surface of the specimen. A 5 µL drop of distilled water was placed on the test specimen surface, and the contact angle was measured, both initially when the drop was placed on the surface (after 5 s have elapsed) and 60 s later. The rate of change in wettability (R, °/s) was calculated as follows (Eq. (2.2)):

$$R = \frac{(A - a)}{55} \tag{2.2}$$

where A is the average angle of contact after 5 s, and a is the average angle of contact after 60 s.

2.3 Results and Discussion

2.3.1 Chemical Characterization and Selection of Biomass Feedstocks

The complex hierarchy structure of lignocellulosic biomass is the main obstacle for nano-components fractionation, where the accessibility of cellulose fibers is hindered by many physicochemical, structural, and compositional factors. Consequently, the relative abundance of cellulose, hemicellulose, lignin and other contaminants is a key factor

for determining the suitability of feedstocks for nanocellulose production (Lee et al., 2014). From a technological point of view, accurate compositional analysis of raw materials enables estimation of CNMs extraction yields and process economics due to changes in process design or additional purification steps. Results of all biomasses compositional analyses are shown in **Table 2.1**.

Obviously, the cellulose content of biomasses is of prime importance because it is directly related to the yield of CNMs in the macro-to-nano deconstruction processes. Considering the potential contribution in terms of cellulose, SH, RH, PRH and both industrial waste (TW and CP) seemed to be the potentially most interesting materials for efficient CNMs production. However, other indicators were considered crucial for the choice of raw materials. Unlike industrial waste, the composition of agricultural biomasses was rich in potential interferences: materials such as RH and PRH had a high ash content, while WB and BFB were high in water-extractable materials. PRS contained significantly more ethanol-soluble extractives than other feedstocks. These 'minor' components in biomass may interfere with acid hydrolysis and do not allow an easy separation of cellulose nanomaterials.

Table 2.1 Shares of main chemical constituents of selected lignocellulosic feedstocks. Results are reported as % on a dry weigh basis.

Constituent		SH	RH	PRH	PRS	WB	BFB	TW	CP
	Ash	4.4	17.8	17.4	7.9	4.4	5.4	0.4	8.3
	$Extractives_{(H2O)}$	9.9	1.9	2.5	9.1	17.7	17.8	1.2	n.d.
	$Extractives_{(EtOH)}$	1.9	0.8	1.0	20.8	4.8	6.8	8.4	1.6
	α-cellulose	55.8	46.8	38.3	5.0	7.6	9.4	55.8	80.5
Lignin	ASL	6.7	3.3	-	-	-	-	5.2	n.d.
	AIL*	2.6	25.5	-	-	-	-	6.3	n.d.
Hemicelluloses	Glucose	41.5	32.5	-	-	-	-	-	-
	Xylose	15.9	28.3	-	-	-	-	21.1	n.d.
	Galactose	12.5	n.d.	-	-	-	-	7.5	n.d.
	Arabinose	13.1	11.1	-	-	-	-	1.1	n.d.
	Mannose	9.4	n.d.	-	-	-	-	1.9	n.d.

* Value corrected for ash; - not evaluated; n.d. not detected.

Quantifying these components enabled a first skimming of raw materials, which picked out (i) soy hulls, (ii) rice husk (despite a high presence of ash it had a good percentage of α-cellulose), (iii) tissue waste and (iv) cotton powder, considered more suitable than the other types of biomass to produce CNMs.

For the selected raw materials, the analysis of structural carbohydrates and lignin (both ASL and AIL) were then carried by HPLC method (**Table 2.1**). Basically, RH consisted of significantly higher amount of lignin compared to SH and TW, for which much more important was instead the hemicellulose content, of 50.9% and 31.6% respectively. This could make RH more recalcitrant and resistant than the others during cellulose separation, since lignin is the hardest chemical component to take away from lignocellulosic biomass (Brinchi et al., 2013). Other than lignin, the accessibility of cellulose in RH could be affected by obstructions caused by hemicellulose, amounting to 39.4%. Both these fractions were instead not detectable for CP that appeared to be the most promising material, as it provided for the highest α-cellulose content (80.5%) and very low influence of other parameters. Furthermore, the presence of numerous foreign interfering materials, mainly small hardly removable plastic particles, were also observed in the TW matrix. Of note, in the agricultural biomasses the glucose share accounted by HPLC was quite different from the corresponding α-cellulose value, which is normally evaluated in cellulose pulps on the assumption that its building unit is glucose only. This denoted a complex composition of the agricultural raw materials and left to presume potential interferences of starch or pectin in the quantification of their α-cellulose fractions (Rowell et al., 1996). Therefore, the

amount of glucose by HPL was assumed as a measure of cellulose in the agricultural biomasses.
Ultimately, from the total chemical characterization soy hulls and cotton powder, respectively as agricultural and industrial waste streams, were selected to be transformed into cellulose nanomaterials. Only the latter are thus discussed in the following sections of this dissertation.

2.3.2 Comparison of CNCs from Different Feedstocks

The fractionation of cotton powder and soy hulls into their constitutive nanocrystalline components led to satisfying yields, assessed at approximately 49 and 36% of the initial cellulose content of CP and SH, respectively (**Table 2.2**). This confirmed the effectiveness of APS as a splitting agent, in place of the more commonly used concentrated inorganic acids.
Differences between the two materials were expected due to the less cellulose content of soy hulls along with its more complex composition compared to cotton powder. Most likely, the presence of hemicellulose and lignin in SH depleted part of the reactant used to extract and oxidize the CNCs (Leung et al., 2012).

Table 2.2 Extraction efficiency (yield %) and quality features of CNCs obtained from cotton powder and soy hulls.

Technique	Parameter	CP_CNCs	SH_CNCs
Gravimetry	Yield (%)	49 ± 12	36 ± 9
TEM	L (nm)[a]	61.32 – 420.47	70.67 – 709.15
	D (nm)[a]	7.3 – 8.2	5.1 – 5.9
	L/D[b]	23 ± 11	42 ± 15
DLS	D_{Hy}[b]	175 ± 2	219 ± 4
	PDI[b] (%)	25.1 ± 0.2	27.2 ± 1.2
ELS	ζ (mV)	-39 ± 1	-44 ± 2

[a] Range from minimum to maximum value.

[b] Average values ± s.d.

Differences were also observed in the morphological features of CNCs, which were strictly dependent from the type of cellulosic sources. Many of the final properties of CNCs-based materials are closely linked to the morphology and the geometric dimensions of cellulose nanocrystals (length, width, aspect ratio) (George & Sabapathi, 2015; Xu et al., 2013). Knowledge of these characteristics can then guide the use of CNCs for as diverse applications. In this study, a comparison of the actual shapes, particle dimensions and size distributions of the two kind of CNCs was performed via transmission electron microscopy (TEM) and by dynamic light scattering (DLS).

The electronic micrographs (**Figure 2.3**) revealed quite different aggregates of the two sets of cellulose nanocrystals.

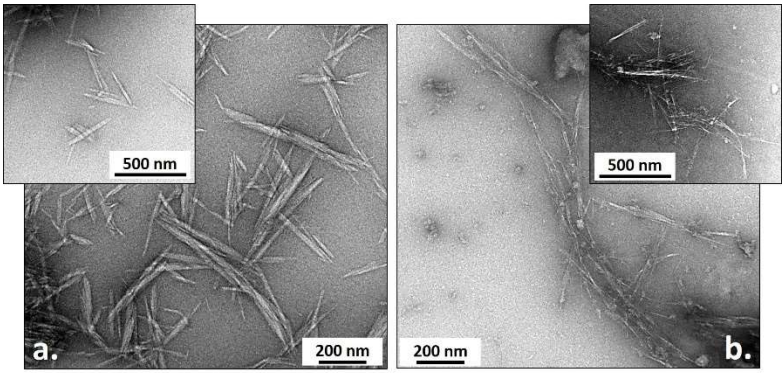

Figure 2.3 Transmission Electron Micrographs (TEM) of dilute suspensions of CNCs from cotton powder (**a.**) and soy hulls (**b.**).

The CNCs achieved from the industrial waste showed typical rod-like structure and dimensions (**Table 2.2**) consistent with common literature values (Brinchi et al., 2013; Morais et al., 2013). On average, the rods were 176 nm long (ranging from minimum ~61 nm to maximum ~420 nm), 7 nm wide (~7 nm to ~8 nm) and had a mean aspect ratio (L/D) of nearly 23. On the other hand, extraction from soy hulls produced a mixture of needle-like nanocrystals, with a length widely ranging between ~71 and ~709 nm (but mainly around 233 nm), a width of ~5 nm and a mean aspect ratio almost double that of CP_CNCs. TEM images also depicted agglomeration of nanocrystals bundles, points with dispersed crystallites and spherical CNCs. Numerous evidences from microscopy and light scattering techniques reveal different types of cellulose crystals exhibiting such a combination of shapes (Dufresne, 2017; Satyamurthy & Vigneshwaran, 2013).

By dynamic light scattering, the equivalent hydrodynamic diameters (D_{Hy}) of diluted CNCs dispersions were also determined, along with their polydispersity index (PDI) and

particle size distributions. Average D_{Hy} values of the two kind of CNCs are shown in **Table 2.2**. Even if the particle size measured by DLS cannot be related precisely to the crystals' diameter and length dimensions (Morais et al., 2013), a good agreement was observed with TEM measurements. For both kind of CNCs, the average values of D_{Hy} closely matched the TEM average lengths of CNCs, hence the DLS appeared to be a rapid method sufficiently accurate to estimate the dimensions of the crystals. CP_CNCs were in a narrow size distribution (**Figure 2.4**) that ranged ($\alpha = 0.1$) from 91 nm to 391 nm, while SH_CNCs broadened within a larger window, being from 66 nm to 690 nm. These were quite similar with the most precise results obtained from TEM, still denoting a good overlap between size distribution in CNCs solutions and electron micrographs of drop casted CNCs.

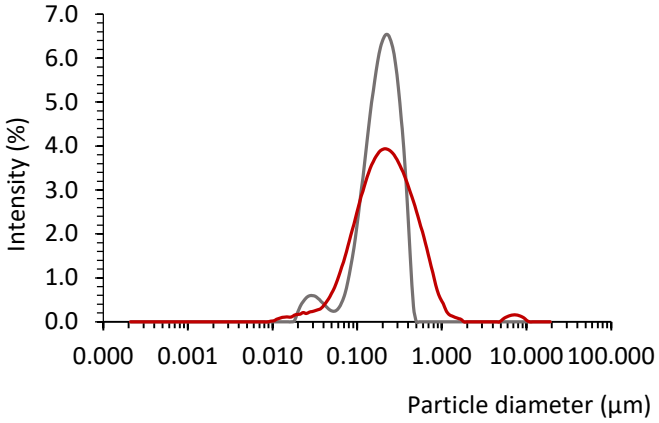

Figure 2.4 Hydrodynamic size distribution by DLS of cellulose nanocrystals from soy hulls (— SH_CNCs, red line) and cotton powder (— CP_CNCs, grey line).

Polydispersity index (PDI) is a measure of the width of particle size distribution, thus indirectly of the quality of CNCs with respect to their size distribution. Usually, in DLS, a numerical value of PDI of < 0.1 refers to a monodisperse particle size population while a PDI > 0.8 refers to a highly polydispersed size distribution (Khandal et al., 2019). In both cases, the PDI was found to be higher than 10%, indicating a moderate degree of polydispersity in the particle size and a bi- or multi-modal distributions.

Both types of CNCs exhibited a zeta potential greater, in absolute value, than -30 mV (**Table 2.2**), assumed as essential to ensure good stability of the crystals in aqueous dispersions ($\zeta < -30$ mV or $\zeta > +30$ mV) (Beyene et al., 2018).

The key functional groups of CNCs were identified through the chemical bonds' absorbance of infrared radiation, using ATR-FTIR spectroscopy. To assess the extraction efficacy, FTIR spectra of CNCs from both types of feedstocks were compared with that of CelluForce NCC® assumed as high quality standard commercial cellulose nanocrystals. As shown in **Figure 2.5**, the absorption bands of CP_CNCs and SH_CNCs were in perfect agreement with those of the commercial reference and surely typical of cellulosic materials.

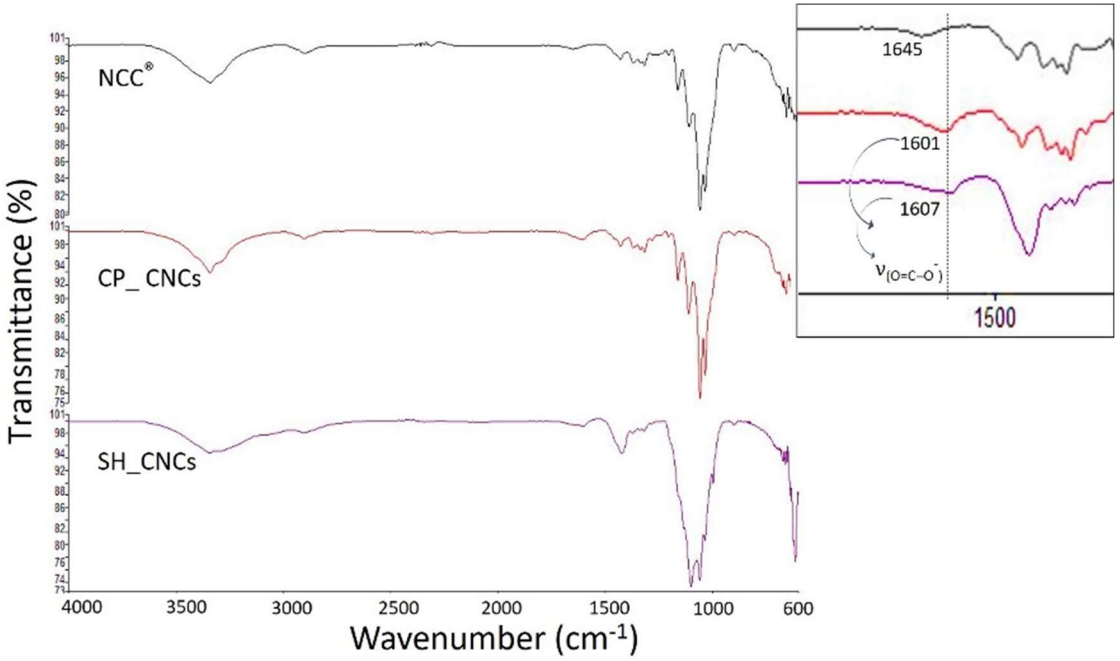

Figure 2.5 FTIR spectra of CNCs from cotton powder and soy hulls in comparison with CelluForce NCC®.

The broad band 3500-3300 cm^{-1}, in all spectra, was ascribed to the stretching vibration of the inter-hydrogen bonded OH group (ν_{OH}), while that near 2900 cm^{-1}, weak and diffused, was attributable to C–H groups of cellulose (Galiwango et al., 2019; Rahbar Shamskar et al., 2016; Rosa et al., 2012). The presence of absorption bands between 1600-1610 cm^{-1}, centred at wavenumber of 1601 cm^{-1} for SH_CNCs and 1607 cm^{-1} for CP_CNCS, could refer to the asymmetric stretching of carboxylate salt (ν_{COO^-}) that was formed because of primary hydroxyl groups oxidation induced by APS treatment (Leung et al., 2012). Similar results were also reported by Li et al. (2015) from their investigation on CNCs modified by TEMPO-mediated oxidation. Furthermore, this peak could be observed only in the spectra of laboratory CNCs products while it was absent in the reference commercial sample produced via sulphuric acid hydrolysis process. The peak absorption at around 1645 cm^{-1} in the NCC® spectrum was instead assigned to O–H bending (δ_{OH}) of absorbed water on a molecular level (Dufresne, 2017; Galiwango et al., 2019; Wang et al., 2006). The presence of signals at 1420-1430 cm^{-1} (–CH_2 scissoring), 1370 cm^{-1} (C–H bending), 1334 cm^{-1} (OH rocking, ρ_{OH}), 1316-1317 cm^{-1} (CH_2 wagging vibrations, ω_{CH2}, at C-6), 1281 cm^{-1} (C–H bending), 1206 cm^{-1} (OH in plane bending), 1161-1162 cm^{-1} (C–C ring stretching), and 1099-1111 cm^{-1} (C–O–C asymmetric stretching), on all spectra, indicated that the CNCs may be primarily in the form of cellulose I (Kumar et al., 2014; Leung et al., 2012). Lacking or overlapping of some of these peaks in the SH_CNCs spectrum may be due to the developed of hydrogen bonding network in crystalline structure that impeded or decreased some bending and out of plan movements. Other characteristic absorption peaks

related to the chemical structure of cellulose were 896 cm^{-1}, resulting from β-glycosidic linkages, 1058 and 1035 cm^{-1} from –C–O and C–O–C stretching vibrations of pyranose skeletal ring (Alemdar & Sain, 2008). These FTIR data suggested that oxidation occurred preferentially at the C6 primary alcohol of crystalline cellulose, since the oxidation of C2 and C3 secondary alcohols is known to induce the cleavage of the glucopyranose ring. The absence of an IR signal relating to hemiacetal formation (880 cm^{-1}) confirmed the intact crystalline structure of CNCs prepared by APS (Leung et al., 2011). By comparing the spectral data of CP_CNCs and SH_CNCs with those of commercial reference, it was possible to state the substantial removal of hemicellulose and lignin and the efficient isolation of pure cellulose nanocrystals.

2.3.3 Comparison of CNFs from Different Feedstocks

Mechanical isolation of CNFs from enzyme-pre-treated soy hulls and cotton powder required tailored process parameters suited to the specific feedstock. Soy hulls, homogenized with high-pressure technology, after 7 passes at 800 bar appeared completely defibrillated, resulting in a very stable gel-like appearance. On the other hand, cotton powder, which could not be treated at 3% due to the flocculation of individual fibers in clusters even of several millimeters in size, hence diluted up to 2 and 1.5%, obtained a good degree of defibrillation after 10 passes at 700 bar, showing much more stable gels after addition of the dispersing additive. Samples collected at any homogenization pass are shown in **Figure 2.6**.

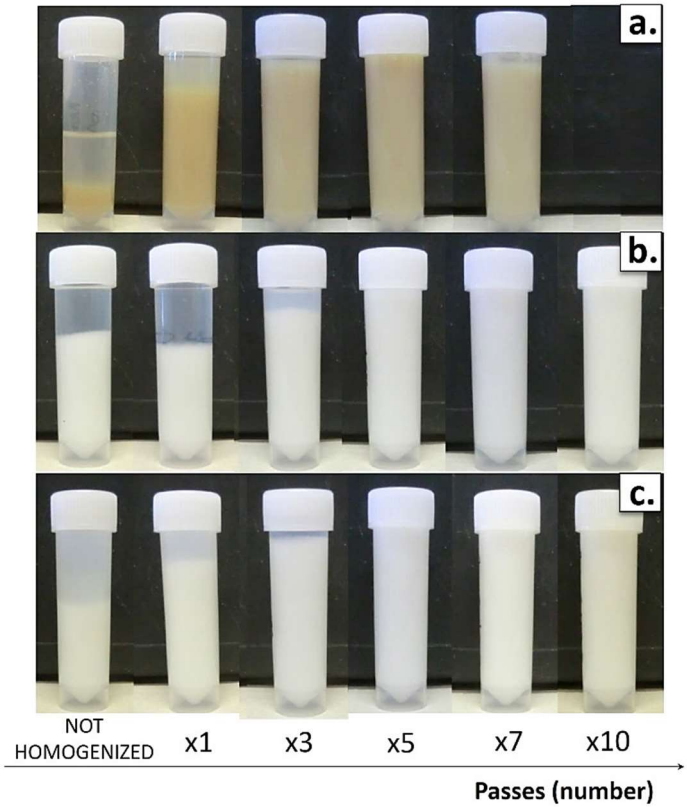

Figure 2.6 Appearance of the suspensions of soy hulls (**a.**) and cotton powder, without (**b.**) and with additive (**c.**), as collected from enzymatic pre-treatment (not homogenized) and after 1, 3, 5, 7 and 10 high-pressure homogenization passes.

It was then observed that CNFs of greater consistency could be produced with fewer homogenization passes when dealing with soy hulls instead of cotton powder, imputing this conclusion to the morphological characteristics of the native fibers, the cellulose content and the repulsive action of

hemicelluloses potentially still present. In the latter respect, it is known that hemicellulose can contribute to efficient fibrillation and dispersion stability of CNFs by electric and/or steric mechanisms that prevent coalescence of CNFs (Iwamoto et al., 2008; Kumagai & Endo, 2020).

It should also be considered that Viscozyme® L is a multi-enzyme complex with a strong pectolytic activity and a wide range of carbohydrases, including arabanase, cellulase, β-glucanase, hemicellulase and xylanase (De Campos et al., 2013). It can therefore be assumed that the synergistic activity of these enzymes was important especially for soy hulls, which contained hemicellulose and pectins, and less important for cotton powder, which was affected only by the β-1,4 cleavage activity of a small fraction of the enzyme complex.

Morphology of the obtained CNFs was one of the most important parameters to control during the production process. No clear difference could be seen between the untreated and enzymatically treated fibers for the tested experimental conditions using optical microscope (images not shown). Oppositely, as a consequence of homogenization steps, the fibers showed a significant progressive decrease in their dimensions compared to untreated ones, first separating themselves into microfibers and then into nanofibril sub-elements. **Figures 2.7-2.9** show optical micrographs of the enzymatically treated fibers for increasing numbers of passes through the homogenizer and for the different sets of samples.

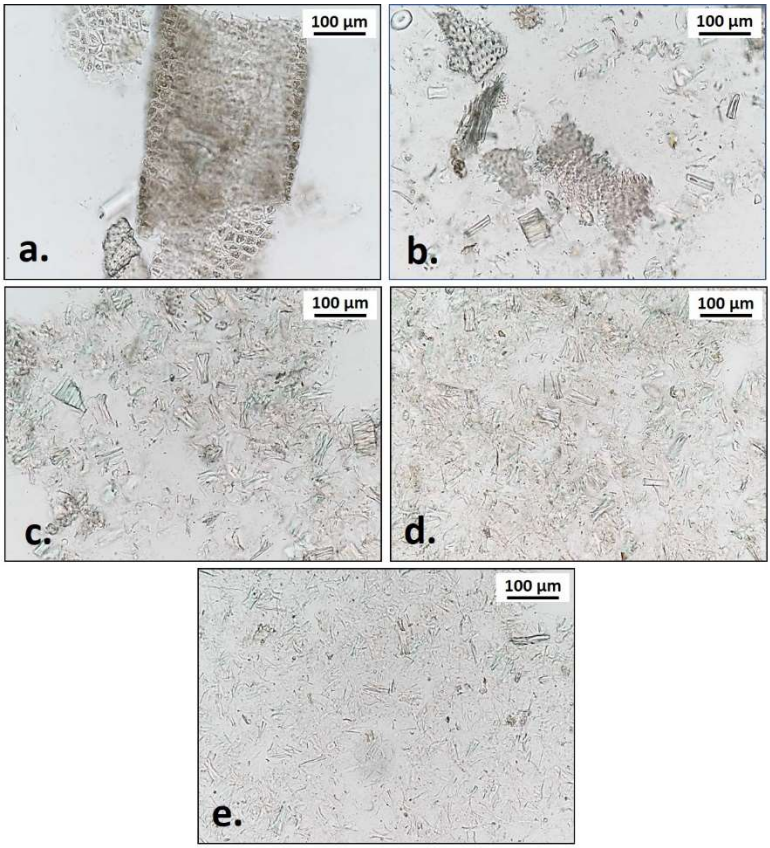

Figure 2.7 Optical microscopy images of enzymatically-treated soy hulls fibers after 0 (**a.**), 1 (**b.**), 3 (**c.**), 5 (**d.**), and 7 (**e.**) passes through the high-pressure homogenizer. Magnification Plan Apo 20x DIC M N2.

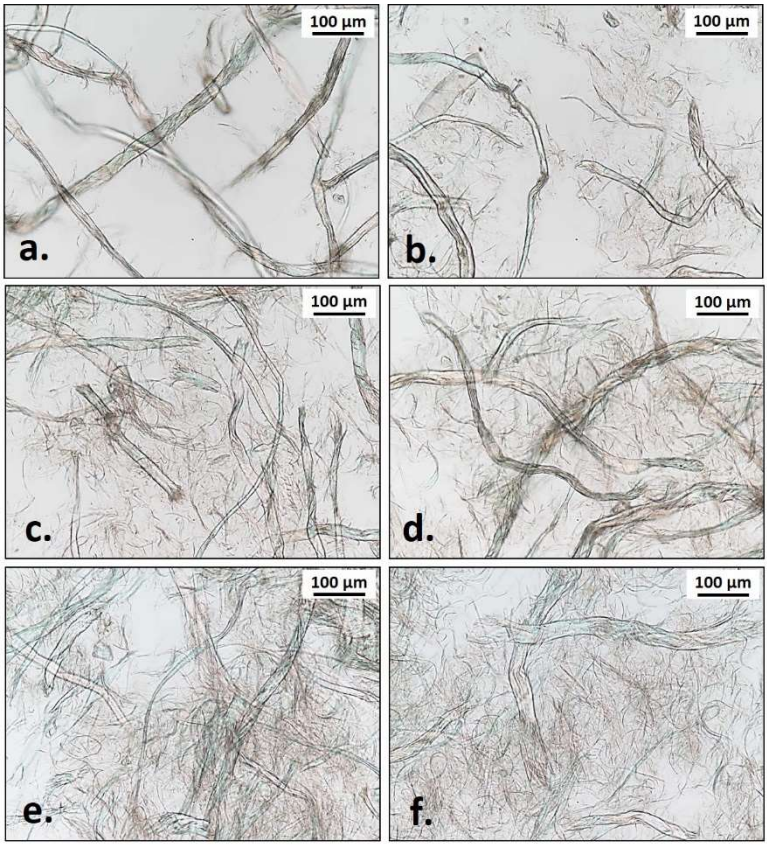

Figure 2.8 Optical microscopy images of enzymatically-treated cotton powder fibers after 0 (**a.**), 1 (**b.**), 3 (**c.**), 5 (**d.**), 7 (**e.**) and 10 (**f**) passes through the high-pressure homogenizer. Magnification Plan Apo 20x DIC M N2.

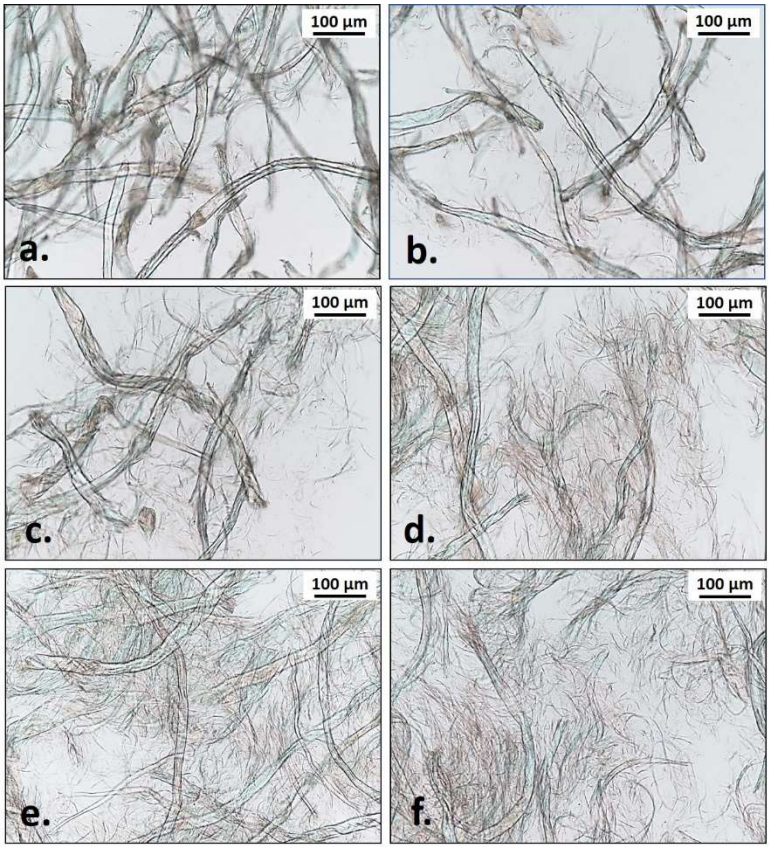

Figure 2.9 Optical microscopy images (Magnification Plan Apo 20x DIC M N2) of enzymatically-treated cotton powder with additive, after 0 (**a.**), 1 (**b.**), 3 (**c.**), 5 (**d.**), 7 (**e.**) and 10 (**f**) passes through the high-pressure homogenizer.

Although these pictures did not allow for size measurement, they rather gave an indication of the extent of fibrillation. No long fibers were observed for soy sample after only 3 homogenization passes (**Figure 2.7c.**), but small broken fragments were still present, which almost disappeared after 7 passes (**Figure 2.7e.**). At 7 passes, most nanofibrils had length lower than 100 µm. Instead, mechanically disintegrated CNFs from both cotton samples possessed much longer fibrils, which could reach several hundred micrometers even after 10 passes (**Figures 2.8f.**, **2.9f.**). The CNFs obtained using the additive appeared more regular and individualized compared to those obtained without the additive, but some large fragments were still visible in both samples.

Figure 2.10 shows scanning electron micrographs of the isolated CNFs obtained after passing SH and CP fibers through the homogenizer 7 and 10 times, respectively. As expected, the isolated CNFs exhibited very high lengths which could not be assessed by SEM technique whatever the sample considered. Moreover, because of the strong interactions between the fibrils, final dispersions remained quite heterogeneous in diameter, and even if the fibers had mostly nanoscale diameters (~50 nm), there were also larger fibril bundles, all being in a high-density network and entangled with each other.

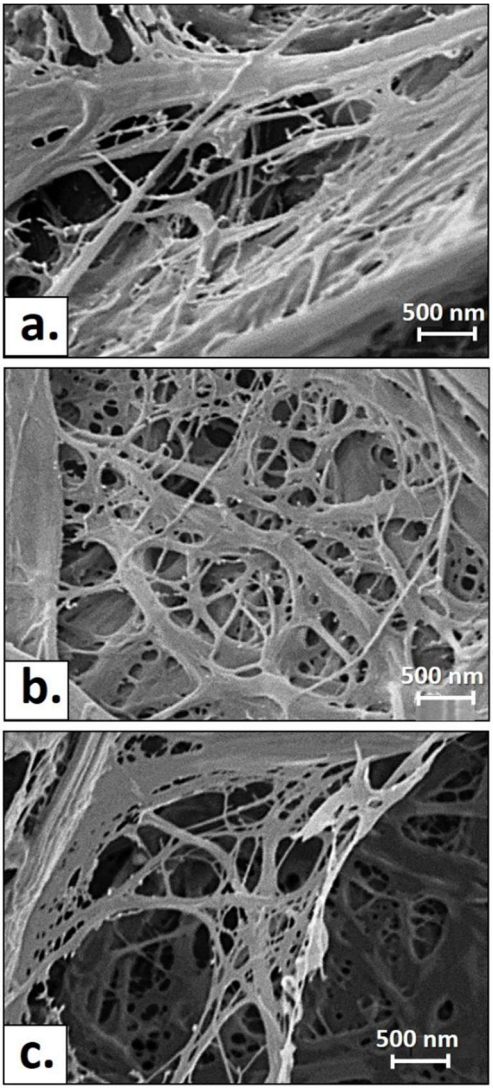

Figure 2.10 SEM images, at 30K x magnifications, of SH_CNFs (**a.**), CP_CNFs (**b.**) and CP_a_CNFs (**c.**) at the end of homogenization process.

The effect of mechanical processing within different number of passes on rheological behaviour of cellulose fibers was detailed in order to optimize the processing steps providing stable fiber suspensions. CNFs suspensions are known to exhibit gel properties even at low cellulose concentrations, which occurs when the percolation threshold concentration of nanofibers is exceeded (Nechyporchuk et al., 2016). As shown in **Figure 2.11**, at a solid content of 1.5%, the steady-shear viscosity values (η, mPa·s) of all samples were positively correlated with the homogenization passes, since along the process a web of fibrils, having nano-size width and much higher surface area, was being created.

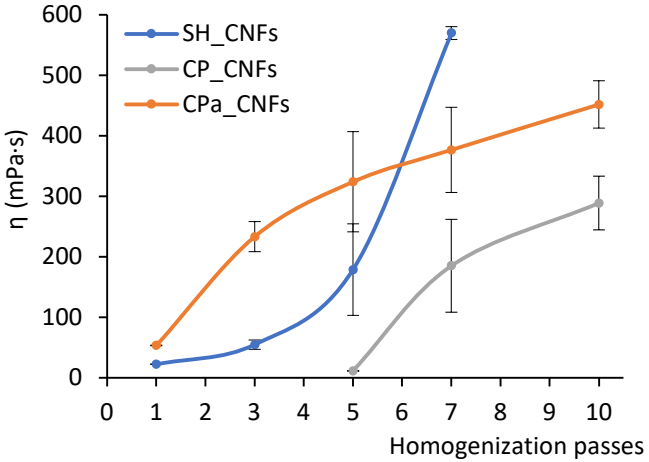

Figure 2.11 Steady-shear viscosity (η) as a function of homogenization passes for SH_CNFs, CP_CNFs and CP_a_CNFs, at a shear rate of 20 s^{-1} and a solid content of 1.5%.

SH_CNFs exhibited lower viscosity trend compared to CP_a_CNFs upon the first 5 homogenization passes, and significantly higher trend with increased the passes. This proved that sol–gel transformation and visco-elastic transition strictly depended on the interfibrillar hydroxyl bonding, the length to diameter ratio and the cross-linking extent of the different cellulosic nanofibers. Thereby, for CP with additive a threshold of 3 passes was assumed to trigger the mechanism of network formation leading to the gel-like behaviour, and at least 5 and 7 passes for SH and CP without additive, respectively. At the end of the considered processes, viscosity values of 570.1 ± 10.4 mPa·s for SH_CNFs and of 452.0 ± 39.2 mPa·s for CP_a_CNFs were recorded. Much less viscous was CP_CNFs reaching 289.0 ± 44.5 mPa·s at the conclusion of mechanical homogenization. From the figure, it is also apparent that no results could be obtained from the first homogenates of CP without additive as these initial suspensions (at 1 and 3 homogenization passes) contained clearly visible millimetre-sized fibre flocs that were expelled from the side of the cone-and-plate system, sometimes causing the rotation of the cone to slow down or even stop completely.

Hand-made CNFs sheets were produced by casting method, using the homogenates collected after several passes (where feasible), and a quantitative comparison of their physico-mechanical properties was carried out. Specimens of all sheets produced are shown in **Figure 2.12**, while the results of the sheets characterization are presented in **Table 2.3**. For all samples, stress-strain curves, showing the change in tensile stress as strain increases, are also available in the supporting information (S.I.).

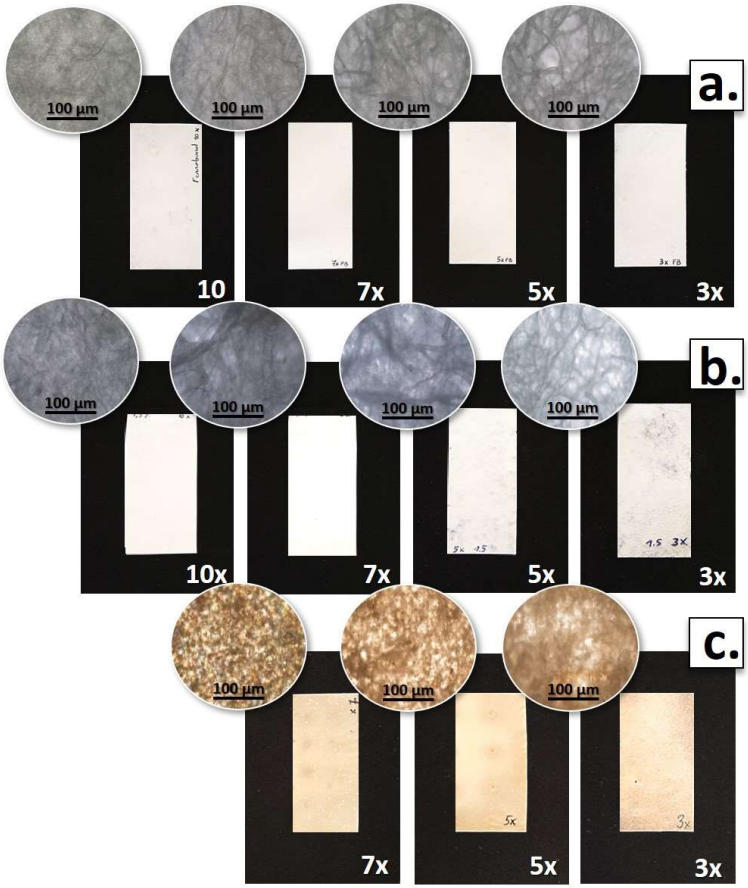

Figure 2.12 Top view photographs of sheet specimens and corresponding surface magnifications (20x) under optical microscope (insets). Homogenates of CP with additive (**a.**), CP without additive (**b.**) and SH (**c.**), at different passes, were used to get the sheets.

Table 2.3 Thickness, mechanical and wettability properties of sheets produced from the homogenates collected along the process.

Sample	Pass	Thickness (mm)	E Modulus (MPa)	Tensile Strength (MPa)	θ_w (°)	R (°/s)
CP_CNFs	3	0.18±0.02	419±34	5.51±1.51	n.d.	n.d.
	5	0.20±0.05	551±36	7.32±1.78	n.d.	n.d.
	7	0.15±0.03	913±55	14.93±4.04	n.d.	n.d.
	10	0.13±0.04	823±17	23.31±3.52	n.d.	n.d.
CP_a_CNFs	3	0.17±0.03	767±80	13.69±1.49	19.55±0.21	0.36±0.04
	5	0.14±0.02	1091±33	23.01±3.08	29.08±4.69	0.30±0.10
	7	0.12±0.02	1479±52	40.47±9.18	33.01±5.61	0.25±0.08
	10	0.10±0.01	1519±73	67.78±9.75	62.64±7.51	0.14±0.05
SH_CNFs	3	0.14±0.05	n.d.	n.d.	56.94±9.22	0.39±0.10
	5	0.11±0.04	1255±24	41.32±4.32	61.58±4.40	0.15±0.09
	7	0.09±0.01	1981±53	56.53±4.24	64.82±3.31	0.13±0.06

n.d. not detected.

In all cases, an increment in the number of passes through the homogenizer meant a more and more tight bonding between fibrils (see **Figure 2.12** insets) and well compact sheets, which in turn resulted in progressively better mechanical properties. All cellulose sheets showed in fact an increase in tensile strength and elastic modulus with decreasing fiber size along the progress in fibrillation. However, when comparing the sheets, some differences were found between the samples. At 7 passes, SH_CNFs sheets showed the stiffest network structure, with the highest *E*-modulus and a tensile strength comparable to that of CP_a_CNFs. Nevertheless, the latter had a greater elastic deformation under tensile load (see **Figure S 2.1** of the Supporting Information for additional details) and, after 10 homogenization passes, showed the highest tensile strength. It is worth noting that, in in the absence of additive, cotton powder fibers were not fibrillated to the same extent as in the presence of additive during the mechanical process, as CNFs sheets with much worse mechanical performances were obtained. Compared to CP_a_CNFs, at 10 homogenization passes CP_CNFs sheets showed a decrease in *E*-modulus and tensile strength of 696 and 44.5 MPa, respectively.

Microstructures of cellulose nanomaterials are known to significantly impact on their mechanical properties (Qing et al., 2015). In general, differences in tensile properties of cellulose networks may be explained in terms of the different density and stiffness of hydrogen bonding between cellulose chains and the diverse contribution of the fiber morphology (Stelte & Sanadi, 2009).

Contact angle measurements were used to study the wetting behaviour and relative sorbtive rates of the different CNFs sheets. As expected, fibrillation had positive effects on wet

fiber performances due to the increase in the length to diameter ratio and in the surface area, thus improving inter-fiber bonding capability. The wettability of the CP_a_CNFs network improved progressively as the number of passes increases, with a raise in the water contact angle (θ_w) of 43.09°, passing from 3 to 10 homogenization steps. The θ_w enhanced moderately of 7.88° from 3 to 7 passes for SH_CNFs, those having the highest initial contact angles since after 3 passes. This could be explained by the presence of residual lignin in the SH_CNFs, since it was previously reported that the films from the lignin-containing cellulose fibrils have less water-wettable surfaces (Jiang et al., 2019). On the other hand, for CP_CNFs the absorption rate of water drops by the sheets surface was not sufficiently to consider the contact angle measurements meaningful and measurable. No result was therefore found for this sample. At 3 passes, both CP_a_CNFs and SH_CNFs sheets showed the greatest relative change in contact angle per unit time (°/s), having the fastest rate of sorption upon initial contact with water. The change in contact angle with time was less rapid with passes increases, indicating a relative decreased degree of water absorption into the sheet. Finally, at 10 and 7 passes, for CP_a_CNFs and SH_CNFs, respectively, very little change in contact angle was seen over the time interval of a typical test (60 s).

2.4 Conclusions

In this work, preparation approaches of nanocellulose (fibers and crystals) from industrial and agricultural residues were proposed, and led to the following main concluding remarks:

- Proper choice of raw materials is a prerequisite for an economically efficient production of nanocellulose due to a broad variety of chemical composition and structure, which can affect the preparation before the CNMs obtaining process, as well as the extraction conditions.
- As exceptional sources of ease accessible cellulose fibers, soy hulls and cotton powder may represent valuable feedstocks for nanocellulose materials. These appeared suitable options for simplifying the extraction processes traditionally used for woody raw materials, thus showing some potential for upscaling.
- Tailored oxidative-hydrolysis and enzyme-mediated homogenization are effective chemical or mechanical deconstruction strategies to obtain good quality CNCs and CNFs, respectively, from the selected feedstocks.
- The choice of raw material, technology applied, and parameters involved for obtaining CNMs change geometry, morphology, surface charge for CNCs, as well as morphology (dimensions and residual fiber fragments), viscosity, strength, and water absorption for CNFs. Therefore, it is possible to take advantage of the customizable functionalities of the CNMs by tuning these variables and targeting them towards specific applications.

2.5 Supporting Information

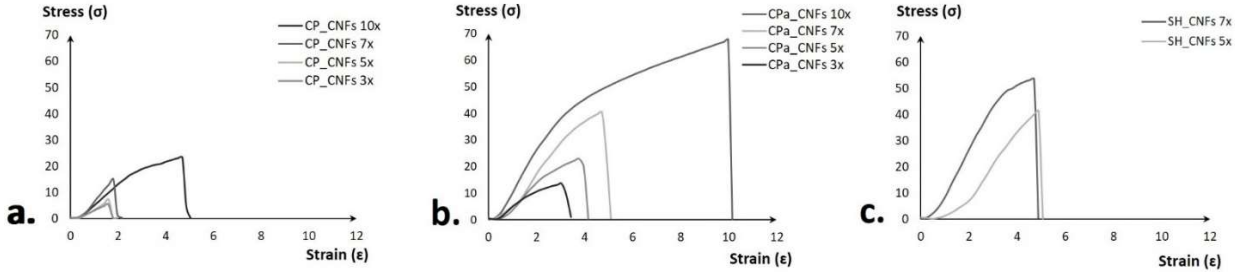

Figure S 2.1 Tensile stress-strain curves of the hand-made sheets from CP_CNF (**a.**), CP_a_CNFs (**b.**) and SH_CNFs (**c.**) at different homogenization passes.

References

Alemdar, A., & Sain, M. (2008). Isolation and characterization of nanofibers from agricultural residues – Wheat straw and soy hulls. *Bioresource Technology*, *99*(6), 1664-1671.

Assocarta. (2019). Rapporto ambientale dell'industria cartaria italiana: dati 2016-2017. Associazione Italiana fra gli Industriali della Carta Cartoni e Paste per Carta (Assocarta),. Milano, Italy: *Associazione Italiana fra gli Industriali della Carta Cartoni e Paste per Carta (Assocarta)*.

ASTM. (2009). *Standard Test Method for Surface Wettability of Paper (Angle-of-Contact Method) (Withdrawn 2009)* (ASTM D724-99(2003)).

ASTM. (2016). *Standard Test Method for Tensile Properties of Paper and Paperboard Using Constant-Rate-of-Elongation Apparatus* (ASTM D828-16).

Bajpai, P. (2015). Generation of Waste in Pulp and Paper Mills. In *Management of Pulp and Paper Mill Waste* (pp. 9-17). Springer International Publishing.

Bano, S., & Negi, Y. S. (2017). Studies on cellulose nanocrystals isolated from groundnut shells. *Carbohydrate Polymers*, *157*, 1041-1049.

Bell, N. C., Lee, P., Riley, K. S., & Slater, S. (2018). Tackling problematic textile waste streams. RESYNTEX project Report. Aylesbury, UK: *Oakdene Hollins Ltd*.

Berglund, L., Noël, M., Aitomäki, Y., Öman, T., & Oksman, K. (2016). Production potential of cellulose nanofibers from industrial residues: Efficiency and nanofiber characteristics. *Industrial Crops and Products*, *92*, 84-92.

Beyene, D., Chae, M., Dai, J., Danumah, C., Tosto, F., Demesa, A. G., & Bressler, D. C. (2018). Characterization of cellulase-treated fibers and resulting cellulose nanocrystals generated through acid hydrolysis. *Materials*, *11*(8), 1272.

Brinchi, L., Cotana, F., Fortunati, E., & Kenny, J. M. (2013). Production of nanocrystalline cellulose from lignocellulosic biomass: Technology and applications. *Carbohydrate Polymers*, *94*(1), 154-169.

Bruce, D. M., Hobson, R. N., Farrent, J. W., & Hepworth, D. G. (2005). High-performance composites from low-cost plant primary cell walls. *Composites Part A: Applied Science and Manufacturing*, *36*(11), 1486-1493.

Camia, A., Robert, N., Jonsson, R., Pilli, R., García-Condado, S., López-Lozano, R., van der Velde, M., Ronzon, T., Gurría, P., M'Barek, R., Tamosiunas, S., Fiore, G., Araujo, R., Hoepffner, N., Marelli, L., & Giuntoli, J. (2018). Biomass production, supply, uses and flows in the European Union: First results from an integrated assessment. EUR - Scientific and Technical Research Reports (EUR 28993 EN, JRC109869). European Commission - Joint Research Centre (JRC). Luxembourg: *Publications Office of the European Union*.

Chen, D., Lawton, D., Thompson, M. R., & Liu, Q. (2012). Biocomposites reinforced with cellulose nanocrystals derived from potato peel waste. *Carbohydrate Polymers*, *90*(1), 709-716.

Cherian, B. M., Leão, A. L., de Souza, S. F., Thomas, S., Pothan, L. A., & Kottaisamy, M. (2010). Isolation of nanocellulose from pineapple leaf fibres by steam explosion. *Carbohydrate Polymers*, *81*(3), 720-725.

De Campos, A., Correa, A. C., Cannella, D., de M Teixeira, E., Marconcini, J. M., Dufresne, A., Mattoso, L. H., Cassland, P., & Sanadi, A. R. (2013). Obtaining nanofibers from curauá and sugarcane bagasse fibers using enzymatic hydrolysis followed by sonication. *Cellulose*, *20*(3), 1491-1500.

de Souza Lima, M. M., & Borsali, R. (2004). Rodlike Cellulose Microcrystals: Structure, Properties, and Applications. *Macromolecular Rapid Communications*, *25*(7), 771-787.

Dufresne, A. (2017). *Nanocellulose: From Nature to High Performance Tailored Materials* (2 ed.). Walter de Gruyter GmbH & Co KG.

Duran, N., Lemes, A. P., & Seabra, A. B. (2012). Review of Cellulose Nanocrystals Patents: Preparation, Composites and General Applications. *Recent Patents on Nanotechnology*, *6*(1), 16-28.

ENTeR - Expert Network on Textile Recycling. (2018). Textile Waste & Recycling - Strategic Agenda on Textile Waste Management and Recycling *Interreg Central Europe's ENTeR Project*.

Euratex - European Apparel and Textile Confederetion. (2015). Annual Report 2015. Euratex. Brussels, Belgium.

European Commission. (2019). Commission Staff working document on Sustainable Products in a Circular Economy -Towards an EU Product Policy Framework contributing to the Circular Economy. (SWD(2019)91/F1). Brussels, Belgium

FAO's Plant Production and Protection Division, & ICAC's Expert Panel on Social Environmental and Economic Performance of Cotton Production. (2015). Measuring Sustainability in Cotton Farming Systems. (ISBN 978-92-5-108614-8). Rome, Italy: *FAO-ICAC*.

Galiwango, E., Abdel Rahman, N. S., Al-Marzouqi, A. H., Abu-Omar, M. M., & Khaleel, A. A. (2019). Isolation and characterization of cellulose and α-cellulose from date palm biomass waste. *Heliyon*, *5*(12), e02937.

García-Condado, S., López-Lozano, R., Panarello, L., Cerrani, I., Nisini, L., Zucchini, A., Van der Velde, M., & Baruth, B. (2019). Assessing lignocellulosic biomass production from crop residues in the European Union: Modelling,

analysis of the current scenario and drivers of interannual variability. *GCB Bioenergy*, *11*(6), 809-831.

García, A. (2016). Industrial and crop wastes: A new source for nanocellulose biorefinery. *Industrial Crops and Products*, *v. 93*, pp. 13-38-2016 v.2093.

George, J., & Sabapathi, S. N. (2015). Cellulose nanocrystals: synthesis, functional properties, and applications. *Nanotechnology, Science and Applications*, *8*, 45.

Haggith, M., Kinsella, S., Baffoni, S., Anderson, P., Ford, J., Leithe, R., Neyroumande, E., Murtha, N., & Tinhout, B. (2018). The State of the Global Paper Industry 2018: New Challenges and Opportunities for Forests, People and the Climate. EPN Annual Report. The Environmental Paper Network (EPN),. North Carolina, USA: *Environmental Paper Network (EPN)*.

Hames, B., Ruiz, R. O., Scarlata, C., Sluiter, A., Sluiter, J., & Templeton, D. (2008). Preparation of Samples for Compositional Analysis. Laboratory Analytical Procedure (LAP) (NREL/TP-510-42620). National Renewable Energy Laboratory (NREL).

Hemmati, F., Jafari, S. M., Kashaninejad, M., & Barani Motlagh, M. (2018). Synthesis and characterization of cellulose nanocrystals derived from walnut shell agricultural residues. *International Journal of Biological Macromolecules*, *120*, 1216-1224.

Hirai, A., Inui, O., Horii, F., & Tsuji, M. (2009). Phase Separation Behavior in Aqueous Suspensions of Bacterial Cellulose Nanocrystals Prepared by Sulfuric Acid Treatment. *Langmuir*, *25*(1), 497-502.

Iwamoto, S., Abe, K., & Yano, H. (2008). The Effect of Hemicelluloses on Wood Pulp Nanofibrillation and Nanofiber Network Characteristics. *Biomacromolecules*, *9*(3), 1022-1026.

Jiang, Y., Liu, X., Yang, Q., Song, X., Qin, C., Wang, S., & Li, K. (2019). Effects of residual lignin on composition, structure and properties of mechanically defibrillated cellulose fibrils and films. *Cellulose*, *26*(3), 1577-1593.

Kallel, F., Bettaieb, F., Khiari, R., García, A., Bras, J., & Chaabouni, S. E. (2016). Isolation and structural characterization of cellulose nanocrystals extracted from garlic straw residues. *Industrial Crops and Products*, *87*, 287-296.

Keijsers, E. R. P., Yılmaz, G., & van Dam, J. E. G. (2013). The cellulose resource matrix. *Carbohydrate Polymers*, *93*(1), 9-21.

Khandal, D., Riedl, B., Tavares, J. R., Carreau, P. J., & Heuzey, M.-C. (2019). Tailoring cellulose nanocrystals rheological behavior in aqueous suspensions through surface functionalization with polyethyleneimine. *Physics of Fluids*, *31*(2), 021207.

Kumagai, A., & Endo, T. (2020). Effects of hemicellulose composition and content on the interaction between cellulose nanofibers. *Cellulose*.

Kumar, A., Negi, Y. S., Choudhary, V., & Bhardwaj, N. K. (2014). Characterization of Cellulose Nanocrystals Produced by Acid-Hydrolysis from Sugarcane Bagasse as Agro-Waste. *Journal of Materials Physics and Chemistry*, *2*(1), 1-8.

Lee, H. V., Hamid, S. B. A., & Zain, S. K. (2014). Conversion of Lignocellulosic Biomass to Nanocellulose: Structure and Chemical Process. *The Scientific World Journal*, *2014*, 20.

Leung, A. C. W., Hrapovic, S., Lam, E., Liu, Y. L., Male, K. B., Mahmoud, K. A., & Luong, J. H. T. (2011). Characteristics and Properties of Carboxylated Cellulose Nanocrystals Prepared from a Novel One-Step Procedure. *Small*, *7*(3), 302-305.

Leung, A. C. W., Luong, J. H. T., Hrapovic, S., Lam, E., Liu, Y., Male, K. B., Mahmoud, K., & Rho, D. (2012). *Cellulose*

nanocrystals from renewable biomass. http://www.google.com/patents/US20120244357

Leung, A. C. W., Luong, J. H. T., Hrapovic, S., Lam, E., Liu, Y., Male, K. B., Mahmoud, K., & Rho, D. (2014). *Cellulose Nanocrystals From Renewable Biomass* (US Patent No. US 8900706 B2). https://lens.org/173-345-283-827-03X

Li, B., Xu, W., Kronlund, D., Määttänen, A., Liu, J., Smått, J.-H., Peltonen, J., Willför, S., Mu, X., & Xu, C. (2015). Cellulose nanocrystals prepared via formic acid hydrolysis followed by TEMPO-mediated oxidation. *Carbohydrate Polymers*, *133*, 605-612.

Li, M., Wang, L.-j., Li, D., Cheng, Y.-L., & Adhikari, B. (2014). Preparation and characterization of cellulose nanofibers from de-pectinated sugar beet pulp. *Carbohydrate Polymers*, *102*, 136-143.

Lu, P., & Hsieh, Y.-L. (2012). Cellulose isolation and core–shell nanostructures of cellulose nanocrystals from chardonnay grape skins. *Carbohydrate Polymers*, *87*(4), 2546-2553.

Manshoven, S., Christis, M., Vercalsteren, A., Arnold, M., Nicolau, M., Lafond, E., Mortensen, L. F., & Coscieme, L. (2019). Textiles in Europe's Circular Economy (ETC/WMGE 2019/6). Boeretang, Belgium: *European Topic Centre on Waste and Materials in a Green Economy*.

Monte, M. C., Fuente, E., Blanco, A., & Negro, C. (2009). Waste management from pulp and paper production in the European Union. *Waste Management*, *29*(1), 293-308.

Morais, J. P. S., Rosa, M. d. F., de Souza Filho, M. d. s. M., Nascimento, L. D., do Nascimento, D. M., & Cassales, A. R. (2013). Extraction and characterization of nanocellulose structures from raw cotton linter. *Carbohydrate Polymers*, *91*(1), 229-235.

Nechyporchuk, O., Belgacem, M. N., & Bras, J. (2016). Production of cellulose nanofibrils: A review of recent advances. *Industrial Crops and Products*, *93*, 2-25.

Nosek, R., Holubcik, M., Jnadacka, J., & Radacovska, L. (2017). Analysis of paper sludge pellets for energy Utilization. *BioResources*, *12*, 7032-7040.

Pelissari, F. M., Sobral, P. J. d. A., & Menegalli, F. C. (2014). Isolation and characterization of cellulose nanofibers from banana peels. *Cellulose*, *21*(1), 417-432.

Qing, Y., Sabo, R., Wu, Y., Zhu, J. Y., & Cai, Z. (2015). Self-assembled optically transparent cellulose nanofibril films: effect of nanofibril morphology and drying procedure. *Cellulose*, *22*(2), 1091-1102.

Rahbar Shamskar, K., Heidari, H., & Alimorad, R. (2016). Preparation and evaluation of nanocrystalline cellulose aerogels from raw cotton and cotton stalk. *Industrial Crops and Products*, *93*, 203-211.

Rajinipriya, M., Nagalakshmaiah, M., Robert, M., & Elkoun, S. (2018). Importance of Agricultural and Industrial Waste in the Field of Nanocellulose and Recent Industrial Developments of Wood Based Nanocellulose: A Review. *ACS Sustainable Chemistry & Engineering*, *6*(3), 2807-2828.

Rasheed, A. (2020). Classification of Technical Textiles. In S. Ahmad, A. Rasheed, & Y. Nawab (Eds.), *Fibers for Technical Textiles* (pp. 49-64). Springer International Publishing.

Ronzon, T., & Piotrowski, S. (2017). Are Primary Agricultural Residues Promising Feedstock for the European Bioeconomy? *Industrial Biotechnology*, *13*(3), 113-127.

Rosa, S. M. L., Rehman, N., de Miranda, M. I. G., Nachtigall, S. M. B., & Bica, C. I. D. (2012). Chlorine-free extraction of cellulose from rice husk and whisker isolation. *Carbohydrate Polymers*, *87*(2), 1131-1138.

Rowell, R. M., Young, R. A., & Rowell, J. K. (1996). *Paper and Composites from Agro-based Resources*. CRC Press.

Satyamurthy, P., & Vigneshwaran, N. (2013). A novel process for synthesis of spherical nanocellulose by controlled hydrolysis of microcrystalline cellulose using anaerobic microbial consortium. *Enzyme and Microbial Technology*, *52*(1), 20-25.

Siqueira, G., Bras, J., & Dufresne, A. (2010). *Cellulosic Bionanocomposites: A Review of Preparation, Properties and Applications* (Vol. 2).

Sluiter, A., Hames, B., Ruiz, R., Scarlata, C., Sluiter, J., & Templeton, D. (2008). Determination of Ash in Biomass. Laboratory Analytical Procedure (LAP) (NREL/TP-510-42622). National Renewable Energy Laboratory (NREL).

Sluiter, A., Hames, B., Ruiz, R., Scarlata, C., Sluiter, J., Templeton, D., & Crocker, D. (2012). Determination of Structural Carbohydrates and Lignin in Biomass. Laboratory Analytical Procedure (LAP). National Renewable Energy Laboratory (NREL).

Sluiter, A., Ruiz, R., Scarlata, C., Sluiter, J., & Templeton, D. (2008). Determination of Extractives in Biomass. Laboratory analytical procedure (LAP). National Renewable Energy Laboratory (NREL).

Sluiter, J. B., Ruiz, R. O., Scarlata, C. J., Sluiter, A. D., & Templeton, D. W. (2010). Compositional analysis of lignocellulosic feedstocks. 1. Review and description of methods. *Journal of Agricultural and Food Chemistry*, *58*(16), 9043-9053.

Smyth, M., García, A., Rader, C., Foster, E. J., & Bras, J. (2017). Extraction and process analysis of high aspect ratio cellulose nanocrystals from corn (Zea mays) agricultural residue. *Industrial Crops and Products*, *108*, 257-266.

Stelte, W., & Sanadi, A. R. (2009). Preparation and Characterization of Cellulose Nanofibers from Two Commercial Hardwood and Softwood Pulps. *Industrial & Engineering Chemistry Research*, *48*(24), 11211-11219.

Suhr, M., Klein, G., Kourti, I., Rodrigo Gonzalo, M., Giner Santonja, G., Roudier, S., & Delgado Sancho, L. (2015). Best Available Techniques (BAT) Reference Document for the Production of Pulp, Paper and Board. Industrial Emissions Directive 2010/75/EU Integrated Pollution Prevention and control. EUR - Scientific and Technical Research Reports (JRC95678, EUR 27235EN). European Commission's Joint Research Centre (JRC) – Institute for Prospective Technological Studies (IPTS). Luxembourg: *Publications Office of the European Union*.

Trache, D., Hussin, M. H., Haafiz, M. K. M., & Thakur, V. K. (2017). Recent progress in cellulose nanocrystals: sources and production. *Nanoscale*, *9*(5), 1763-1786.

Tsukamoto, J., Durán, N., & Tasic, L. (2013). Nanocellulose and bioethanol production from orange waste using isolated microorganisms. *Journal of the Brazilian Chemical Society*, *24*(9), 1537-1543.

Uddin, F. (2019). Introductory Chapter: Textile Manufacturing Processes. In F. Uddin (Ed.), *Textile Manufacturing Processes*. IntechOpen.

Ütebay, B., Çelik, P., & Çay, A. (2020). Textile Wastes: Status and Perspectives. In *Textile Industry and Waste*. IntechOpen.

Varanasi, S., Henzel, L., Sharman, S., Batchelor, W., & Garnier, G. (2018). Producing nanofibres from carrots with a chemical-free process. *Carbohydrate Polymers*, *184*, 307-314.

Wang, Q., Fan, X., Gao, W., & Chen, J. (2006). Characterization of bioscoured cotton fabrics using FT-IR ATR spectroscopy and microscopy techniques. *Carbohydrate Research*, *341*(12), 2170-2175.

Xu, X., Liu, F., Jiang, L., Zhu, J. Y., Haagenson, D., & Wiesenborn, D. (2013). Cellulose Nanocrystals vs. Cellulose Nanofibrils: A Comparative Study on Their

Microstructures and Effects as Polymer Reinforcing Agents. *ACS Applied Materials & Interfaces*, *6*.

3 Fast Production of Cellulose Nanocrystals by Hydrolytic Oxidative Microwave Assisted Treatment

Luana Amoroso[1], Giuseppe Muratore[1], Marco A. Ortenzi[2], Stefano Gazzotti[2], Sara Limbo[3] and Luciano Piergiovanni[3*].

1. *Department of Agricultural, Food and Environment (Di3A), Università degli Studi di Catania, Via Santa Sofia 100, 95123 Catania, Italy.*
2. *CRC Laboratorio di Materiali e Polimeri (LaMPo), Department of Chemistry, Università degli Studi di Milano, Via Golgi 19, 20133 Milano, Italy.*
3. *DeFENS, Department of Food, Environmental and Nutritional Sciences—PackLAB Università degli Studi di Milano, Via Celoria 2, 20133 Milano, Italy.*

This chapter is published in *Polymers*, 2020, *12*(1), 68.

For the hydrolytic-oxidative microwave-assisted method described in this chapter, the following patents were deposited:

- Piergiovanni L. & Amoroso L. (2018). Procedimento per la produzione di nanocristalli di cellulosa (CNC). Brevetto italiano n. IT 201800007870 A1 (domanda di brevetto n. 102018000007870, depositata il 06.08.2018, pubblicata il 06.11.2018).
- Piergiovanni L. & Amoroso L. (2020). Method for Producing Cellulose Nanocrystals (CNCs). European patent EP 3608342 A1 (application number: 19000360.8, date of filing 02.08 2019, date of publication 12.02.2020).

Abstract

In contrast to conventional approaches, which are considered energy and time intensive, expensive, and not green, herein we report an alternative microwave-assisted ammonium persulfate (APS) method for cellulose nanocrystals (CNCs) production, under pressurized conditions in a closed reaction system. The aim was to optimize the hydrolytic-oxidative patented procedure (US 8,900,706), replacing the conventional heating with a faster process that would allow the industrial scale production of the nanomaterial and make it more appealing to green economy. Microwave-assisted process was performed according to different time-temperature programs, varying the ramp (from 5 to 40 min) and the hold heating time (from 60 to 90 min), at fixed reagent concentration and weight ratio of raw material/APS solution. Differences in composition, structure, and morphology of the nanocrystals, raising from traditional and microwave methods, were studied by several techniques (TEM, FTIR-ATR, DLS, ELS, TgA, XRD), beside the extraction yields were calculated. Fine tuning the microwave treatment variables, it was possible to realize a simple, cost-effective way for faster materials preparation, that allowed to get high quality CNCs, with defined hydrodynamic diameter (150 nm) and zeta potential (-0,040 V), comparable to those obtained using conventional heating, in only 90 min instead of 16 h.

Keywords: microwave technology; cellulose nanocrystals; energy-saving, fast-production.

3.1 Introduction

Cellulose-based materials have been used by our society for thousands of years for many daily-usage items. Nowadays, on this widespread natural polymer, the most recent and innovative researches are oriented, in an attempt to increase the application of its properties, especially at nano-scale level: the nanometric and crystalline forms of cellulose, known as Cellulose Nanocrystals (CNCs), have garnered a huge level of attention from the international scientific community and an exceptional appealing throughout the world that does not appear to be relenting. In particular, food packaging industry, which is still heavily dependent on synthetic materials, is interested in the wider use of these new bio-nanoparticles, in order to increase the sustainability of its products and reduce their environmental impact. In our previous works, we have widely demonstrated that cellulose nanocrystals offer a barrier to gas diffusion comparable to that offered by synthetic barrier polymers nowadays employed (EVOH, PVOH, PVDC), even applying considerably lower coating thicknesses (Fotie et al., 2017; Li et al., 2013; Mascheroni et al., 2016; Rampazzo et al., 2017). Actually, cellulose nanocrystals have long been regarded as a laboratory interest, evidenced by the significant rise in spin-offs and pilot-scale initiatives and in the number of patents published over the last few years on this theme (Gómez H et al., 2016). At the time of the TAPPI Nanotechnology for Renewable Nanomaterials Conference (TAPPI Nano), in June 2014, there was only one commercial entity producing nanocellulose for market development: the Canadian CelluForce Co.. Since then, the market has exploded and today, only few years later, we can report that worldwide

there are many commercial entities, producing nanocellulose at capacities beyond pilot plant scale (CelluForce, American Process Inc., Paperlogic, Borregaard). Beside these, numerous research facilities are producing nanocellulose, and several new lab and pilot plants have been announced, and we believe there are numerous unreported lab scale facilities at universities, paper mills, and other sites. Furthermore, the global nanocellulose market is expected to register a very high CAGR (Compound Annual Growth Rate), during the forecast period, 2018 to 2023 (MarketsandMarkets, 2019; Tan et al., 2019), so, these emerging nanoparticles, have the potential to play a major role in the 21st century in the development of advanced materials (Dufresne, 2017).

However, although nanocellulose applications has being studied since around 1980, only recently its manufacturing became at least technically feasible (Jongaroontaprangsee et al., 2018). To date, the production of nanocellulose at industrial scale is restricted to still limited number of companies with a narrow production (totalling ca. 6000 kg per day) (de Melo et al., 2017). Encouraged by the growing industrial interest, especially of food packaging sector, for cellulose nanocrystals (CNCs), further research efforts and alternative methods must be explored to make the industrial scale-up of nanocellulose production increasingly convenient and more simply achievable.

It is fair to assert that, most of existing literature to date reports the typical procedure currently employed for the preparation of cellulose nanocrystals (CNCs) consisting of subjecting an appropriate cellulosic feedstock to strong acid hydrolysis under strictly controlled conditions of temperature, agitation, and time. The most common protocol involves the use of mineral acids (typically sulfuric acid ca

64% w/w) at a temperature range from 45 to 70 °C, for times varying according to the temperature (Bondeson et al., 2006; Favier et al., 1995; Filson et al., 2009; Kos et al., 2014). These procedures are expensive, require considerably high initial capital investment and have high operating costs due to the corrosiveness, safety issues, and hazardous waste treatment/disposal requirements of such acids and their by-products. Additionally, they require relatively pure cellulosic starting materials, such as steam-exploded wood pulp and microcrystalline cellulose, or alkaline and bleaching agents, as pre-treatments to remove non-cellulosic fiber contents (e.g., lignin, pectin, hemicelluloses). The use of highly corrosive mineral acids, requiring expensive corrosion resistant equipment, multiple treatment steps or tedious isolation techniques, impedes large-scale production and real-world applications of CNCs (Leung et al., 2011). However, recent international scientific literature reported a simple and versatile one-step procedure to produce highly crystalline CNCs, that involves the use of ammonium persulfate ($(NH_4)_2SO_8$), an oxidant with low long-term toxicity, high water solubility and low cost. Recent studies have shown that the latter allows to obtain, in a single step, the hydrolytic fragmentation of cellulose, with the formation of nanocrystals, and the oxidation of some primary hydroxyl group into carboxylic ones, that is of great utility in the incorporation or grafting of CNCs in packaging materials and in the possibility of binding functionalizing molecules to CNCs (Mascheroni et al., 2016). This hydrolytic-oxidative process, also covered since 2014 by a patent (US 8,900,706) of Leung and co-workers (Leung et al., 2014), describes, for preparing cellulose nanocrystals, a heating treatment time that is substrate-dependent, ranging from 5 and 24 h for

complex substrates and typically of 16 h for most common cellulosic materials such as hemp, flax etc. The APS method is broadly applicable to a variety of native plant fibers and other cellulose sources, simultaneously removing lignin and amorphous cellulose to yield high-quality CNCs.

In the APS protocol, as for the ones with mineral acids, heating has traditionally been conventional one, meaning that energy is conveyed through convection, conduction, and radiation. However, the rate of conventional heating is slow compared to microwave (MW) heating. In the latter way of heating, electromagnetic energy converts thermal energy through direct interaction of the incident radiation with molecules of a target material. Many experiments have shown that under MW irradiation conditions, chemical reactions can be significantly accelerated by several orders of magnitude (Zhu & Chen, 2014) and selectivity of the ensuing products can be obtained by choosing appropriate MW parameters, thus offering several advantages over conventional heating (Polshettiwar & Varma, 2008). As a result, microwave heating technique has emerged as a valuable alternative in the production of organic compounds, polymers, inorganic materials, and even nanomaterials, with shorter reaction time and higher reaction rate, selectivity, and yield compared to the conventional heating methods (Caddick & Fitzmaurice, 2009; Nüchter et al., 2004; Venkatesh & Raghavan, 2004; Zhu & Chen, 2014). In recent years, some review articles have been published on the microwave irradiation-assisted synthesis of nanostructured materials, such as metal nanostructures (Nadagouda et al., 2011), nanostructured carbon materials (Zhang & Liu, 2012), nanoporous nanomaterials (Tompsett et al., 2006), colloidal nanocrystals (Baghbanzadeh et al., 2011), inorganic

nanomaterials (Bilecka & Niederberger, 2010), metal oxide nanoparticles supported on carbon nanotubes (Motshekga et al., 2012), and polymer nanocomposites (Dariusz et al., 2011). Some researchers have explored it for nanocellulose production (de Melo et al., 2017; Filson et al., 2009; Kos et al., 2014) or modification processes including acetylation (Li et al., 2009) and carboxymethylation (Biswas et al., 2014), but no one commented on oxidative hydrolysis by means of microwave heating. Simple procedures, instantaneous and rapid heating, high temperature homogeneity, decreased energy costs, unique transformations, and ease of scalability, are the major advantages that are becoming apparent when using microwave-assisted chemistry. Moreover, as a result of the more efficient heating in the processes, microwave energy is understood to be more environmentally friendly, requiring less energy consumption than the conventional heating processes (de la Hoz, 2011). By controlling the specific MW parameters (temperature, pressure, and ramping of temperature) and choice of solvents, researchers can now move into the next generation of advanced nanomaterial design and development (Gawande et al., 2014).

In contrast to conventional approaches, which are considered energy and time intensive, expensive, and not green, herein we report an alternative microwave-assisted APS method for cellulose nanocrystals production, under pressurized conditions in a closed reaction system. The aim was to optimize the hydrolytic-oxidative procedure described by Leung et al.'s patent, replacing the conventional heating with a faster heating, based on microwave technology that could allow the industrial scale production of the nanomaterials and make it more appealing to green economy. In this paper, several features were evaluated in order to compare the

nanocrystals raising from traditional and microwave processes and to investigate the influence of different thermal conditions on production and properties of nanocellulose materials (CNCs).

3.2 Materials and Methods

3.2.1 Materials

The cotton powder as raw material to be used for CNCs production was supplied by Sanitars S.p.A. (Flero, Brescia, Italy) who obtained it as waste product from cotton processing. The chemical reagents (ammonium persulfate ≥98%, sodium hydroxide ≥97%) were purchased from Sigma-Aldrich (Milan, Italy).

3.2.2 Design of Experiment

For the design of the experiment a multilevel general factorial design was used, exploring two quantitative factors: the ramp time (X_1), i.e. the time required to reach a predefine heating temperature of 120 °C; and the hold time (X_2), or time for temperature maintenance. Based on some previous experiences, 4 levels for the ramp time (5, 15, 30, 40 min), and two levels for the hold time (60, 90 min) have been set, with 4 replicates for each combination of experimental conditions. Moreover, 4 central points were employed to the design, for a total of 36 runs (runs), performed with a completely randomized blocks sequence. The effect of all the possible combinations of the levels of the two factors, X_1 and X_2, on some parameters of the nanocrystals were analysed:

(I) hydrodynamic diameter (D_{Hy}), (II) polydispersity index (PDI), (III) zeta potential (ζ) and (IV) yield (Y). The experiment design was supported by the Design-Expert software (version 7.0.0) of Stat-Ease® (Stat-Ease Inc., Minneapolis, USA).

3.2.3 Cellulose Nanocrystals Extraction Processes

3.2.3.1 Heating Programs

Cellulose nanocrystals from the same raw material (i.e., cotton powder) were obtained using the two methodologies as outlined next. For conventional heating process, the milled cotton powder was subjected to an oxidative hydrolysis with ammonium persulfate (APS) 1M solution according to Leung and co-workers method (Leung et al., 2011). The reaction mixture (ratio between fibers and APS 10:1 g/L) was thus placed into a large beaker, onto a magnetic stirrer hotplate, equipped with a Vertex Digital thermoregulatory (VELP Scientifica, Usmate, Italy), heated at 75 °C and continuously stirred for 16 h, limiting the evaporation by means of a plastic foil cover.

Instead, microwave-assisted preparation of CNCs involved that cellulosic material was introduced into microwave pressure vessels (HVT50, teflon, 50 mL) and 1M APS solution was added, maintaining the same rapport between fibers and reactive solution than conventional heating method. The suspension was homogenised through stirring for 5 min and transferred to a laboratory microwave digestion system (Multiwave GO, Anton Paar, Graz, Austria) during the whole heating procedure. The equipment was provided with a single magnetron that delivers up to 850 W microwave

power over the full power range. For accurate reaction control the vessel temperature was continuously monitored with an IR temperature sensor, measuring from the bottom of the cavity. The sensor system of the instrument enabled automatic detection of each reaction vessel, as well as monitoring of the rotor revolution, to ensure uniform microwave heating and prevent localized overheating. The microwave-assisted process was performed according to sequential heating steps, choosing different time-temperature programs: the reaction mixture has initially been ramped to a set temperature of 120 °C and then held to the fixed temperature before final cooling (till 40 °C). The rate of temperature increase ($\Delta T/t$) remained constant according to selected ramp time. The reaction conditions, for conventional and microwave heating, are summarized in **Table 3.1**.
The microwave reactor allowed precise control of reaction conditions and homogeneous temperature profiles, closely fitting with those programmed, as shown in **Figure 3.1**

Table 3.1 Microwave and conventional heating programs for cellulose nanocrystals production

Microwave Heating Method	Heating Program			Temperature (°C)	Total Heating Time (hh:mm)	Cooling (°C)
	Ramp (mm:ss)	ΔT/t (°C min^{-1})	Hold (mm:ss)			
M_1	05:00	20	60:00	120	01:05	40
M_2	15:00	7	60:00	120	01:15	40
M_3	30:00	3	60:00	120	01:30	40
M_4	40:00	2.5	60:00	120	01:40	40
M_5	05:00	20	90:00	120	01:35	40
M_6	15:00	7	90:00	120	01:45	40
M_7	30:00	3	90:00	120	02:00	40
M_8	40:00	2.5	90:00	120	02:10	40
Conventional Heating Method				**Temperature (°C)**	**Total Heating Time (hh:mm)**	**Cooling (°C)**
C_1				75	16:00	40

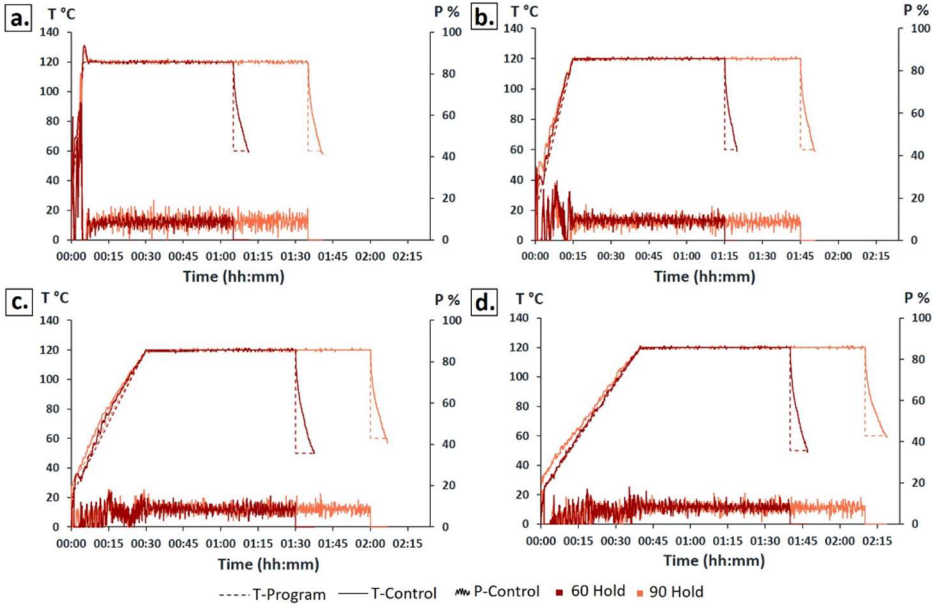

Figure 3.1 Monitoring of the temperature (°C) and microwave power supplied (%) during predefined heating programs: (**a.**) M_1, M_5; (**b.**) M_2, M_6; (**c.**) M_3, M_7; (**d.**) M_4, M_8.

3.2.3.2 Purification Steps

Aiming to concentrate the cellulose and remove excess acid, the CNCs suspensions were subjected to subsequently centrifugation-washing procedures, at 4,000 rpm for 20 min, using deionized water, until the pH level increased from around 0.2 to 4 (pH correction was then performed, increasing it to 8 ± 0.5 with NaOH to avoid aggregation of the crystals in acidic environment). An ultrasonic treatment (UP200St 200W, Hielscher Co., Germany) was then carried out, at 0.7 cycles of 20 min and 70% output, to distribute CNCs evenly in the suspensions. The suspensions were vacuum filtered using Munktell filter paper (grade 1-2 μm) to remove fibers that did not completely react with APS, and other big cellulose agglomerates and large contaminants that may have been introduced during the process. The purified suspensions were finally freeze-dried (LyoQuest -55/230V 50Hz, Telstar, Spain) for 3-4 days to get white CNCs powder.

3.2.4 CNCs Extraction Yield

The yield of CNCs production (%) was estimated, using a gravimetric method, by Eq. (3.1), as the ratio of freeze-dried CNCs weight (w_2, g) and cellulosic content of raw material (w_1, g), which is equal to 80.5% of the fresh weight of cotton powder:

$$Yield\ \% = \left(\frac{w_2}{w_1}\right) \times 100 \qquad (3.1)$$

The yield was calculated based on an average of four replicates for each heating condition.

3.2.5 Morphological Characterization of CNCs

The morphological characteristics of the CNCs were evaluated via Transmission Electron Microscopy, using a LEO 912AB TEM with Omega energy filter (Zeiss, Oberkochen, Germany) at an accelerating voltage of 120 kV. For the microscopic observations, drops of dilute aqueous suspension of CNCs (≈ 4 wt %), previously sonicated for 1 min, were deposited on carbon-coated electron microscope grids, negatively stained with 2% uranyl acetate and allowed to dry. Representative micrographs were selected for measuring the diameter (D), length (L) and the aspect ratio (L/D) of the nanocrystals by digital image analysis (iTEM Olympus software). In addition, the dimensions of CNCs from all heating programs, in dilute suspensions (at pH 8), were also investigated by dynamic light scattering (DLS) measurements (mod. Litesizer500, Anton Paar, Graz, Austria), performed at 25.0 ± 0.1 °C with a 35 mW laser diode light (λ = 658 nm) and collecting the scattered light at 15° and 90°. By applying correlation analysis and the Stokes–Einstein relation, the equivalent hydrodynamic diameters (D_{Hy}), the polydispersity index (PDI) and size distributions of the scatters were calculated. Four runs have been performed, withdrawing three different aliquots for each set of experimental conditions.

3.2.6 Zeta Potential Measurement

The diluted suspensions of the CNCs (pH 8) were analysed by electrophoretic light scattering (ELS) (mod. Litesizer 500, Anton Paar, Graz, Austria) which allows to measure the

electrophoretic mobility of the particles suspended in a liquid, directly proportional to their Zeta potential (ζ, mV), according to Henry's equation. Measures were replicated four times, at 25.0 ± 0.1 °C, by means of a 35 mW diode laser (λ = 658 nm) and at 15° detection angle.

3.2.7 Statistical Analysis

The two independent variables, ramp time (X_1) and hold time (X_2), were statistically explored, subjecting the data to a two-way analysis of variance (ANOVA) to determine the effects of factorial combination of X_1 (quantitative factor on 4 levels) and X_2 (quantitative factor on 2 levels), each of which repeated 4 times. The statistical significance of the model was determined by evaluating the p-value, F-value and lack of fit at 95% confidence level. The statistical treatment of the experimental data also consisted in fitting a polynomial function to the set of data collected from multilevel factorial design, by means of the least squares method. The extent of fitting was expressed by the adjusted determination coefficient (R^2_{adj}). Response surfaces were then obtained using the fitted model and keeping one independent variable constant varying the other variable. Furthermore, to obtain the process settings achieving peak performance, numerical optimization function has been used to find maximum desirability for all responses simultaneously, combining all the data into a single desirability function (D), through the geometric mean (D_j) of the individual desirability. Finally, to differentiate the CNCs samples of each series of microwave heating programs from those of conventional heating, the mean values of measured parameters were compared using

Fisher's least significance difference (LSD) test, when the F-test was significant and with a significance level of $p \leq 0.05$. To this aim, a one-factor comparative experiment was performed, whose levels were represented by the different heating programs adopted (M_1, M_2, M_3, ..., C_1).

3.2.8 FTIR-ATR Analysis of Cellulose Nanocrystals

The Presence of CNCs have been verified and further investigated using Fourier transform infrared spectroscopy (FTIR), that allowed to identify key chemical compounds through the chemical bonds' absorbance of infrared radiation. The FTIR-ATR spectroscopy was performed, in duplicate, on the native cotton powder and on freeze-dried CNCs samples resulting from conventional heating and from the microwave heating program that provided the best results in terms of yield, size and zeta potential. A Perkin Elmer instrument (Spectrum 100) have been used, equipped with attenuated total reflectance (ATR) accessory and a spherical Ge crystal, fixed at an incident angle of 45°. All spectra were collected at a spectrum resolution of 4 cm^{-1}, with 180 scans and recorded, in transmittance mode, over the wavenumber range of 4000-600 cm^{-1}. A background scan of clean Ge crystal was acquired before scanning the samples.

3.2.9 X-Ray Diffraction (XRD) Characterization

X-Ray diffraction (XRD) measurements were performed on the same freeze-dried powders that were analysed in FTIR-ATR, to gain insight into details of the crystalline structure of CNCs from the two heating methods. The diffraction patterns

were detected, at room temperature, on a Panalytical X'pert PrO diffractometer (Malvern Panalytical S.r.l., Lissone, Italy) equipped with a copper (Cu-K_α, λ = 1.5405 Å) rotating anode source, at an operating voltage of 40 kV and a filament current of 40 mA. The 2θ angles were recorded from 10° to 45°, with a step size of 0.02°, scanning rate 2s/step, divergence slit 0.25°, soller slit 0.04 rad and antiscatter slit 0.5°. The collected data were analyzed using Origin® 2019b data analysis software to provide peaks position (2θ), full width at half maximum (FWHM) and peaks deconvolution. Diffraction peaks were profile-fitted assuming Gaussian-Lorentzian functions as stated by the common experience (Duchemin, 2017; Hult et al., 2003; Ioelovich, 2016; S. Park et al., 2010). Baseline anchor points, based on raw data, were automatically located through a 2nd derivative baseline function, and subsequently connected by interpolation. The interplanar distances in crystallites (d_{hkl}-spacing) were calculated using the Bragg's Eq. (3.2):

$$d_{hkl} = \frac{\lambda}{2 \sin \theta} \tag{3.2}$$

where d_{hkl} (nm) is the spacing between the planes in the atomic lattice, λ is the wavelength of X-ray radiation (nm) and θ is the angle between the incident ray and the scattering planes *(Ioelovich, 2016; Ju et al., 2015)*.

In addition, the x-ray diffraction patterns were used to determine the size τ (nm) of cellulose crystallites, through the Scherrer Eq. (3.4):

$$\tau_{hkl} = \frac{K\lambda}{\beta \cos \theta} \tag{3.3}$$

Where τ_{hkl} (nm) is the crystallite size perpendicular to the lattice plane, *K* is the Scherrer constant (0.94), β is the FWHM of the diffraction peak in radians (Aguayo et al., 2018; Scherrer, 1918).

3.2.10 Thermogravimetric analysis (TGA)

The thermal behaviour of the two kind of CNCs (from conventional and the best microwave program) was studied by employing a thermogravimetric analyzer Perkin Elmer, TGA 4000, under an air and nitrogen flow, with a purge rate of 20 mL min^{-1}. Samples, weighing from ca. 7 to 10 mg, were heated from 30 °C to 600 °C, at a heating rate of 10°C min^{-1}. Two replications were done for each of the two CNCs type. The DTG curves were also obtained using differentials of TGA values by the following Eq. (3.4).

$$DTG = \frac{(w_{T+\Delta T} - w_{T-\Delta t})}{2\Delta T} \quad (3.4)$$

where $w_{T+\Delta T}$ and $w_{T-\Delta t}$ are the residual weights of the sample at temperature T+ΔT and T-ΔT, respectively, and ΔT is the interval of temperature for reading residual sample weight *(Oun & Rhim, 2017)*. The onset and endset degradation temperatures of the samples were obtained from TGA curves, as the intersection of the tangents to the point of deviation from the initial and final weight, respectively, and the inflection point of the curve.
To further define the degradation, the temperature of maximum degradation rate (Tv_{max}) was determined as the minimum point of the derivative curve, DTG, and therefore

corresponding to the inflection point of the TGA curve. The peak of the first derivative indicates the point of greatest rate of change on the weight loss curve.

3.3 Results

3.3.1 Evaluation of the Yield of Cellulose Nanocrystals

As shown in **Table 3.2**, the choice of heating program, with the other process conditions being equal, considerably affected the yield of CNCs, which is essential to decree the extraction success. It is worth to note that, the reported yields, are only indicative and related to a specific lab-scale production process, since they strongly depend on the preparation procedure and post-treatment filtration.
The hydrolysis by conventional heating gave 48.85 ± 11.99% of cellulose nanocrystals, while the yields recorded for microwave-assisted hydrolysis were at most 45.81±3.79 %, when ramp-hold combination was set according to M_3 program and tended to decrease when the ramp times progressively decreased, reaching just 22.09 ± 1.64 % and 23.37 ± 2.98 % for the shorter ones (i.e., 5 min, M_1 and M_5 respectively). On the other hand, no important differences between the two hold times were detected: the extraction efficiency of the process at 60 min hold time was, in fact, comparable to that obtained at 90 min, except for the yield of 30-minute ramp processes, for which the procedure with the shorter hold time (60') was significantly better.

Table 3.2 Mean values ±SD of experimental parameters for CNCs produced by conventional and different microwave heating programs. Analysis of variance (ANOVA) below.

	Heating Method	Y (%)	D_{Hy} (µm)	PDI (%)	ζ (mV)
Microwave	M_1	22.093 ± 1.634	0.212 ± 0.014	23.491 ± 0.926	-27.388 ± 3.280
	M_2	32.314 ± 1.474	0.174 ± 0.008[a]	23.550 ± 1.637	-30.520 ± 1.638
	M_3	45.814 ± 3.795[a]	0.153 ± 0.005	21.901 ± 1.172	-40.575 ± 2.534[a]
	M_4	36.894 ± 3.236	0.165 ± 0.006	22.996 ± 2.649	-35.735 ± 2.077
	M_5	23.370 ± 4.124	0.244 ± 0.026	22.760 ± 2.215	-26.559 ± 1.171
	M_6	32.422 ± 2.985	0.178 ± 0.005[a]	21.842 ± 2.475	-32.095 ±2.466
	M_7	34.411 ± 2.011	0.174 ± 0.009[a]	24.418 ± 2.999	-33.229 ± 2.844
	M_8	35.031 ± 1.935	0.159 ± 0.008	22.714 ± 1.783	-35.874 ± 2.127
Conv	C_1	48.850 ± 11.991[a]	0.176 ± 0.002[a]	25.067 ± 0.231	-39.52 ± 1.141[a]
	Model	***	***	NS	***
	Lack of Fit	NS	NS	NS	NS
	Main effect				
	Ramp time (X_1)	***	***	NS	***
	Hold time (X_2)	*	NS	NS	NS
	Ramp time^2 (X_1^2)	***	***	NS	**
	Interaction				
	Ramp x Hold (X_1X_2)	NS	NS	NS	NS
	Ramp^2 x Hold ($X_1^2X_2$)	NS	NS	NS	NS
	Performance index of fitted model				
	R^2_{Adj}	0.8	0.8	-	0.7

***, **, and * indicate significant at $p \leq 0.001$, $p \leq 0.01$, and $p \leq 0.05$. NS, not significant.
[a] Same letter indicates statistical differences smaller than least significant difference (LSD) (not significant for $p \leq 0.05$).

Comparatively, the yield of conventional heating (C_1) was very close to the highest for the microwave mode of heating (M_3). Note that, in other previous works, the APS treatment applied to the cotton raw material has led to CNCs with average yields that were comparable or even lower than that achieved by using M_3 method (Castro-Guerrero & Gray, 2014; Oun & Rhim, 2017; Ye et al., 2018). Additionally, the results were, in all MW heating programs, more repeatable, with standard deviations significantly lower than the conventional CNCs preparation procedure, thanks to the rigid control of the reaction conditions allowed by microwave reactor.

3.3.2 Morphology of Cellulose Nanocrystals

The morphology and geometric dimensions of the nanocrystals (length, width, aspect ratio) strictly depend on the exact conditions in which the hydrolysis occurred, beside on the cellulose source used (Habibi et al., 2010). Based on this consideration, a characterization of the actual shapes, particle dimensions and length distributions of CNCs, via Transmission Electron Microscopy (TEM) and by dynamic light scattering (DLS), was performed. The electronic micrographs (**Figure 3.2**) revealed rather similar aggregates of the two sets of nanocrystals produced, with typical rod-like crystal structure and quite high aspect ratio (greater than 20). The measured widths were approximately in the order of few nanometres (around 7 nm), for both kind of CNCs, while their length ranged over a larger window, from some tens (≈ 80 nm) to a few hundreds of nanometres (≈ 400 nm), with an average value of around 170 nm. However, it is known

from the literature that CNCs generally have a relatively wide length distribution, due to the controlled nature of the progress of the hydrolytic process (Dufresne, 2013). Moreover, the dimensions of the cellulose nanocrystals were comparable to previously reported works (Dufresne, 2017).

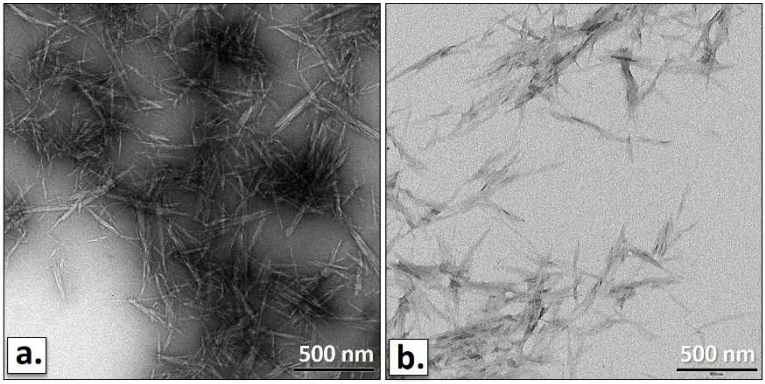

Figure 3.2 TEM micrographs of diluted suspensions of cellulose nanocrystals obtained by traditional (**a.**), and MW (**b.**) heating methods.

The average CNCs lengths achieved from TEM observations closely matched the DLS mean values of hydrodynamic diameter (**Table 3.2**). It is to highlight that the average D_{Hy} tended to be lower as the ramp time increased, varying from 212 ± 14 nm and 244 ± 26 nm of M_1 and M_5, to 165 ± 6 and 159 ± 8 nm of M_4 and M_8 respectively. However, by setting the heating program M_3, the smallest D_{Hy}, 153 ± 5 nm, was reached, which increased from M_3 to M_4 or by prolonging the hold time to 90'.

The CNCs dilute dispersions exhibited a bimodal frequency length distribution, that mainly ranged ($\alpha = 0.1$) from 91 nm to around 330 nm, except for M_1, from 116 to 498 nm, and for M_5, from 126 to 460 nm (data not shown): these were

comparable to the range of lengths obtained using the electronic microscope, still indicating the good overlap between size distribution in CNCs solution and electron micrographs of drop casted CNCs. Polydispersity index (PDI) is a measure of the width of particle size distribution. A value below or equal to 10% refers that the sample is monodisperse (Baalousha & Lead, 2012; Rampazzo et al., 2017). The higher polydispersity indexes of the CNCs obtained (**Table 3.2**), were therefore indicative of a more complex morphology and a bi- or multi-modal distributions.

3.3.3 Zeta Potential Analysis

For each heating methods, average zeta potential of diluted suspensions of cellulose nanocrystals are shown in **Table 3.2**. Except for M_1 and M_5, with zeta potential (ζ) of -27.39 ± 3.28 mV and -26.56 ± 1.17 mV, respectively, the conventional heating and the remaining microwave programs recorded voltage value lower than -30 mV, which reflect cellulose nanocrystals stably dispersed in the colloidal suspension (Zhong et al., 2012). In particular, the combination of process factors (ramp time, hold time) defined in the M_3 program produced crystals with the highest zeta potential (-40.57 ± 2.53 mV), comparable to those of the nanoparticles resulting from C_1. It should be noted the progressive increase (in absolute value) of the zeta potentials with the increase of the ramp time, while no important change was found with the changing of the hold time. The only exception, once again, is M_3 program, that emerged with higher potentials than M_7, having a longer hold time (90 min) but the same ramp time (30 min).

3.3.4 Statistical Evaluation of the Responses and Model Fitting

The statistical processing of collected data was carried out using a quadratic model, considering the superior abilities to predict and explain the variability of the data compared to the linear model (it ensured the highest R^2_{Adj}). As shown in the **Table 3.2**, for hydrodynamic diameter, zeta potential and yield responses, ANOVA confirmed the adequacy of the second-order model, falling the model probability value (p-value) below 0.001 and exhibiting a Lack of Fit not significant (p-value > 0.05). For these responses, the model showed a good fit with the experimental data, as the values of adjusted determination coefficient (R^2_{adj}) were quite high, of 0.8 for D_{Hy}, 0.7 for ζ, 0.8 for Y.

Both factors studied, X_1 (beside its quadratic term X_1^2) and X_2, showed significant main effects for the hydrodynamic diameter, while the interaction between the two (X_1X_2) showed a p-values greater than 5% ($p > 0.05$) that made it not significant for the same responses. However, the F-value for X_2 was very small compared to the F-value of X_1 (data not shown), and this implied that the latter factor had a much larger effect on the response variable. Instead, for the zeta potential and yield responses, only X_1 and X_1^2 were significant for ANOVA analysis. Moreover, it should be noted that, neither of the two factors examined (ramp and hold time), nor their interaction, were significant as far as the polydispersity index (PDI) is concerned.

In order to know the effect of non-experimental intermediate levels, the interpolation equations of the response variables were calculated, quantitatively describing the behaviour of

the system. The final equations of the regression predictive models are reported below, in terms of coded factors (Eq. (3.5-3.7)):

$$\left(D_{Hy}\right)^{-1,8} = +30.08 + 6.92\,X_1 - 1.40\,X_2 - 5.93\,{X_1}^2 \quad (3.5)$$

$$\zeta = -0.034 - 0.0047\,X_1 + 0.0034\,{X_1}^2 \quad (3.6)$$

$$\mathrm{Y} = 36.60 + 6.91\,X_1 - 8.18\,{X_1}^2 \quad (3.7)$$

By default, in the equation in terms of coded factors, the high levels of the factors are coded as +1 and the low levels as -1. The equations show the factor coefficients, calculated using the least square technique, each of which represents the expected change in the response per unit of variation of independent variable, when all the remaining factors are kept constant. The intercept is the overall average response of all executions. For the hydrodynamic diameter response, the power transformation was applied, using the Box Cox diagram of Design Expert, in order to improve the matching of the model to the data. Three-dimensional surfaces and contour plots were generated based on Eq. (3.5-3.7) and are shown in **Figure 3.3-3.6**. In the graphs, the model with quadratic terms highlighted the presence of curvature, but no marked torsions have been found, due to the not significant interaction of the two factors for the analysis of variance.
With the aim of optimizing the responses, criteria and target values maximizing the desirability function (d_j) were assigned. It has been assumed the need to minimize the hydrodynamic diameter, maximize (in absolute value) the zeta potential setting the lowest acceptable threshold to -30 mV, and maximize the extraction yield. Adopting the

constrained optimization algorithm (Myers et al., 2016), it has been constructed the contour plot of the desirability function, with all the equivalent solutions able to satisfy the restriction criteria set, finding a maximum d_j of 0.77 (d_j ranges from zero to one for any given response) by combine a ramp time of about 29 min and a hold time of 60 min.

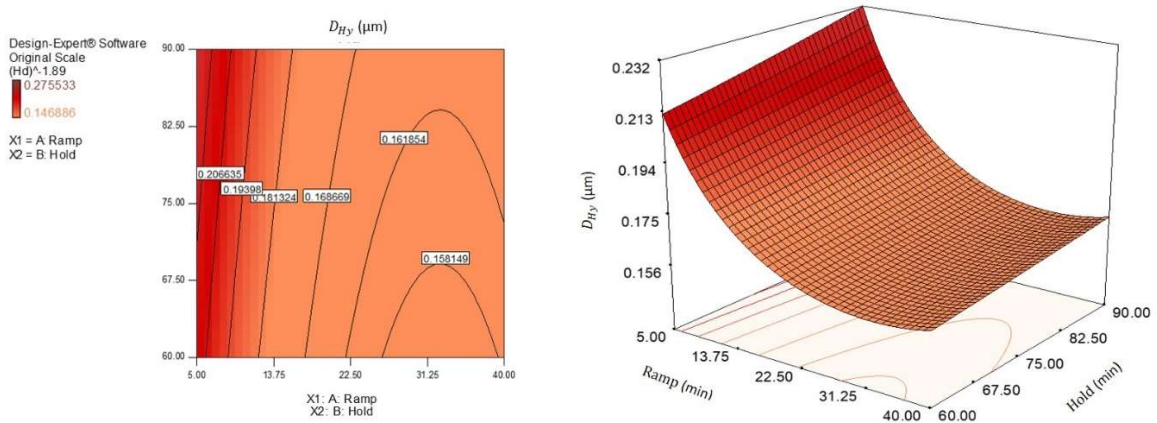

Figure 3.3 Response surface and contour plot showing the effect of ramp (X_1) and hold (X_2) on the response variable hydrodynamic diameter (D_{Hy}).

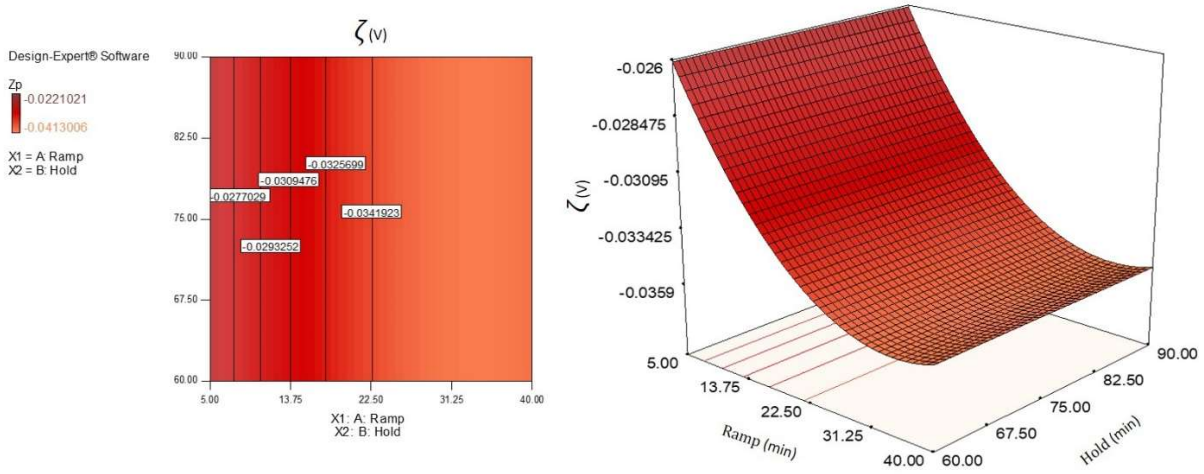

Figure 3.4 Response surface and contour plot showing the effect of ramp (X_1) and hold (X_2) on the response variable zeta potential (ζ).

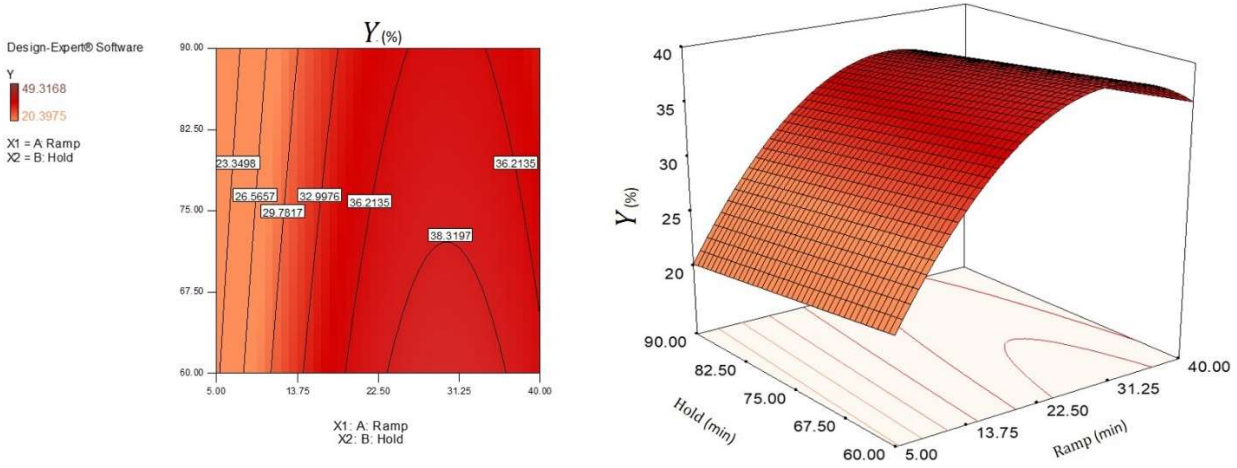

Figure 3.5 Response surface and contour plot showing the effect of ramp (X_1) and hold (X_2) on the response variable zeta potential (Y)

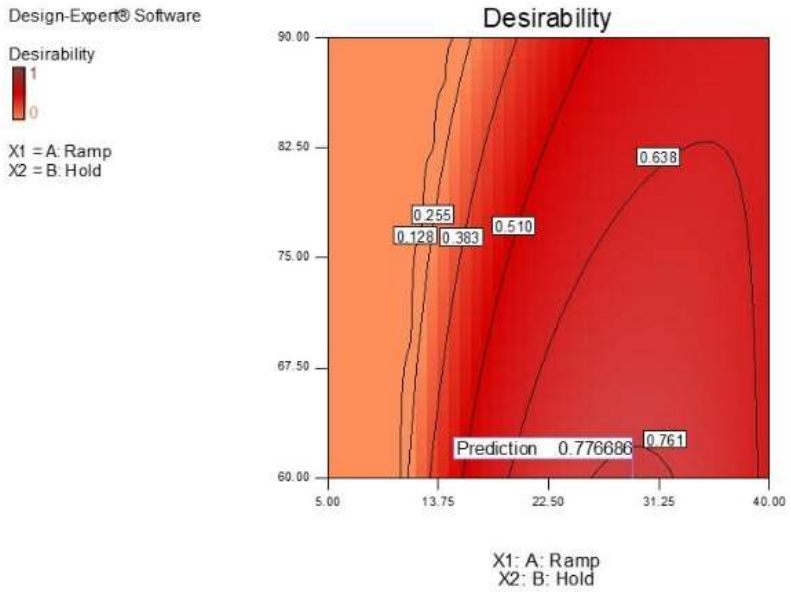

Figure 3.6 Contour plot of desirability function (desirability plot) showing the prediction values satisfying the restriction criteria in the desirability area.

Finally, aiming to explore further the differences of the two heating systems, all the possible pairwise comparisons between the mean of each one MW program with the mean of C_1 (conventional) were analysed, following one-way analysis of variance, and using Fisher's Least Significant Difference (LSD) test, given that the null hypothesis had already been rejected. The results of LSD test confirmed the significative differences existing among heating programs in terms of yield, particle size and zeta potential. However, as shown in **Table 3.2**, for yield and zeta potential responses, no significant differences between C_1 and M_3 emerged, and for M_2, M_6 and M_7 methods with regard to the hydrodynamic diameter.

3.3.5 FTIR-ATR Analysis of Cellulose Nanocrystals

By observing the changes occurred in the initial chemical structure due to APS treatment, the characterization of the crystals by infrared analysis has led to the double result of verifying the positive outcome of cellulose nanocrystals extraction process, as well as comparing the nanocrystals obtained with the two heating methods. FTIR-ATR spectra, of both type of CNCs produced, showed absorption bands surely typical of cellulosic materials and consistent with others' reports. They revealed similarities, in transmittance, in the main regions highlighted in **Figure 3.7**. The broad band centred at around 3340 cm^{-1}, in all spectra, is attributed to the intramolecular hydrogen bonded O–H stretching vibration (ν_{OH}) (Rahbar Shamskar et al., 2016), in particular, that formed between O(3)H–O(5) positions, adjacent to the β-glycosidic bond of cellulose I (Leung et al., 2014).

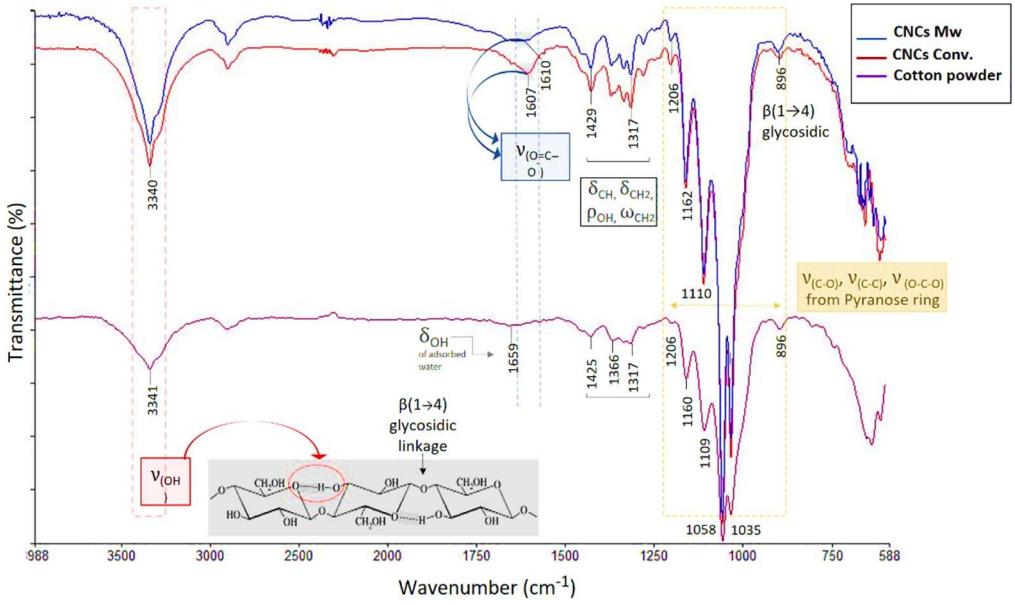

Figure 3.7 FTIR-ATR spectra (4000-600 cm^{-1}) of CNCs from microwave (— blue line) and conventional (— red line) methods in comparison with the raw cotton powder (— purple line).

It is known that the hydroxyls, linked to C(2), C(3) and C(6) carbons of cellulose, contribute to the formation of various types of inter- and intra-molecular hydrogen bonds, whose presence not only has a strong influence on the physical properties of cellulose, as solubility, hydroxyl reactivity and crystallinity, but plays an important role in the mechanical properties of the polymer too (Fan et al., 2012). It is possible to observe that the amplitude relative to this absorption peak could be affected in the chain cleavage process, due to the weakening of the hydrogen bonds throughout the hydrolysis (Xiong et al., 2012). In the spectra of CNCs, unlike raw materials, this band becomes, in fact, narrower and longer. Next to this region, FTIR peaks at 2900 cm^{-1}, weak and diffused, are the result of $–CH_2$ and C–H stretching vibrations in cellulose structure (Orasugh et al., 2018). The lower range of cellulose IR spectra, from 1800-600 cm^{-1}, had relatively well-defined peaks. It is certainly worth to highlight the presence of absorption peaks at around 1600-1610 cm^{-1}, probably attributable to carboxylate asymmetric stretching (ν_{COO-}), which is formed because of primary hydroxyl groups oxidation, induced by APS treatment. In the conventional treatment this band is emerged slightly stronger than microwave one. However, it should be noted that, the identification of carbonate ion band around 1700–1600 cm^{-1} by FT-IR ATR, is quite difficult because the O–H bending (δ_{OH}) of absorbed water (1633-1659 cm^{-1}) was also observed in this region (Pirani & Hashaikeh, 2013; Zianor Azrina et al., 2017). FTIR data also suggested that oxidation occurred preferentially at the C6 primary alcohol of crystalline cellulose. The oxidation of C2 and C3 secondary alcohols is known to induce the cleavage of the glucopyranose ring, resulting in harmful lowering of crystallinity (Potthast et al.,

2007). The absence of an IR signal relating to hemiacetal formation (880 cm^{-1}) confirmed the intact crystalline structure of CNCs prepared by APS (Leung et al., 2011) with two adopted heating methods.

Cellulose molecules also contain several C-C and C-H bonds, which require numerous absorptions throughout the spectral range, but especially in the fingerprint region. The presence of signals at 1420-1430 cm^{-1} is assigned to the $–CH_2$ scissoring in cellulose (Kumar et al., 2014), as well as the 1317 cm^{-1} relative to the $–CH_2$ wagging deformation mode (ω_{CH2}) at C6, and 1281 cm^{-1} to the C–H bending. The medium weak peaks, around 1370 cm^{-1} and 1334 cm^{-1}, are attributed, instead, to OH out-of-plane bending vibrations (Ibrahim et al., 2010; Oun & Rhim, 2015) and to the rocking of –OH (ρ_{OH}), respectively. The peak at 1110 cm^{-1}, present in all the spectra, is attributed to the asymmetric stretching of the C-O-C group of cellulose. Other characteristic absorption peaks, related to the chemical structure of cellulose, were 896 cm^{-1}, resulting from the β-glycosidic linkage (Zianor Azrina et al., 2017), 1058 (the strongest band across the cellulose spectra) and 1035 cm^{-1}, referable to the –C–O and C–O–C bonds of the pyranose ring. It can also be observed that, the presence of these very strong absorption bands, referable to the glucopyranose unit vibrations, demonstrate that the degradation of cellulose could hardly have taken place at glucose rings. The main degradation point should be, in fact, the glycosidic bonds (Xiong et al., 2012). Absorption patterns of cellulose remained unchanged after persulfate treatment; this confirms that there are no significant changes related to the conformation of the cellulosic structure. With regard to the glycosidic bond, it is to be noted that, although the C1-O-C4 bond is highlighted in the FTIR analysis, the structure of

cellulose molecules does not easily allow those vibrational movements that the infrared ray is able to trigger and the FTIR to detect. For this reason and due to the relatively small number of broken glycosidic bonds (compared to the thousands present), the FTIR technique is not suitable to signal a decrease in the degree of polymerization following hydrolytic cleavage. Therefore, in the spectra of both CNCs, the peak at around 896 cm^{-1} remained substantially identical with respect to the cotton powder raw material.
In general, the comparison of these spectral data revealed that, all CNCs are composed of crystalline cellulose I (Kumar et al., 2014; Leung et al., 2014), with minimal differences in some peaks, while the absorption peaks around 1338, 1507, 1734 cm^{-1}, typically referable to the aliphatic carboxylic groups, aryl ester, and acetyl groups in the xylan, due to the presence of characteristic groups of hemicellulose and lignin, were totally missing. The reduction in the intensity of some peaks, in the infrared spectrum of the raw material (cotton powder), may be due to the presence of a network of bonds (hydrogen, glycosidic) that prevented or reduced some flexing and out of plane movements, which instead appeared in the crystalline structure of the CNCs.

3.3.6 X-ray Powder Diffraction Analysis (XRD)

From the XRD characterization of CNCs a few considerations have been made on the type of crystalline allomorph and sizes of crystallites, as well as the integrity of the crystalline structure of both CNCs type was confirmed. Four characteristic peaks, at around 15°, 16.5°, 22.8° and 34.5° 2θ, were deconvoluted from the background scattering

by the curve-fitting process (deconvoluted peaks are plotted in **Figure 3.8** insets), corresponding to the (1 $\bar{1}$ 0), (1 1 0), (2 0 0) and (0 0 4) crystallographic planes, respectively (Lin & Dufresne, 2014; Nam et al., 2016; Zhang et al., 2016). **Table 3.3** provides a comparison of the crystallite sizes and *d*-spacing values of the two CNCs type, evaluated along the three main planes (1 $\bar{1}$ 0), (1 1 0) and (2 0 0), that were consistent with the most references (Ioelovich et al., 2010; Ju et al., 2015; Nishiyama et al., 2002; Sunkyu Park et al., 2010). Such features, including the *d*-spacing and average crystallite size, as determined by the Bragg's and Scherrer's equations, resembled the diffraction pattern of Cellulose I_β, according to crystallographic data reported in our previous work (Mascheroni et al., 2016). The peaks discussed in the following crystalline analysis also indicated that crystal structures of CNCs were unchanged during APS oxidative hydrolysis both with conventional and microwave heating. Diffractograms also exhibited a shoulder on the (2 0 0) peak, at around 20.5 2θ angles, which was ascribed to (1 0 2) crystallographic plane of cellulose I_β phase (Nam et al., 2016). Comparing the diffraction patterns of the two samples, this peak was more discernible and intense for MW CNCs than the conventional one. This is a characteristic for crystals with Miller index (1 0 2) in cellulose type I polymorph, that does not always appear in all type I cellulose samples (Aguayo et al., 2018; S. Park et al., 2010). Five crystalline peaks (1 $\bar{1}$ 0, 1 1 0, 1 0 2, 2 0 0, and 0 0 4) have been separated in many cases (Mariano et al., 2018), but four crystalline peaks (1 $\bar{1}$ 0, 1 1 0, 2 0 0, and 0 0 4) have been assumed in other studies (He et al., 2008; Oun & Rhim, 2017).

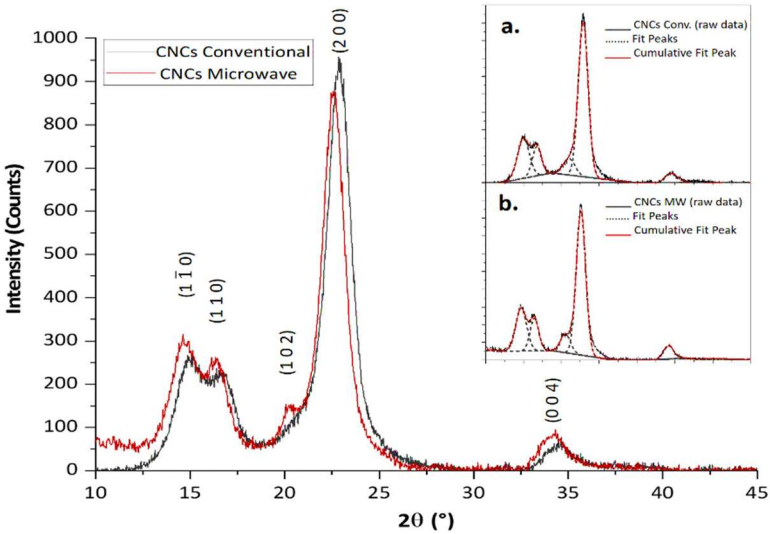

Figure 3.8 Experimental X-ray diffractograms for cellulose nanocrystals from conventional (tick black line) and microwave (tick red line) heating methods. In the insets, the fitted crystalline peaks (dashed grey line) and total fitted patterns (thin red line) for conventional (**a.**) and microwave (**b.**) CNCs are shown.

Table 3.3 Crystallographic parameters for conventional and microwave CNCs samples.

	Crystalline Plane (Miller Index of I_β)	FWHM (°)	Peak position 2θ (°)	*d*-spacing (nm)	Crystallite size τ (nm)
CNCs Conventional	1 $\bar{1}$ 0	1.7	15.0	0.59	4.8
	1 1 0	1.4	16.7	0.52	6.0
	1 0 2		21.0		
	2 0 0	1.5	22.9	0.39	5.6
	0 0 4		34.5		
CNCs Microwave	1 $\bar{1}$ 0	1,7	14.7	0.60	5.0
	1 1 0	1,4	16.4	0.53	6.1
	1 0 2		20.6		
	2 0 0	1,5	22.6	0.39	5.7
	0 0 4		34.2		

3.3.7 Thermal Properties of Cellulose Nanocrystals

Thermal stability was also tested given its importance in highlighting the potential differences between the two nanocrystals. Furthermore, it plays a critical role in the preparation of melt processed CNCs-composites for thermoplastic applications (Mokhena et al., 2018). The thermogravimetric (TGA) and differential thermogravimetric (DTG) profiles of the conventional CNCs and those of the MW treated CNCs are shown in **Figure 3.9**.

Interestingly, in comparison with conventional nanocrystal samples, microwave CNCs exhibited higher thermal stability for all the phases of thermal decomposition. The onset degradation temperature (Td_{onset}), obtained from TGA curves, was a few tens of degrees lower for conventional nanocrystals (event shown in **Figure 3.9**).

It could be appreciably observed, from the thermograms, that increments of 47.82 (ΔTd_{15}) and 29.78 °C (ΔTd_{30}) occur in the MW-CNCs at the temperature corresponding to the 15% and 30% of weight loss, respectively. Likewise, the value of Td_{60} for conventional nanocrystals weakly decreased to about 347.62 °C compared with 367.19°C of MW crystals (ΔTd_{60} = 19.57 °C). The endset (Td_{endset}) and the temperature of maximum degradation rate ($T\nu_{max}$) (deduced by peak calculation of the 1st derivative of the weight loss curve), in N_2 atmosphere, were also shifted to a higher temperature, from 360 °C to 375 °C and from 327.58°C to 343.16 °C, respectively, in the case of MW CNCs.

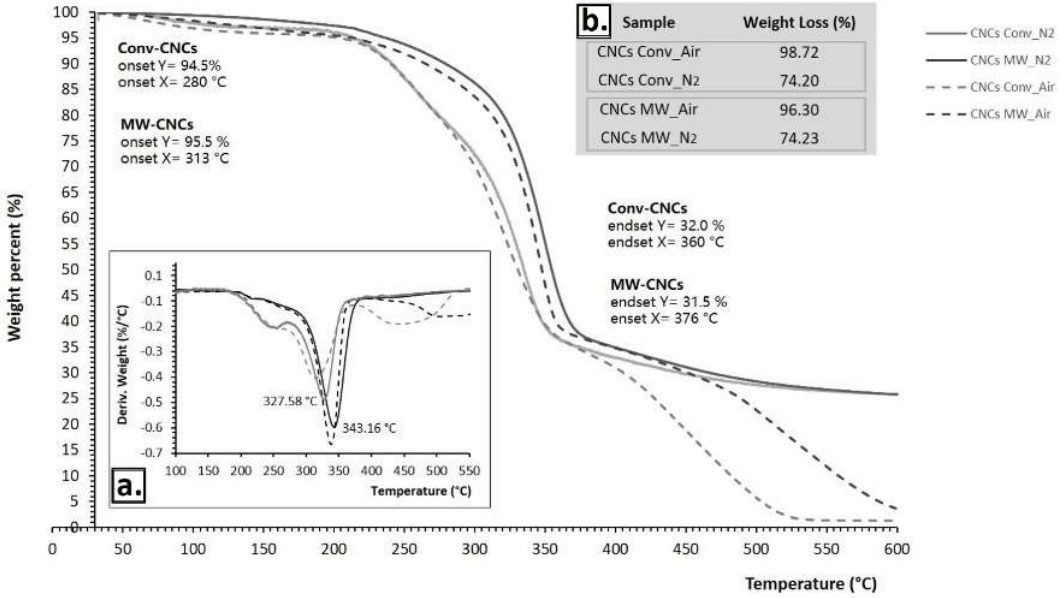

Figure 3.9 Thermogravimetric analysis (TGA) and differential thermogravimetric (DTG) curves (inset **a.**) of CNCs samples in air and nitrogen atmosphere. Final weight losses (%) of CNCs in both atmospheres (inset **b.**).

The difference in thermal degradation behaviour could be justified by the presence of a higher carboxyl content on the conventional CNCs surface, being supported by the FT-IR spectra. Finally, heating in air induced a significant decline in the decomposition profile, leaving significantly lower final residues, nearly 4 and 1.3% (**Figure 3.9** inset), than those of nitrogen atmosphere, around 26%.

3.4 Discussion

The APS oxidative-hydrolysis, performed with both heating modes, was effective in reducing the particle dimensions of native cellulose allowing satisfactory yields, although rather variable according to the different heating programs. In particular, too rapid achievement of high temperatures (i.e., the use of shorter ramp) has probably depleted part of the reagent used to extract and oxidize the CNCs, before free radical ions, generated by persulfate, could actually penetrate through the lumen of the fibers and perform the shortening of cellulose into crystallites. This left an important fraction of the polymer undissolved and led to lower yields. Furthermore, during the heating run the generation of a lot of energy and heat (self-heating) was observed, attributable to the triggering of spontaneous and exothermic reactions. The exothermic reactions can be recognized in **Figure 3.1** by an increase of temperature while the microwave power is reduced or even shut off. At that point, significant amounts of reaction gases and heat are generated by the decomposition of the sample. As result, the microwave power input is reduced to keep the temperature value at or below the set limit. However, using the short ramp methods, the offsetting of this phenomenon with the drastic power drop was not

enough and, therefore, temperature spikes were generated (overshoot), failing the set temperature (**Figure 3.1a.** and **b.**). Moreover, the high-temperature hydrolysis was accompanied by darkening of nanoparticles due to the intensification of oxidation, dehydration, and carbonization, which was also accompanied by caramelization of dissolved by-products of cellulose hydrolysis such as oligosaccharides (Ioelovich, 2018). Conversely, a slow ramp (≈ 30 min) enabled an appropriate heating rate for the type of sample that had to be digested. This made sure that no overloading and/or overheating of the vessels occurred, keeping a reliable control of the process: using a slow ramp, all sample temperatures was equal to the target temperature and the exothermic reactions had enough time to happen at low reaction temperatures.

Another consideration is that, for the 30 min ramp processes, the yield achieved with the shorter hold time (60') was significantly better than that obtained prolonging the hold time up to 90'. This was ascribed to the creation of irreversible tight connections between the individual crystals released, due to the extension of the heating time, and to the subsequent loss of these larger particles, during the purification steps (filtration above all). About that, it has been reported that the crystallites can grow in size, because of the large freedom of motion, after hydrolytic cleavage (Dufresne, 2017). Taking this result into account, it could be considered more advantageous, in terms of energy and time saving, the adoption of thermal programs with shorter hold time. It should also be noted that M_3 heating program allowed extraction yield comparable to that obtained from conventional heating in a much longer reaction time. This may reflect the relative efficiency and specificity of

microwaves in heating raw material since it needs a very short time, of only 90 min instead of 16 h required by conventional one, leading to energy saving and high convenience in CNCs production. The treatment of raw material has in fact generated ionic species, derived from the thermal decomposition of persulfate in water solution (Mascheroni et al., 2016), creating an in situ catalytic environment which proved to be advantageous under microwave irradiation (Zhu & Chen, 2014), in hydrolysing hemicellulose, amorphous cellulose and other components.

The results obtained through digital micrographs (TEM) was in a good agreement with those of dynamic light scattering (DLS), thus the latter appeared to be a rapid method sufficiently accurate to estimate the sizes of CNCs. On this regard, it should be noted that the DLS technique analyses the data in spherical approximation, mathematically processing the CNCs as spheres that move with Brownian motion, regardless of their real physical morphology. The hydrodynamic diameter (D_{Hy}) of a non-spherical particle thus corresponds to the diameter of a sphere that has the same translational diffusion speed as the particle. If the shape of a particle changes in a way that affects the diffusion speed, then the hydrodynamic size will change. For example, small variations in the length of a rod-shaped particle will directly affect the size, while changes in the rod's diameter (cross-section of the particle), which will hardly affect the diffusion speed, will be difficult to detect. In the case of CNCs, the average lengths achieved from TEM observations closely matched the DLS mean values of hydrodynamic diameter. These values tended to be lower as the ramp time increased but reached the smallest value by using M_3 heating program. Moreover, D_{Hy} increased from M_3 to M_4 or by prolonging the

hold time to 90'. This confirmed the hypothesis of an irreversible rearrangement of the crystals that could also explain the reduction in yield.
Further chemical feature was evaluated to compare the CNCs obtained from the two different heating methods. By means of light scattering, besides the hydrodynamic diameter, the zeta potential (ζ) of CNCs were assessed using the electrophoretic light scattering (ELS) technique. Zeta potential value is an assessment of the electro-kinetic potential in colloid dispersions, being related to the degree of repulsion between ions of same charges and to the particle–particle interaction. It provides information about the particles' surface–solvent interface, and its absolute magnitude is critical to understand the suspension stability and aggregation phenomena, therefore is fundamental to know it for the potential use of CNCs as coatings for flexible packaging materials. Not all kind of CNCs produced exceed -30 mV, assumed as essential to guarantee favourable stability of colloid dispersions for an extended time ($\zeta < -30$ mV or $\zeta > +30$ mV) (Zhong et al., 2012). In particular, the average zeta potential of nanocrystals was determined to be below this threshold (in absolute value) only for the two microwave programs that involved the shortest ramp times, M_1 and M_5 respectively.
Interpreting the response surfaces generated by the final equations of regression predictive models, it could be concluded that, within the experimental domain, smaller nanocrystals with a higher zeta potential and greater yield, would be obtained by adjusting the process conditions to a high ramp level (i.e., by choosing longer ramp time) and at a low hold level (i.e. by choosing shorter hold time). However, the ramp factor (and its quadratic term producing the

curvature) contributed greatly to influence the answers, while only the hydrodynamic diameter was little affected by the hold time (X_2), much less significant than the first factor (highly significant).
Through the contour plot of the desirability function, prediction values really close to the M_3 method were found to be the optimal reaction conditions able to achieve peak performances. Under these conditions, the best reaction environment for the isolation of CNCs could occur, i.e., greater availability of the acid molecules at higher concentrations, enough time available for simultaneous hydrolysis and oxidation process of cellulose fibers. Otherwise, the optimal potential of the reaction would decrease, due to the premature degradation of the reagent and the triggering of carbonization reactions.
The cellulose I_β crystalline structure remained unchanged during APS oxidative hydrolysis both with conventional and microwave heating, as shown in the XRD measurements. The CNCs crystalline planes can be ordered in a different way depending on the synthesis conditions: a potential variation between the distances of the crystalline planes could be related to the stress and deformation present within the CNCs crystallites, and finally influencing physical properties at macroscopic level. It has been previously reported that this affects the barrier behaviour of CNCs in permeability and migration phenomena as well as their mechanical properties, that are very important for the future packaging materials that can be developed using these CNCs (Aguayo et al., 2018; Li et al., 2015). Therefore, the similar patterns and intensity preservation of diffraction peaks, after replacement of conventional heating with microwave one, implied that the latter has not destroyed or converted the inherent crystalline

structure of nanocrystals and this contribute to validate the designed MW method (M_3) for CNCs production from cotton powder.

The thermogravimetric patterns confirmed the higher thermal stability of microwave CNCs for all phases of the thermal decomposition. Indeed, the higher carboxyl content on the conventional CNCs surface, in comparison with MW CNCs, as it appeared in the FTIR spectra, might result in worse thermal stability. This would be in good accordance with the results reported by others (Mascheroni et al., 2016; Sharma & Varma, 2014; Zhang et al., 2016). In addition, by determining the TG patterns in air, it seemed that more carboxylate groups on the latter nanocrystals could be introduced, in such oxidizing atmosphere, inducing a significant decline in the decomposition profile and leaving significantly lower final residues than those of nitrogen atmosphere. Heating in air causes in fact oxidation of the hydroxyl groups, resulting, as the temperature increases, in increases of carbonyl, carboxyl and hydroperoxide groups, with free radicals also appearing. The thermal degradation in this case is accelerated (Dufresne, 2017).

3.5 Conclusions

Compared with conventional heating, MW-assisted APS method has been proven to be an advanced technology in reducing the hydrolysis time of cellulosic amorphous regions, since it need shorter time, of only 90 min instead of 16 h required by conventional heating, leading to energy saving and high efficiency in CNCs production. Fine tuning the treatment variables (ramp and hold heating time), we

developed a simple, cost-effective way for a rapid and reproducible preparation of the nanocrystals, using cotton powder as raw material.

At optimal reaction conditions (M_3 method), CNCs with a narrow size distribution, average particle length of 153 nm (hydrodynamic diameter) and average particle width of 7 nm were prepared in 45% of yield, comparable to those obtained by conventional method in a much longer reaction time. The nanoparticles formed stable suspensions in water with an average zeta potential of -0,040 V, as measured by ELS. The resulting products retained the cellulose I_β crystalline structure as shown in the XRD measurements, and the FT-IR spectral data were in perfect agreement with the data of conventional method. Of further importance to compare the two types of nanoparticles, were the thermogravimetric patterns, confirming the higher thermal stability of microwave CNCs for all phases of the thermal decomposition.

Considering the environmental, chemical, and economic advantages introduced by this novel approach, microwave-assisted technology combined with other green chemistry strategies such us the use of APS, could make the CNCs production more interesting from an economical and industrial point of view, as well as more appealing to green economy, which should be greatly advocated and encouraged as a promising research trend.

The uniformity, small diameter and the high values of aspect ratio, zeta potential, crystallinity, and thermal stability of such nanocrystals, which are assured by the good process control of the microwave reactor, allow to hypothesize their real applications as nanofillers or nanocoating in the food packaging field. However, in order to better characterize the

properties of CNCs and their performances once they have been coated or introduced into food packaging materials, further investigations will be necessary in order to verify the analogy of CNCs resulted from the two heating methods. Moreover, the microwave assisted technology could pave the way for observation of an increase in the carboxylation degree of CNCs by combining the oxidizing action of APS with the addition of an auxiliary oxidizing gaseous agent.

References

MarketsandMarkets. Nanocellulose Market by Type (Microfibrillated Cellulose, Cellulose Nanocrystals), Application (Pulp& Paper, Composites & Packaging, Biomedical & Pharmaceuticals, Electronics & Sensors), and Region (Europe, North America, APAC)-Global Forecast to 2023. Availabe online: https://www.marketsandmarkets.com/MarketReports/nano-cellulose-market-56392090.html (accessed on 22 October 2019).

Aguayo, M. G., Pérez, A., Reyes, G., Oviedo, C., Gacitua, W., Gonzalez, R., & Uyarte, O. (2018). Isolation and Characterization of Cellulose Nanocrystals from Rejected Fibers Originated in the Kraft Pulping Process. *Polymers*, *10*, 1145.

Baalousha, M., & Lead, J. (2012). Rationalizing nanomaterial sizes measured by atomic force microscopy, flow field-flow fractionation, and dynamic light scattering: sample preparation, polydispersity, and particle structure. *Environmental Science & Technology*, *46*(11), 6134-6142.

Baghbanzadeh, M., Carbone, L., Cozzoli, P. D., & Kappe, C. O. (2011). Microwave-Assisted Synthesis of Colloidal Inorganic Nanocrystals. *Angewandte Chemie International Edition*, *50*(48), 11312-11359.

Bilecka, I., & Niederberger, M. (2010). Microwave chemistry for inorganic nanomaterials synthesis. *Nanoscale*, *2*(8), 1358-1374.

Biswas, A., Kim, S., Selling, G. W., & Cheng, H. N. (2014). Conversion of agricultural residues to carboxymethylcellulose and carboxymethylcellulose acetate. *Industrial Crops and Products*, *60*, 259-265.

Bondeson, D., Mathew, A., & Oksman, K. (2006). Optimization of the isolation of nanocrystals from microcrystalline cellulose by acid hydrolysis. *Cellulose*, *13*(2), 171-180.

Caddick, S., & Fitzmaurice, R. (2009). Microwave enhanced synthesis. *Tetrahedron*, *65*(17), 3325-3355.

Castro-Guerrero, C. F., & Gray, D. G. (2014). Chiral nematic phase formation by aqueous suspensions of cellulose nanocrystals prepared by oxidation with ammonium persulfate [journal article]. *Cellulose*, *21*(4), 2567-2577.

Dariusz, B., Aleksander, P., & Slawomir, M. (2011). Synthesis of Polymer Nanocomposites Under Microwave Irradiation. *Current Organic Chemistry*, *15*(2), 178-188.

de la Hoz, A. (2011). *Microwave heating as a tool for sustainable chemistry* (N. E. Leadbeater, Ed. 1 ed.). CRC Press.

de Melo, E. M., Clark, J. H., & Matharu, A. S. (2017). The Hy-MASS concept: hydrothermal microwave assisted selective scissoring of cellulose for in situ production of (meso)porous nanocellulose fibrils and crystals [paper]. *Green Chemistry*, *19*(14), 3408-3417.

Duchemin, B. (2017). Size, shape, orientation and crystallinity of cellulose Iβ by X-ray powder diffraction using a free spreadsheet program. *Cellulose*, *24*.

Dufresne, A. (2013). Nanocellulose: a new ageless bionanomaterial. *Materials Today*, *16*(6), 220-227.

Dufresne, A. (2017). *Nanocellulose: From Nature to High Performance Tailored Materials* (2 ed.). Walter de Gruyter GmbH.

Fan, M., Dai, D., & Huang, B. (2012). Fourier transform infrared spectroscopy for natural fibres. In S. M. Salih (Ed.), *Fourier transform-materials analysis*. IntechOpen.

Favier, V., Chanzy, H., & Cavaille, J. Y. (1995). Polymer Nanocomposites Reinforced by Cellulose Whiskers. *Macromolecules*, *28*(18), 6365-6367.

Filson, P. B., Dawson-Andoh, B. E., & Schwegler-Berry, D. (2009). Enzymatic-mediated production of cellulose nanocrystals from recycled pulp. *Green Chemistry*, *11*(11), 1808-1814.

Fotie, G., Rampazzo, R., Ortenzi, M. A., Checchia, S., Fessas, D., & Piergiovanni, L. (2017). The Effect of Moisture on Cellulose Nanocrystals Intended as a High Gas Barrier Coating on Flexible Packaging Materials. *Polymers (Basel)*, *9*(9), 415.

Gawande, M. B., Shelke, S. N., Zboril, R., & Varma, R. S. (2014). Microwave-Assisted Chemistry: Synthetic Applications for Rapid Assembly of Nanomaterials and Organics. *Accounts of Chemical Research*, *47*(4), 1338-1348.

Gómez H, C., Serpa, A., Velásquez-Cock, J., Gañán, P., Castro, C., Vélez, L., & Zuluaga, R. (2016). Vegetable nanocellulose in food science: A review. *Food Hydrocolloids*, *57*, 178-186.

Habibi, Y., Lucia, L. A., & Rojas, O. J. (2010). Cellulose Nanocrystals: Chemistry, Self-Assembly, and Applications. *Chemical Reviews*, *110*(6), 3479-3500.

He, J., Cui, S., & Wang, S.-y. (2008). Preparation and crystalline analysis of high-grade bamboo dissolving pulp for cellulose acetate. *Journal of Applied Polymer Science*, *107*(2), 1029-1038.

Hult, E.-L., Iversen, T., & Sugiyama, J. (2003). Characterization of the supermolecular structure of cellulose in wood pulp fibres. *Cellulose*, *10*(2), 103-110.

Ibrahim, M. M., El-Zawawy, W. K., & Nassar, M. A. (2010). Synthesis and characterization of polyvinyl alcohol/nanospherical cellulose particle films. *Carbohydrate Polymers*, *79*(3), 694-699.

Ioelovich, M. (2018). Influence of hydrolysis conditions on production of cellulose nanocrystalline particles. SITA, Mohammedia, Morocco.

Ioelovich, M., Leykin, A., & Figovsky, O. (2010). Study of cellulose paracrystallinity. *Bioresources*, *5*, 1393-1407.

Ioelovich, M. Y. (2016). Models of supramolecular structure and properties of cellulose [journal article]. *Polymer Science Series A*, *58*(6), 925-943.

Jongaroontaprangsee, S., Chiewchan, N., & Devahastin, S. (2018). Production of nanocellulose from lime residues using chemical-free technology. *Materials Today: Proceedings*, *5*(5, Part 1), 11095-11100.

Ju, X., Bowden, M., Brown, E. E., & Zhang, X. (2015). An improved X-ray diffraction method for cellulose crystallinity measurement. *Carbohydrate Polymers*, *123*, 476-481.

Kos, T., Anžlovar, A., Kunaver, M., Huskić, M., & Žagar, E. (2014). Fast preparation of nanocrystalline cellulose by microwave-assisted hydrolysis [journal article]. *Cellulose*, *21*(4), 2579-2585.

Kumar, A., Negi, Y. S., Choudhary, V., & Bhardwaj, N. K. (2014). Characterization of Cellulose Nanocrystals Produced by Acid-Hydrolysis from Sugarcane Bagasse as Agro-Waste. *Journal of Materials Physics and Chemistry*, *2*(1), 1-8.

Leung, A. C. W., Hrapovic, S., Lam, E., Liu, Y. L., Male, K. B., Mahmoud, K. A., & Luong, J. H. T. (2011). Characteristics and Properties of Carboxylated Cellulose Nanocrystals Prepared from a Novel One-Step Procedure. *Small*, *7*(3), 302-305.

Leung, A. C. W., Luong, J. H. T., Hrapovic, S., Lam, E., Liu, Y., Male, K. B., Mahmoud, K., & Rho, D. (2014). *Cellulose Nanocrystals From Renewable Biomass* (US Patent No. US 8900706 B2). https://lens.org/173-345-283-827-03X

Li, F., Biagioni, P., Bollani, M., Maccagnan, A., & Piergiovanni, L. (2013). Multi-functional coating of cellulose nanocrystals for flexible packaging applications. *Cellulose*, *20* (5), 2491-2504.

Li, F., Mascheroni, E., & Piergiovanni, L. (2015). The Potential of NanoCellulose in the Packaging Field: A Review. *Packaging Technology and Science*, *28*(6), 475-508.

Li, J., Zhang, L.-P., Peng, F., Bian, J., Yuan, T.-Q., Xu, F., & Sun, R.-C. (2009). Microwave-assisted solvent-free acetylation of cellulose with acetic anhydride in the presence of iodine as a catalyst. *Molecules (Basel, Switzerland)*, *14*(9), 3551-3566.

Lin, N., & Dufresne, A. (2014). Surface chemistry, morphological analysis and properties of cellulose nanocrystals with gradiented sulfation degrees. *Nanoscale*, *6*(10), 5384-5393.

Lu, P., & Hsieh, Y. L. (2010). Preparation and properties of cellulose nanocrystals: Rods, spheres, and network. *Carbohydrate Polymers*, *82*(2), 329-336.

Mariano, M., El Kissi, N., & Dufresne, A. (2018). Cellulose nanomaterials: size and surface influence on the thermal and rheological behavior. *Polímeros*, *28*(2), 93-102.

Mascheroni, E., Rampazzo, R., Ortenzi, M. A., Piva, G., Bonetti, S., & Piergiovanni, L. (2016). Comparison of cellulose nanocrystals obtained by sulfuric acid hydrolysis and ammonium persulfate, to be used as coating on flexible food-packaging materials [journal article]. *Cellulose*, *23*(1), 779-793.

Mokhena, T., Sefadi, J., Sadiku, E., John, M., Mochane, M., & Mtibe, A. (2018). Thermoplastic processing of PLA/cellulose nanomaterials composites. *Polymers*, *10*(12), 1363.

Morán, J., Alvarez, V., Cyras, V., & Vázquez, A. (2008). Extraction of cellulose and preparation of nanocellulose from sisal fibers. *Cellulose*, *15*(1), 149-159.

Motshekga, S. C., Pillai, S. K., Ray, S. S., Jalama, K., & Krause, R. W. M. (2012). Recent trends in the microwave-assisted synthesis of metal oxide nanoparticles supported on carbon

nanotubes and their applications. *J. Nanomaterials*, *2012*, 51-51.

Myers, R. H., Montgomery, D. C., & Anderson-Cook, C. M. (2016). *Response surface methodology: process and product optimization using designed experiments*. John Wiley & Sons.

Nadagouda, M. N., Speth, T. F., & Varma, R. S. (2011). Microwave-Assisted Green Synthesis of Silver Nanostructures. *Accounts of Chemical Research*, *44*(7), 469-478.

Nam, S., French, A. D., Condon, B. D., & Concha, M. (2016). Segal crystallinity index revisited by the simulation of X-ray diffraction patterns of cotton cellulose Iβ and cellulose II. *Carbohydrate Polymers*, *135*, 1-9.

Nishiyama, Y., Langan, P., & Chanzy, H. (2002). Crystal Structure and Hydrogen-Bonding System in Cellulose Iβ from Synchrotron X-ray and Neutron Fiber Diffraction. *Journal of the American Chemical Society*, *124*(31), 9074-9082.

Nüchter, M., Ondruschka, B., Bonrath, W., & Gum, A. (2004). Microwave assisted synthesis – a critical technology overview. *Green Chemistry*, *6*(3), 128-141.

Orasugh, J. T., Saha, N. R., Sarkar, G., Rana, D., Mondal, D., Ghosh, S. K., & Chattopadhyay, D. (2018). A facile comparative approach towards utilization of waste cotton lint for the synthesis of nano-crystalline cellulose crystals along with acid recovery. *International Journal of Biological Macromolecules*, *109*, 1246-1252.

Oun, A. A., & Rhim, J.-W. (2015). Preparation and characterization of sodium carboxymethyl cellulose/cotton linter cellulose nanofibril composite films. *Carbohydrate Polymers*, *127*, 101-109.

Oun, A. A., & Rhim, J.-W. (2017). Characterization of carboxymethyl cellulose-based nanocomposite films reinforced with oxidized nanocellulose isolated using

ammonium persulfate method. *Carbohydrate Polymers*, *174*, 484-492.

Park, S., Baker, J., Himmel, M., Parilla, P., & Johnson, D. (2010). Cellulose crystallinity index: measurement techniques and their impact on interpreting cellulase performance. Biotech Biofuels 3:10. *Biotechnology for biofuels*, *3*, 10.

Park, S., Baker, J. O., Himmel, M. E., P.A., P., & Johnson D.K. (2010). Cellulose crystallinity index: measurement techniques and their impact on interpreting cellulase performance. *Biotechnology for Biofuels*, *3*(10).

Pirani, S., & Hashaikeh, R. (2013). Nanocrystalline cellulose extraction process and utilization of the byproduct for biofuels production. *Carbohydrate Polymers*, *93*(1), 357-363.

Polshettiwar, V., & Varma, R. S. (2008). Microwave-Assisted Organic Synthesis and Transformations using Benign Reaction Media. *Accounts of Chemical Research*, *41*(5), 629-639.

Potthast, A., Kostic, M., Schiehser, S., Kosma, P., & Rosenau, T. (2007). Studies on oxidative modifications of cellulose in the periodate system: Molecular weight distribution and carbonyl group profiles. *Holzforschung*, *61*, 662-667.

Rahbar Shamskar, K., Heidari, H., & Alimorad, R. (2016). Preparation and evaluation of nanocrystalline cellulose aerogels from raw cotton and cotton stalk. *Industrial Crops and Products*, *93*, 203-211.

Rampazzo, R., Alkan, D., Gazzotti, S., Ortenzi, M. A., Piva, G., & Piergiovanni, L. (2017). Cellulose Nanocrystals from Lignocellulosic Raw Materials, for Oxygen Barrier Coatings on Food Packaging Films. *Packaging Technology and Science*, *30*(10), 645-661.

Scherrer, P. (1918). Bestimmung dergrosse und der inneren struktur yon kolloiteilchen mittels. *Gottinger Nachr Math Phys*, *2*, 98-100.

Sharma, P. R., & Varma, A. J. (2014). Thermal stability of cellulose and their nanoparticles: Effect of incremental increases in carboxyl and aldehyde groups. *Carbohydrate Polymers*, *114*, 339-343.

Tan, K., Heo, S., Foo, M., Chew, I. M., & Yoo, C. (2019). An insight into nanocellulose as soft condensed matter: Challenge and future prospective toward environmental sustainability. *Science of the Total Environment*, *650*, 1309-1326.

Tompsett, G. A., Conner, W. C., & Yngvesson, K. S. (2006). Microwave Synthesis of Nanoporous Materials. *Chemphyschem*, *7*(2), 296-319.

Venkatesh, M. S., & Raghavan, G. S. V. (2004). An Overview of Microwave Processing and Dielectric Properties of Agri-food Materials. *Biosystems Engineering*, *88*(1), 1-18.

Xiong, R., Zhang, X., Tian, D., Zhou, Z., & Lu, C. (2012). Comparing microcrystalline with spherical nanocrystalline cellulose from waste cotton fabrics. *Cellulose*, *19*.

Ye, S., Yu, H.-Y., Wang, D., Zhu, J., & Gu, J. (2018). Green acid-free one-step hydrothermal ammonium persulfate oxidation of viscose fiber wastes to obtain carboxylated spherical cellulose nanocrystals for oil/water Pickering emulsion [journal article]. *Cellulose*, *25*(9), 5139-5155.

Zhang, K., Sun, P., Liu, H., Shang, S., Song, J., & Wang, D. (2016). Extraction and comparison of carboxylated cellulose nanocrystals from bleached sugarcane bagasse pulp using two different oxidation methods. *Carbohydrate Polymers*, *138*, 237-243.

Zhang, X., & Liu, Z. (2012). Recent advances in microwave initiated synthesis of nanocarbon materials. *Nanoscale*, *4*(3), 707-714.

Zhong, L., Fu, S., Peng, X., Zhan, H., & Sun, R. (2012). Colloidal stability of negatively charged cellulose nanocrystalline in aqueous systems. *Carbohydrate Polymers*, *90*(1), 644-649.

Zhu, Y.-J., & Chen, F. (2014). Microwave-Assisted Preparation of Inorganic Nanostructures in Liquid Phase. *Chemical Reviews*, *114*(12), 6462-6555.

Zianor Azrina, Z. A., Beg, M. D. H., Rosli, M. Y., Ramli, R., Junadi, N., & Alam, A. K. M. M. (2017). Spherical nanocrystalline cellulose (NCC) from oil palm empty fruit bunch pulp via ultrasound assisted hydrolysis. *Carbohydrate Polymers*, *162*, 115-120.

4 Carbon dioxide diffusion at different relative humidity through coating of cellulose nanocrystals for food packaging applications

Ghislain Fotie[a], Luana Amoroso[b], Giuseppe Muratore[b] and Luciano Piergiovanni[a*]

[a.] *DeFENS, Department of Food, Environmental and Nutritional Sciences—PackLAB Università degli Studi di Milano, Via Celoria 2, 20133 Milano, Italy.*

[b.] *Department of Agricultural, Food and Environment (Di3A), Università degli Studi di Catania, Via Santa Sofia 100, 95123 Catania, Italy.*

The present chapter has been published in *Food Packaging and Shelf Life*, *2018*, *18, 62-70*.

Abstract

In this paper, the investigation was focused on the CO_2 permeability through CNCs coating at various RH values, comparing with the O_2 one, aiming to evaluate the potential usage in all the applications of modified atmosphere packaging for intermediate-low moisture foods where the role of carbon dioxide is essential for shelf life extension. For this purpose, PET films were coated with characterized CNCs, obtained from cotton linters, and the CO_2 permeance was measured as a function of increasing RH values (from 0% to 80%). After calculating the diffusion and solubility coefficients, and estimating the CO_2/O_2 selectivity, the possible evolution of different modified atmospheres has been theoretically calculated. The results obtained, let hypothesize

that, in consequence of a very high CO_2/O_2 permeability selectivity, the CNCs coated films can be useful in some modified atmosphere packaging applications, in a range of RH typical of many medium-high RH food products.

Keywords: cellulose nanocrystals; carbon dioxide barrier; moisture effects; modified atmosphere packaging.

4.1 Introduction

An intensive research and a general wide interest in the cellulose nanomaterials (CNM) have greatly increased over the last years, up to the point that the "ISO Technical Committee (ISO/TC 229) for Nanotechnologies" recently published a standard vocabulary (ISO, 2017), for cellulose nanomaterials, whose indications are strictly followed in this paper. CNMs are anticipated to have significant commercial impact because for their renewable nature and unique properties. They are believed to have potential applications in a wide range of products including those that currently use non-renewable, oil-based materials or ingredients. In particular, the interest in possible packaging applications of cellulose nanocrystals (CNCs) and cellulose nano-fibrils (CNFs) is continuously and very rapidly growing all around the world (Hubbe et al., 2017; Johansson et al., 2012; Khan et al., 2014; Li et al., 2015; Rebouillat & Pla, 2013; Reig et al., 2014). In addition to the biodegradability and their origin in renewable sources, there is a strong interest in the potential for activating feasible paradigms of circular economy, related to the chance of producing CNCs and CNFs from cellulose-containing biomasses of food companies or by-products of packaging materials industries.

Actually, very attractive properties can be detected when the size of cellulose molecules is broken down into the nanoscale (Dufresne, 2017). Extraordinary gas barrier functionalities and improved mechanical properties, differently expressed by CNCs and CNFs, lead to very promising applications in bio-based flexible packaging and cellulosic materials for food products. The perspective of optimizing diffusional properties with the purpose of packaging material minimization and possible shelf life extension seems, in particular, a very interesting and current strategy for food packaging innovation, and for high sustainability targets. Several researches have been carried out on the gas barrier properties of cellulose nanocrystals and cellulose nanofibrils (Aulin et al., 2010; Gicquel et al., 2017; Li, Biagioni, Bollani, et al., 2013; Minelli et al., 2010).

In all our previous works, which were carried out on CNCs obtained from different raw materials and coated onto conventional and biobased films for food packaging, we always found permeance values much lower than those of conventional synthetic barrier layers, even if very thin coatings were applied (less than 1 μm) (Fotie et al., 2017; Li, Biagioni, Bollani, et al., 2013; Li, Biagioni, Finazzi, et al., 2013; Mascheroni et al., 2016; Rampazzo et al., 2017).

These peculiar and interesting barrier properties of CNCs coatings are not totally surprising, taking into account the main requirements for getting low gas permeability through polymers (Ashley, 1985; Dhoot et al., 2002; McKeen, 2017; Siracusa, 2012; Yam, 2010). In fact, it is well known that highly polar polymers have low gas permeability; having high cohesive energy and strong chain-to-chain attractions, their void volume is small and diffusional phenomena are limited (Salame, 1986) at low humidity. Cellulose can be

defined a polar polymer since it has many polar oxygen–hydrogen (—OH) groups, with small differences in whatever crystalline forms (Gardiner & Sarko, 1985), even if net dipoles, i.e. a result of opposite charges, are absent.
Un-saturations which lead to a greater ease of chains rotation and consequently to high gas diffusion, are completely absent in cellulose molecules. Short lateral chains which hinder the close packing of macromolecules, increasing free volume and enhancing permeability, as well, are absent in the linear polymers such as cellulose. On the contrary, the crosslinking that restrains the segmental mobility of the polymer and makes the diffusion process slower, is extensively possible due to the crystalline conformation of cellulose, through hydrogen bonds between chains alongside and intramolecular. The crystallinity degree, that in whatever polymer leads to tortuous path in the diffusion pathway of permeants, is always high in cellulose nanocrystals: depending on the different source and preparation process used, the crystallinity index reaches even 80–90% (McKeen, 2017). Finally, the glass transition temperature, which when higher than service temperature is consistent with very stiff chains and gives relatively better barrier properties, is well above 200 °C in the cellulose biopolymers (Fakhraai et al., 2005; Gajdoš et al., 2000).
All that is currently known about morphology and chemical properties of polymers, which positively affect high barrier performance, is noticeable in cellulose and, particularly in cellulose nanocrystals. At the same time, however, it has been noted that the lack of intramolecular hydrogen bonding in the surface chains of cellulose makes possible extensive interactions with water molecules. Various studies dealing with these kinds of phenomena, showed that the water content

and interactions with the material's components have a great influence on final properties of cellulosic materials (Engelund et al., 2013; Froix & Nelson, 1975; Ioelovich et al., 2010). For more than 70 years, bulk amorphous regions have been indicated to be an ideal place for water adsorption, and the relationship between the availability of surface hydroxyl groups and crystallinity of cellulose is well established (Howsmon, 1949; Mihranyan et al., 2004).

The moisture sensitivity is a serious critical point for preserving the outstanding gas barrier properties of CNCs coatings, particularly if they are expected to be used in food packaging applications. Actually, we always observed a strong reduction of oxygen barrier properties at medium-high relative humidity values (Fotie et al., 2017; Rampazzo et al., 2017) and recently (Fotie et al., 2017), by a multidisciplinary approach, we tried to better understand the basics and the entity of water-cellulose nanocrystals interaction. Starting from about 40% of equilibrium relative humidity (RH), we assessed a 65% of freezable water in the CNCs and the XRPD (X-Ray Powder Diffraction) patterns gave clear indications of loss of structural coherence in the increasing of the RH values, and that the amorphous regions in the sample expanded at the expense of the crystalline part.

In this paper, the investigation was continued and focused on both the O_2 and CO_2 permeability of CNCs coatings at various relative humidity values. A potential application for such a high barrier material is in fact, the modified atmosphere packaging of food products, where the role of carbon dioxide is essential for shelf life extension of perishable foods which have medium or high relative humidity values.

4.2 Materials and methods

4.3.1 Materials

The cotton linters used for CNCs production were obtained from Innovhub (Milan, Italy), the chemical reagents were purchased from Sigma-Aldrich (Milan, Italy) and the 12 μm thick polyethylene terephthalate (PET) film, used as coating substrate, was achieved by Sapici spa (Cernusco sul Naviglio, Italy).

4.3.2 CNCs Obtainment and Coating Deposition

The Leung and co-workers method was followed for the CNCs preparation, throughout the oxidative hydrolysis process by ammonium persulfate (APS) 1 M, in the ratio APS (cm^3)/cotton linters (g) 100:1 (Leung et al., 2011). The yield of CNCs production (%) was calculated as the ratio of freeze-dried CNCs weight (g) and cellulosic content of 100 g of raw materials. The steps of CNCs purification and the coating application on PET films, were followed as described in previous works (Mascheroni et al., 2016; Rampazzo et al., 2017); the coating suspension was a CNCs 4% (m/m), adjusted at pH 8 with NaOH 1 M. For the thickness assessment of CNCs coating, a gravimetric method was used. After weighing 4 samples (M1, g) of 100 cm^2, the coating was washed out under hot water (~70 °C) and the resulting uncoated PET films were dried and weighed (M2, g). The coating thickness (L, cm) was estimated by Eq. (4.1):

$$L = \frac{M1 - M2}{\rho} \times 100 \qquad (4.1)$$

where ρ=1.58 g cm^{-3} is assumed as the density of the CNCs (Mazeau & Heux, 2003).

4.3.3 Characterization of CNCs Morphology and Coating Uniformity

Either equivalent hydrodynamic diameters of the dispersed CNCs, and particle number distributions were determined by dynamic light scattering (DLS) measurements (mod. Litesizer500, Anton Paar, Graz, Austria). The measurements were performed at 25.0 ± 0.1 °C with a 35 mW laser diode light (λ = 658 nm) and collecting the scattered light at 15°and 90°. Prior to proceeding with the measurements, the samples were diluted at 3 different concentrations with distilled water adjusted to pH 8 and maintained at 25 °C through stirring until measurement. The diluted solutions were flowed in the measurement cell after 30 s homogenization by ultrasonic (UP 200 St, Hielscher ultrasonics GMBH, Teltow, Germany) in a cool water bath to prevent overheating. The dimensions of the CNCs were next evaluated via Transmission Electron Microscopy (TEM). Drops of aqueous dispersions of CNCs (1%) were settled on carbon-coated electron microscope grids, negatively stained with uranyl acetate and left to dry. Samples were analysed with a Hitachi Jeol-10084 TEM operated (Brugherio, Italy) at an accelerating voltage of 80 kV.
Surface structure of the PET coated films was also evaluated by Atomic Force Microscope. Three different samples were measured with Tosca™ 400 AFM (Anton Paar, Graz, Austria) in tapping mode. Three randomly selected positions were measured for each sample. All images were recorded

with the same scan size of 5 x 5 μm and resolution 500 × 500. Surface roughness (Sq, root mean square) has been calculated from AFM images following standard procedure (ISO, 2012). The transparency of the CNCs coated PET was also measured at 550 nm, according to the ASTM D 1746-70, by means of a UV-VIS spectrophotometer (mod. L650, Perkin-Elmer, Milano, Italy). Each sample was replicated three times, analyzing at least four spots on each replicate.

4.3.4 CNCs Zeta Potential and Conductivity

Zeta potential (mV) and conductivity (mS cm^{-1}) of the CNCs in the diluted suspension at 3 different concentrations at pH 8 were performed by electrophoretic light scattering (ELS), using the PALS technology (mod. Litesizer 500, Anton Paar, Graz, Austria). Measures were replicated 5 times, at 25.0 ± 0.1 °C, by means of a 35 mW diode laser (λ = 658 nm) and at 15° detection angle.

4.3.5 O_2 and CO_2 Permeance at Various Relative Humidities (RH)

Oxygen and Carbon dioxide permeance measures were performed by an isostatic permeabilimeter (mod. Multiperm, PERMTECH S.r.l., Pieve Fosciana, Italy) according to ASTM standard method D-3985. The gasses' permeance (P_G, $cm^3\ m^{-2}\ d^{-1}\ bar^{-1}$) of CNCs coated and uncoated PET films were measured at 25 °C under 80%, 70%, 60%,40%, 20% and 0% RH on the coated side of the film, both increasing and decreasing the RH values for CO_2 and just increasing RH for O_2 and uncoated PET film. The CO_2 permeability coefficients

at different RH ($KP_{CO2/CNCs}$, $cm^3\ \mu m\ m^{-2}\ d^{-1}\ bar^{-1}$) of the CNCs coating alone were estimated from the average values of both increasing and decreasing RH, using Eq. (4.2) (Crank, 1979)(Crank, 1979), and assuming that the PET surface did not interact with the CNCs coating layer of thickness L (μm) and considering that the interface PET-CNCs minimally affected the carbon dioxide permeation.

$$L / [KP_{CO2/CNCs}\ (\text{CNCs coating})] = [1/P_{CO2}(\text{coated PET film})] - [1/P_{CO2}\ (\text{uncoated PET film})] \quad (4.2)$$

From the isostatic CO_2 permeation curves obtained from the permeance measures, the apparent diffusion coefficients ($D_{CO2/CNCs}$, $cm^2\ s^{-1}$) in the coating, at each RH value were evaluated by using this Eq. (4.3) (Hernandez & Gavara, 1999; Rampazzo et al., 2017):

$$D_{CO2/CNCs} = L^2/(7.2 \times t_{1/2}) \quad (4.3)$$

where L is the thickness (cm) and $t_{(1/2)}$ (s) is the time required to reach half of the maximum permeance value. Actually, this lag-time was measured on the coated film, not on the coating alone. However, we know that the limiting factor for CO_2 permeation is the CNCs coating and assumed as meaningless the barrier contribution of the bare (uncoated) substrate. From Eq. (4.2), in fact, we estimated that the CO_2 permeance of the uncoated PET is 125-1500 times higher than the coating (see **Table 4.2**). Therefore, we assumed Eq. (3) as a reliable estimation of apparent CO_2 diffusion coefficient of the CNCs coating. From the permeability and diffusion coefficients ($KP_{CO2/CNCs}$ and $D_{CO2/CNCs}$), the gases solubility in the CNCs

coating ($S_{CO2/CNCs}$, bar^{-1}) were also calculated at each RH value as follows (Eq. (4.4)):

$$S_{CO2/CN} = KP_{CO2/CNCs}/D_{CO2/CNCs} \quad (4.4)$$

For determining the selectivity parameter (P_{CO2}/P_{O2}) at different RH values, the average permeance values obtained increasing and decreasing RH, were used.

4.3 Results and Discussion

4.2.1 CNCs Production and Coating onto PET Film

The cellulose nanocrystals obtained resulted very similar to the ones already described in previous works (Mascheroni et al., 2016; Rampazzo et al., 2017), for their morphological and main chemical characteristics, which are reported in **Table 1** and in the TEM image of **Figure 4.1a**.

Table 4.1 Main characteristics of cellulose nanocrystals and CNCs coated PET film (± s.d.).

Hydrodynamic diameter (nm), by DLS	101.15 ± 3.65 (n=3)
Zeta potential (mV), by ELS	−44.40 ± 4.12 (n=3)
Conductivity (mS cm^{-1}), by ELS	0.095 ± 0.024 (n=3)
Thickness of CNCs coating (nm)	756.3 ± 22.3 (n=3)
Transparency of the CNCs coated PET film (T% at 550 nm)	85.67 ± 0.3 (n=2)
Roughness of the CNCs coated PET film (Sq)	14.5 ± 4.9 (n=9)

The coating process, carried out with a 4% CNCs suspension in water at pH 8, were very similar as reported in previous papers. The roughness, assessed by AFM, and the transmittance measured at 550 nm, confirmed the uniformity

of the CNCs layer coated onto the PET film, for a thickness lower than 1 μm. In **Table 4.1** and in the AFM image of **Figure 4.1b** these results are summarized.

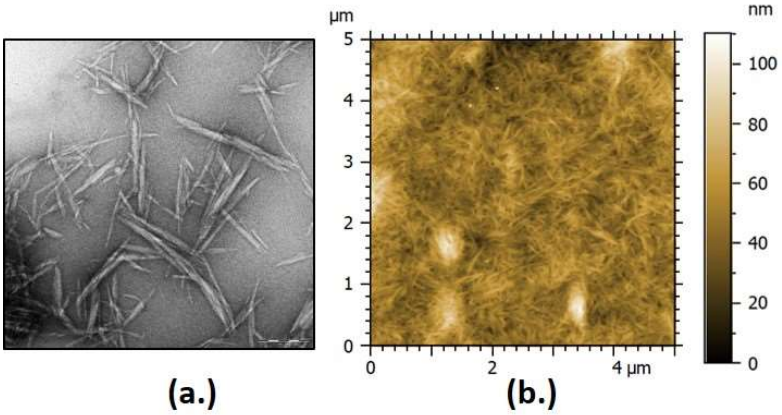

Figure 4.1 TEM picture of cellulose nanocrystals in the suspension used for coating (**a.**) and AFM picture of the coating applied onto PET film (**b.**).

4.2.2 O_2 and CO_2 Permeance of the Coated Film, at Various Relative Humidities

The oxygen and carbon dioxide permeance of PET film, as a function of RH, is state of the art (Auras et al., 2004; Zhang et al., 2001) and in our previous paper (Fotie et al., 2017) we have already shown the negligible differences observed in measuring the oxygen permeance of the CNCs coated PET film increasing and decreasing the relative humidity. Therefore, in this case we assessed the carbon dioxide permeance, both increasing (ads) and decreasing (des) the RH value, for CNCs coated PET film only. The overall results are reported in **Table 4.2**, as average values ± standard deviation,

and also in this case the permeance values in adsorption and desorption are quite similar, so in **Figure 4.2** the global averages values are shown.
The carbon dioxide barrier of the CNCs coating decreases very greatly with increasing the relative humidity, much faster than the oxygen barrier. At around 50% RH the resistance to carbon dioxide permeance is meaningless and the permeance values is very close to the one of uncoated PET. The same phenomenon appears for oxygen just above 80% RH. This unexpected and quite peculiar behaviour of CO_2 permeability throughout the cellulose nanocrystals coating, obviously affects the so called "selectivity", the ratio between the permeance of CO_2 and O_2 (van Krevelen & Nijenhuis, 2009), which increases more than 55 times from 0 to about 25% relative humidity, slowly decreasing thereafter, and going back to typical values (about 6–7) just for RH above 70%. This trend is reported in **Figure4.3**, showing the peak in selectivity at approximately 25% RH.
Herrera, Mathew, and Oksman (2014) investigated various gases permeability and selectivity of cellulose nanocrystals films (layers) deposited by spin coating and obtained by acid hydrolysis using both sulphuric and hydrochloric acid. For the P_{CO2}/P_{O2} ratio, they found values in the range 2.4–11.2, presumably at 0% RH (temperature and RH of measure not published).

Table 4.2 Oxygen and Carbon dioxide permeance at 25 °C under different relative humidity (RH) values, through the CNCs-coated and uncoated PET film ($cm^3m^{-2}d^{-1}bar^{-1}$, average ± s.d.).

	0% RH	20% RH	40% RH	60% RH	70% RH	80% RH
Uncoated PET O_2 permeability (*ads*)	128.5*±6.4 (n=3)	123.4±6.2 (n=3)	115.2±5.8 (n=3)	109.7±5.5 (n=3)	107.1±5.4 (n=3)	104.9±5.2 (n=3)
Uncoated PET CO_2 permeability (*ads*)	597.7±29.9 (n=3)	541.1±27.0 (n=3)	514.1±25.7 (n=3)	500.0±25.0 (n=3)	500.1±25.0 (n=3)	501.1±25.0 (n=3)
CNCs Coated PET O_2 permeability (*ads*)	0.4±0.4 (n=2)	1.0±0.1 (n=2)	2.0±0.1 (n=2)	23.17±3.1 (n=2)	56.4±5.1 (n=2)	84.0±2.9 (n=2)
CNCs Coated PET CO_2 permeability (*ads*)	4.7±4.6 (n=3)	338.8±152. 1 (n=3)	474.5±54.0 (n=3)	494.7±14.8 (n=3)	494.2±14.7 (n=3)	494.2±13.4 (n=3)
CNCs Coated PET CO_2 permeability (*des*)	4.8±4.2 (n=3)	244.3±73.5 (n=3)	480.7±24.0 (n=3)	491.6±14.7 (n=3)	492.1±12.8 (n=3)	494.2±13.4 (n=3)

(ads): increasing RH from 0 to 80 %; (des): decreasing RH from 80 to 0 %; * RH = 8%.

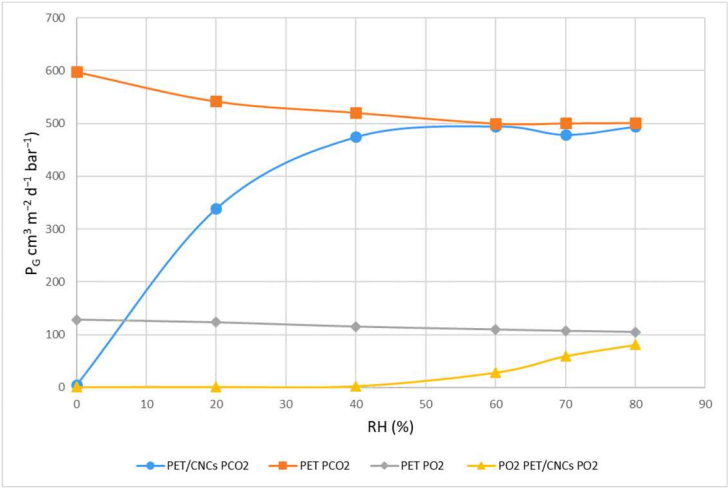

Figure 4.2 Global average values of O_2 and CO_2 permeability for CNCs-coated and uncoated PET film.

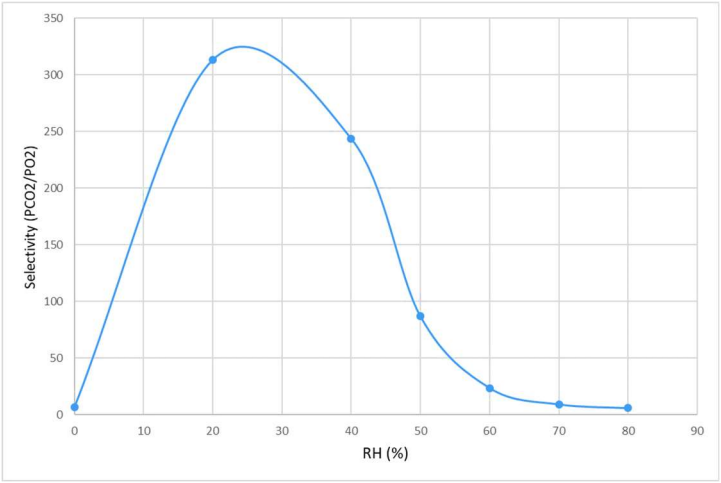

Figure 4.3 Trend of PCO_2/PO_2 ratio (selectivity) according to relative humidity

In order to better understand the role of RH on the carbon dioxide transmission across the CNCs coating, and thereafter on selectivity, the permeability ($KP_{CO2/CNCs}$), diffusion ($D_{CO2/CNCs}$) and solubility ($S_{CO2/CNCs}$) apparent coefficients, in the cellulose nanocrystals thickness only, were assessed at relative humidity from 0 to 80%. According to the gas permeation theory, in fact, permeability is influenced by these two main factors: diffusion and solubility of gases, which are mostly related respectively to the crystallinity of the structure and to the nature of the gas (Barrer & Rideal, 1939; Hernandez & Gavara, 1999). The related values are reported in **Table 4.3** as average ± standard deviation, while in **Figure 4.4a**. and **b.**, the trends of apparent diffusion and solubility coefficients (average values) are shown as function of RH values.

Table 4.3 Permeability ($KP_{CO2/CNCs}$), diffusion ($D_{CO2/CNCs}$) and solubility ($S_{CO2/CNCs}$) apparent coefficients of carbon dioxide in the CNCs coating at 25 °C, under different relative humidity (RH) values.

	0% RH	20% RH	40% RH	60% RH	70% RH	80% RH
Permeability coefficient ($KP_{CO2/CNCs,}$ cm^3 µm m^{-2} d^{-1} bar^{-1})	3.18±2.9 (n=6)	397.3±272 (n=6)	10219±8590 (n=6)	17141±8234 (n=6)	20137±10119 (n=6)	21663±4814 (n=3)
Diffusion apparent coefficient ($D_{CO2/CNCs}$, cm^2 s^{-1})	4.32 E-13±5.1 E-14 (n=6)	6.39 E-13±1.1 E-13 (n=6)	6.69 E-13±9.2 E-14 (n=6)	7.84 E-13±1.6 E-14 (n=6)	8.04 E-13±9.0 E-15 (n=6)	8.07 E-13±6.2 E-15 (n=6)
Solubility apparent coefficient ($S_{CO2/CNCs}$, bar^{-1})	1.01±0.9 (n=5)	78.2±42.9 (n=5)	1555±1070 (n=3)	4714±3779 (n=5)	7596±6717 (n=5)	219640±23615 1 (n=3)

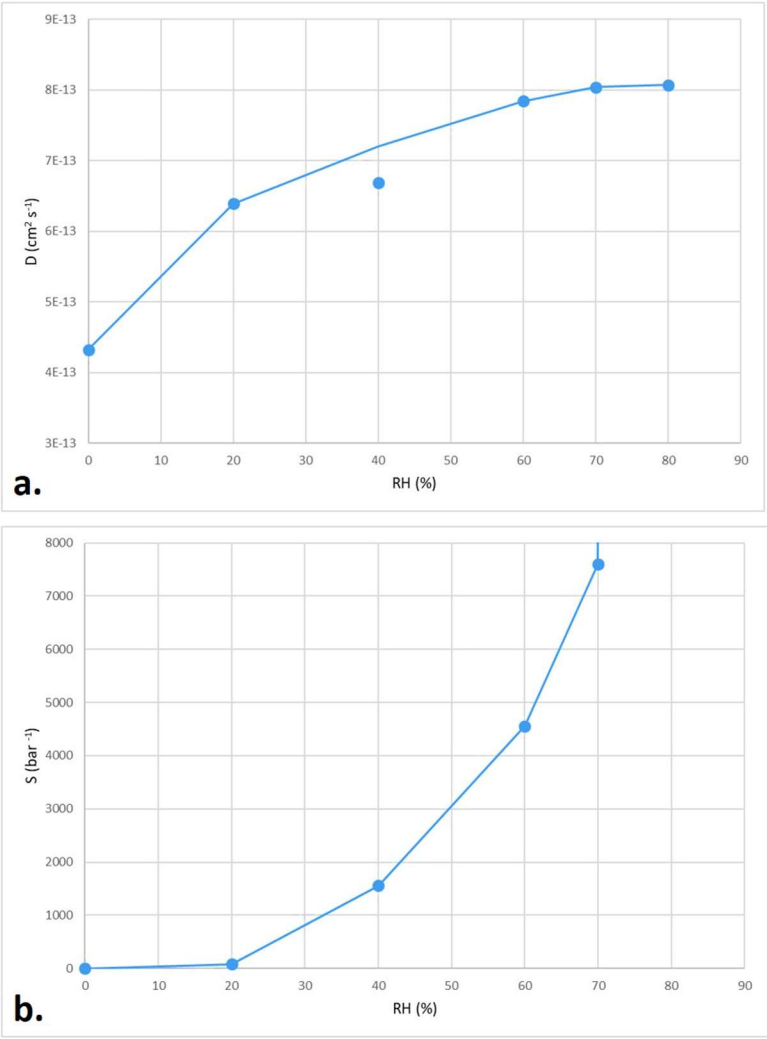

Figure 4.4 Trends of apparent diffusion (**a.**) and solubility (**b.**) coefficients of carbon dioxide in CNCs at 25 °C, as function of RH values.

From the overall data presented, is quite evident the huge increase in CO_2 permeability of CNCs layer, from 0 to 70–80% relative humidity. In the same range of RH values, diffusion and solubility show different trends: the increase of $D_{CO2/CNCs}$ is less than double and it seems to be terminated around 50–60 %RH, while the apparent solubility coefficient $S_{CO2/CNCs}$ increases more than 1000 times and in an exponential way approximately.

When the evaluation of gas permeability is performed on very hydrophilic coatings such as CNCs, in presence of the humidity, it is appropriate to consider a three-dimensional interaction profile that is configured between water, cellulose nanocrystals and gas. In the absence of water (0% RH), we only have the CNCs-gas interaction; therefore, it can be assumed that the permeance of CO_2 is faster than that of O_2, due to the smaller kinetic diameter (Mehio et al., 2014) and higher condensability of CO_2 which facilitate its transmission through any polymer; the value of common selectivity is around 6-7. In the presence of moisture, it can be hypothesized that there would be an interaction between the gas and water and between water and cellulose nanocrystals, i.e. the water could affect the CNCs structure.

At low humidity, since the CNCs shape has not yet been modified, a part of the water will occupy the free volume of the CNCs network, probably assuming a pH value close to the one at which the coating suspension has been dried (pH 8) and affecting the permeability due to the gas solubility in the media. Since the pH value, before coating, was adjusted with sodium hydroxide, it is reasonable to presume a residual of anions, able to affect the pH value of the media, even upon a small hydration. Increasing the RH value, we can assume that the water also swells the coating, increasing the distance

among the nanocrystals' chains and, progressively, changes and modifies the conformational organization of the crystalline network.
The observed increase in the apparent diffusion coefficient ($D_{CO2/CNCs}$) from 0 to 40–50% RH is consistent with this interpretation and might be related to a moderate and initial swelling of CNCs network, while the fast increase of apparent solubility $S_{CO2/CNCs}$ explains the very high value of the selectivity parameter. In fact, carbon dioxide is much more soluble in water than oxygen, especially at high pH values, leading to a very high permeability of CO_2. About this, it is advisable to report that the pH value of the CNCs suspension can be modulated in a certain range; therefore, this seems a useful chance for modulating permeability and selectivity of the coated film in real packaging applications.
The further increase of RH, however, is certainly related to a progressive loss of coherence of the structure, already observed in previous work (Fotie et al., 2017), which equally, and significantly affects both the O_2 and the CO_2 permeability that increase, reaching the PET permeability that acts as limiting factor and decreases the selectivity ratio to standard values of uncoated PET. In fact, at 50% RH for carbon dioxide and above 80% RH for oxygen, the gas barrier of CNCs coating is completely lost. It is worth noting, however, that the barrier properties of CNCs coating are always completely recovered by the drying phase of the coated film, without any defect in the original performance.
In any case, the opportunity of having such a high ratio between carbon dioxide and oxygen permeation, might be useful in many circumstances, where respiring or fermented or toasted food products are packaged. Although carbon dioxide is useful in various modified-atmosphere packaging

applications, a residual CO_2 accumulation in some packages can be detrimental to the quality or the integrity of the package (Lee, 2016).

4.2.3 Modified Atmosphere Evolution Modelling

Considering the potential interest in having such high selectivity values, the possible evolution of various modified atmospheres has been theoretically calculated. The volume concentrations (%) of oxygen, carbon dioxide and nitrogen were forecasted based on gas volumes transmission expected, every 30 min, by the permeance data at 4 different relative humidity, and for 3 different atmospheres. All the variables considered for the computing are proposed in **Table 4.4** (P_{N2} figures are estimations based on common selectivity values).

Table 4.4 Parameters used for forecasting the modified atmosphere evolution.

Permeable surface (cm^2)		600			
Unfilled volume (cm^3)		1000			
Time of iterative forecasting (min)		30			
MAP_1	CO_2(%)	60	**RH 0%**	P_{CO2}*	4.7
	O_2(%)	0		P_{O2}*	0.4
	N_2(%)	40		P_{N2}*	0.1
MAP_2	CO_2(%)	60	**RH 35%**	P_{CO2}*	474
	O_2(%)	5		P_{O2}*	2.4
	N_2(%)	35		P_{N2}*	0.5
MAP_3	CO_2(%)	20	**RH 70%**	P_{CO2}*	494
	O_2(%)	0		P_{O2}*	59.4
	N_2(%)	80		P_{N2}*	13.5

[a] ($cm^3 m^{-2}$ d^{-1} bar^{-1}, at 25 °C).

The expected gas volumes transmissions were estimated taking into account 600 cm^2 of permeable surface, 1 L of initial unfilled volume (UFV) and the initial relative concentrations of oxygen, nitrogen and carbon dioxide, as from MAP_1, MAP_2 and MAP_3. We have also assumed that the gas volumes permeated inside the ideal package did not change during time for phenomena different from permeability. By iterative calculation, the permeated amounts, new UFV value and corresponding gas concentrations every 30 min were accounted as follows:

$$\mathrm{UFV}^{\mathrm{n}} = \pm \mathrm{vO_2}^{\mathrm{n}} \pm \mathrm{v}N_2{}^{n} \pm \mathrm{v}CO_2{}^{n} + UFV^{n-1}$$

$$\%\mathrm{O_2}^{\mathrm{n}} = 100 \times \left(\mathrm{vO_2}^{\mathrm{n}} \pm \mathrm{vO_2}^{\mathrm{n-1}}\right)/\mathrm{UFV}^{\mathrm{n}}$$

$$\%N_2{}^{\mathrm{n}} = 100 \times \left(\mathrm{vN_2}^{\mathrm{n}} \pm \mathrm{vN_2}^{\mathrm{n-1}}\right)/\mathrm{UFV}^{\mathrm{n}}$$

$$\%CO_2{}^{\mathrm{n}} = 100 \times \left(\mathrm{vCO_2}^{\mathrm{n}} \pm \mathrm{vCO_2}^{\mathrm{n-1}}\right)/\mathrm{UFV}^{\mathrm{n}}$$

Where $\mathrm{vO_2}^{\mathrm{n}}$, $\mathrm{vN_2}^{\mathrm{n}}$, $\mathrm{vCO_2}^{\mathrm{n}}$n are the volumes of O_2, N_2 and CO_2, respectively, permeated in the time of iterative forecasting interval (30 min), positive (+) for gas volume permeated inside, while negative (–) for gas permeated outside. This theoretical-iterative approach was experimentally verified in a previous work (Piergiovanni et al., 1993).

In **Figure 4.5** the speculative atmosphere changes are reported during a possible 24 h storage at 25 °C, assuming that the coating immediately equilibrates with the environmental humidity, and no interaction between the gases and a food product inside, take place during the storage time. The relative humidity values have been selected as central point of the common classes of intermediate (IMF,

aw = 0.90 – 0.60), low moisture (LMF, aw = 0.60 – 0), and for dry foods (aw ≈ 0), while the three different modified atmospheres tested were representative of high (MAP_1), low carbon content (MAP_3), and assuming a possible residue of oxygen (MAP_2).

It is quite evident how selectivity can affect the modified atmosphere evolution, at different relative humidity and in different way depending on the atmosphere composition. The influence of the food relative humidity, as well as the environmental conditions, is thus quite important both for the carbon dioxide exit and for the oxygen entrance. These results, which need an experimental confirmation in real packaging applications or in reliable model systems, might be useful for a smart design of modified atmosphere food packaging applications, aimed at targeted shelf life for different food products.

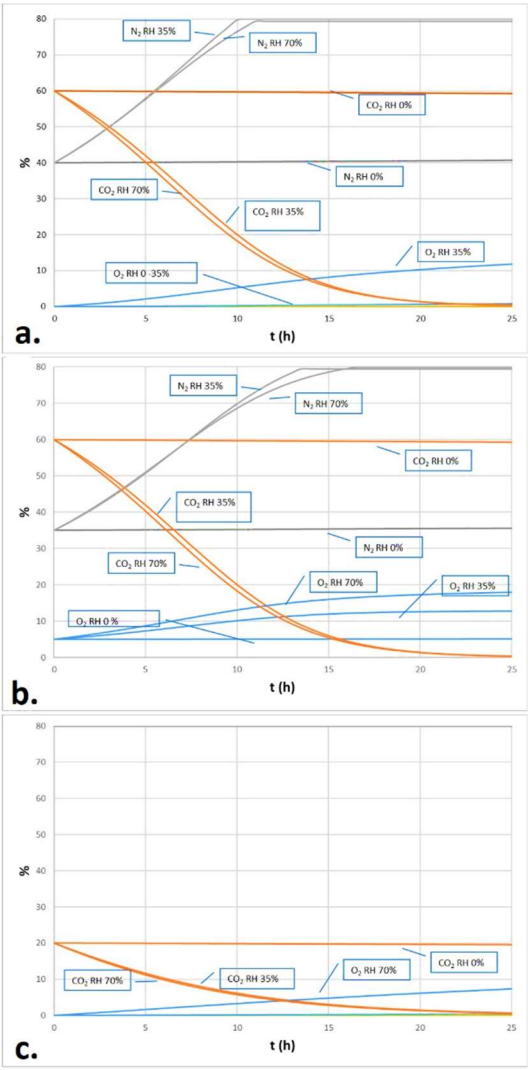

Figure 4.5 Theoretical evolution of three different modified atmospheres (**a.** MAP_1; **b.** MAP_2; **c.** MAP_3) compositions, according to different relative humidity values (0, 35 and 70% RH).

4.4 Conclusions

A deep investigation on the oxygen and carbon dioxide permeability at different relative humidity values, revealed a huge sensitivity of the CO_2 diffusion through the cellulose nanocrystals coated onto a PET film, already at RH values around 20% and above. Increasing the relative humidity, the carbon dioxide permeance greatly increased, much more than oxygen permeance and well before any indication of loss of structural coherence of the CNCs layer. Because of this behaviour, the permeability selectivity (the ratio of CO_2 and O_2 permeance) reached very, very high values in a range of RH, which are typical of many low and intermediate moisture food products. The solubility of CO_2 and the pH of the coating used, have been assumed as the main explications of this unexpected behaviour of the coated film. The carbon dioxide solubility, in particular, is strongly dependent on the pH of permeated matrix and the pH of the coating preparations is adjustable in a certain range, evoking a potential tool for O_2/CO_2 selectivity and CO_2 permeance design. This leads to the hypothesis that such CNCs coated films can be useful in some active or passive modified atmosphere packaging applications. Several commodities, like fruits, lettuce, potato, artichoke, and many others are sensitive to relatively low CO_2 concentrations, leading to symptoms of CO_2 injury, including off-flavour development, discoloration and internal tissue breakdown. In such cases, as well as for some fermented or toasted products, the application of a CNCs coatings may be beneficial for preserving the food quality.

References

Ashley, R. J. (1985). Permeability and Plastics Packaging. In J. Comyn (Ed.), *Polymer Permeability* (pp. 269-308). Springer Netherlands.

Aulin, C., Gallstedt, M., & Lindstrom, T. (2010). Oxygen and oil barrier properties of microfibrillated cellulose films and coatings. *Cellulose*, *17*(3), 559-574.

Auras, R., Harte, B., & Selke, S. (2004). Effect of water on the oxygen barrier properties of poly(ethylene terephthalate) and polylactide films. *Journal of Applied Polymer Science*, *92*(3), 1790-1803.

Barrer, R. M., & Rideal, E. K. (1939). Permeation, diffusion and solution of gases in organic polymers. *Transactions of the Faraday Society*, *35*(0), 628-643.

Crank, J. (1979). *The Mathematics of Diffusion* (2nd ed.). Oxford University Press.

Dhoot, S. N., Freeman, B. D., & Stewart, M. E. (2002). Barrier Polymers. *Encyclopedia of Polymer Science and Technology*.

Dufresne, A. (2017). *Nanocellulose: From Nature to High Performance Tailored Materials* (2 ed.). Walter de Gruyter GmbH & Co KG.

Engelund, E. T., Thygesen, L. G., Svensson, S., & Hill, C. A. S. (2013). A critical discussion of the physics of wood–water interactions. *Wood Science and Technology*, *47*(1), 141-161.

Fakhraai, Z., Valadkhan, S., & Forrest, J. A. (2005). Qualitative discrepancy between different measures of dynamics in thin polymer films⋆. *The European Physical Journal E*, *18*(2), 143-148.

Fotie, G., Rampazzo, R., Ortenzi, M., Checchia, S., Fessas, D., & Piergiovanni, L. (2017). The Effect of Moisture on Cellulose Nanocrystals Intended as a High Gas Barrier

Coating on Flexible Packaging Materials. *Polymers*, *9*(9), 415.

Froix, M. F., & Nelson, R. (1975). The Interaction of Water with Cellulose from Nuclear Magnetic Resonance Relaxation Times. *Macromolecules*, *8*(6), 726-730.

Gajdoš, J., Galić, K., Kurtanjek, Ž., & Ciković, N. (2000). Gas permeability and DSC characteristics of polymers used in food packaging. *Polymer Testing*, *20*(1), 49-57.

Gardiner, E. S., & Sarko, A. (1985). Packing analysis of carbohydrates and polysaccharides. 16. The crystal structures of celluloses IVI and IVII. *Canadian Journal of Chemistry*, *63*(1), 173-180.

Gicquel, E., Martin, C., Yanez, J. G., & Bras, J. (2017). Cellulose nanocrystals as new bio-based coating layer for improving fiber-based mechanical and barrier properties. *Journal of Materials Science*, *52*(6), 3048-3061.

Hernandez, R. J., & Gavara, R. (1999). *Plastics Packaging: Methods for Studying Mass Transfer Interactions: a Literature Review*. Pira International.

Herrera, M. A., Mathew, A. P., & Oksman, K. (2014). Gas permeability and selectivity of cellulose nanocrystals films (layers) deposited by spin coating. *Carbohydrate Polymers*, *112*, 494-501.

Howsmon, J. A. (1949). Water Sorption and the Poly-Phase Structure of Cellulose Fibers. *Textile Research Journal*, *19*(3), 152-162.

Hubbe, M. A., Ferrer, A., Tyagi, P., Yin, Y., Salas, C., Pal, L., & Rojas, O. J. (2017). Nanocellulose in thin films, coatings, and plies for packaging applications: A review. *BioResources*, *12*(1), 2143-2233.

International Organization for Standardization - ISO. (2012). *Geometric Product Specifications (GPS) – Surface texture: Areal – Part 2: Terms, definitions and surface texture parameters.* (ISO 25178-2:2012).

International Organization for Standardization – ISO. (2017). *Nanotechnologies — Standard terms and their definition for cellulose nanomaterial* (ISO/TS 20477:2017).

Ioelovich, M., Leykin, A., & Figovsky, O. (2010). Study of cellulose paracrystallinity. *Bioresources*, *5*, 1393-1407.

Johansson, C., Bras, J., Mondragon, I., Nechita, P., Plackett, D., Simon, P., Svetec, D. G., Virtanen, S., Baschetti, M. G., Breen, C., Clegg, F., & Aucejo, S. (2012). Renewable Fibers and Bio-Based Materials for Packaging Applications - a Review of Recent Developments. *BioResources*, *7*(2), 2506-2552.

Khan, A., Huq, T., Khan, R. A., Riedl, B., & Lacroix, M. (2014). Nanocellulose-Based Composites and Bioactive Agents for Food Packaging. *Critical Reviews in Food Science and Nutrition*, *54*(2), 163-174.

Lee, D. S. (2016). Carbon dioxide absorbers for food packaging applications. *Trends in Food Science & Technology*, *57*, 146-155.

Leung, A. C. W., Hrapovic, S., Lam, E., Liu, Y. L., Male, K. B., Mahmoud, K. A., & Luong, J. H. T. (2011). Characteristics and Properties of Carboxylated Cellulose Nanocrystals Prepared from a Novel One-Step Procedure. *Small*, *7*(3), 302-305.

Li, F., Biagioni, P., Bollani, M., Maccagnan, A., & Piergiovanni, L. (2013). Multi-functional coating of cellulose nanocrystals for flexible packaging applications. *Cellulose*, *20* (5), 2491-2504.

Li, F., Biagioni, P., Finazzi, M., Tavazzi, S., & Piergiovanni, L. (2013). Tunable green oxygen barrier through layer-by-layer self-assembly of chitosan and cellulose nanocrystals. *Carbohydrate Polymers*, *92*(2), 2128-2134.

Li, F., Mascheroni, E., & Piergiovanni, L. (2015). The Potential of NanoCellulose in the Packaging Field: A Review. *Packaging Technology and Science*, *28*(6), 475-508.

Mascheroni, E., Rampazzo, R., Ortenzi, M. A., Piva, G., Bonetti, S., & Piergiovanni, L. (2016). Comparison of cellulose nanocrystals obtained by sulfuric acid hydrolysis and ammonium persulfate, to be used as coating on flexible food-packaging materials [journal article]. *Cellulose*, *23*(1), 779-793.

Mazeau, K., & Heux, L. (2003). Molecular Dynamics Simulations of Bulk Native Crystalline and Amorphous Structures of Cellulose. *The Journal of Physical Chemistry B*, *107*(10), 2394-2403.

McKeen, L. W. (2017). 2 - Introduction to Plastics and Polymers. In L. W. McKeen (Ed.), *Permeability Properties of Plastics and Elastomers (Fourth Edition)* (pp. 21-40). William Andrew Publishing.

Mehio, N., Dai, S., & Jiang, D.-e. (2014). Quantum Mechanical Basis for Kinetic Diameters of Small Gaseous Molecules. *The Journal of Physical Chemistry A*, *118*(6), 1150-1154.

Mihranyan, A., Llagostera, A. P., Karmhag, R., Strømme, M., & Ek, R. (2004). Moisture sorption by cellulose powders of varying crystallinity. *International Journal of Pharmaceutics*, *269*(2), 433-442.

Minelli, M., Baschetti, M. G., Doghieri, F., Ankerfors, M., Lindström, T., Siró, I., & Plackett, D. (2010). Investigation of mass transport properties of microfibrillated cellulose (MFC) films. *Journal of Membrane Science*, *358*(1–2), 67-75.

Piergiovanni, L., Fava, P., & Moro, M. (1993). Shelf-life Extension of Taleggio Cheese by Modified Atmosphere Packaging. *Italian Journal of Food Science*, *5*(2), 115–120.

Rampazzo, R., Alkan, D., Gazzotti, S., Ortenzi, M. A., Piva, G., & Piergiovanni, L. (2017). Cellulose Nanocrystals from Lignocellulosic Raw Materials, for Oxygen Barrier Coatings on Food Packaging Films. *Packaging Technology and Science*, *30*(10), 645-661.

Rebouillat, S., & Pla, F. (2013). State of the Art Manufacturing and Engineering of Nanocellulose: A Review of Available Data and Industrial Applications. *Journal of Biomaterials and Nanobiotechnology*, *4*(2), 165-188.

Reig, C. S., Lopez, A. D., Ramos, M. H., & Ballester, V. A. C. (2014). Nanomaterials: a Map for Their Selection in Food Packaging Applications. *Packaging Technology and Science*, n/a-n/a.

Salame, M. (1986). Prediction of gas barrier properties of high polymers. *Polymer Engineering & Science*, *26*(22), 1543-1546.

Siracusa, V. (2012). Food Packaging Permeability Behaviour: A Report. *International Journal of Polymer Science*, *2012*, 302029.

van Krevelen, D. W., & Nijenhuis, K. (2009). *Properties of Polymers: Their Correlation with Chemical Structure; their Numerical Estimation and Prediction from Additive Group Contributions* (4th ed.). Elsevier Science.

Yam, K. L. (2010). *The Wiley Encyclopedia of Packaging Technology*. Wiley.

Zhang, Z., Britt, I. J., & Tung, M. A. (2001). Permeation of oxygen and water vapor through EVOH films as influenced by relative humidity. *Journal of Applied Polymer Science*, *82*(8), 1866-1872.

5 Sustainable Cellulose Nanofiber films from Carrot as Sprayable Coatings for Food Packaging Applications

Luana Amoroso[1,2†], Kevin J. De France[1†], Gilberto Siqueira[1], Tanja Zimmermann[1*], Gustav Nyström[1,3*].

1. *Laboratory for Cellulose & Wood Materials, Empa – Swiss Federal Laboratories for Materials Science and Technology, Überlandstrasse 129, 8600 Dübendorf, Switzerland.*
2. *Department of Agricultural, Food and Environment (Di3A) – Università degli Studi di Catania, Via Santa Sofia 100, 95123 Catania, Italy;*
3. *Department of Health Science and Technology, ETH Zürich, Schmelzbergstrasse 9, 8092 Zürich, Switzerland.*

For this chapter, a European patent request is pending as follow:

- Zimmermann T., De France K., Siqueira G., Nyström G., Amoroso L. (2021). Bio-based spray-packaging for food applications. Application n. 21169748.7.

Abstract

In order to limit the excessive use of non-renewable plastics as materials for food packaging, research into the development of more environmentally friendly packaging materials/practices has grown rapidly over the last few decades. Although cellulose nanofibers (CNF) have emerged as a promising material for such purposes, the use of new lignocellulosic sources for CNF production remains a challenge. Herein, we investigate the use of carrot pomace from both fresh and stale carrots, along with a one-pot

bleaching pretreatment to produce CNF. The energy required for homogenization of the carrot pomace along with resulting CNF fiber morphology and quality (surface area, degree of polymerization, carbohydrate content) are analyzed. In addition, model films are prepared via vacuum filtration and hot-pressing, whereby film quality, as related to morphological, optical, and mechanical properties is assessed. Finally, carrot CNF suspensions are sprayed onto the surface of bananas, demonstrating a substantial delay in enzymatic browning for up to one week. The results presented herein represent a significant advancement in the development of sustainable materials for food packaging.

Keywords: cellulose nanofibers; carrot pomace; bleaching, microfluidizer; sprayable coating.

5.1 Introduction

Research into the development of more sustainable and environmentally friendly packaging materials/practices has grown rapidly over the last few decades (Garcia et al., 2016; Pauer et al., 2019). In this context, cellulose nanofibers (CNF) are one of such material that has been proposed as a potential solution for applications within the field of food packaging (Gómez H et al., 2016; Hubbe et al., 2017; Khan et al., 2014; Li et al., 2015).

CNFs are made by mechanically (and optionally enzymatically/chemically) fibrillating bulk cellulose fibers from a variety of lignocellulosic starting materials (Chinga Carrasco, 2011), yielding long flexible nanofilaments (length

> 1 μm, diameter ~ 4 – 100 nm), having both crystalline and amorphous domains (Dufresne, 2017; Thomas et al., 2019). Due to a combination of high surface area, good film-formability, good mechanical and optical properties, potential for chemical modification, and low oxygen permeability (De France et al., 2017; Ferrer et al., 2017; Hsieh et al., 2017; Li & Lee, 2017), CNFs have been reported as suitable raw materials for the formulation of films and coatings, as they offer several benefits and key features for effective performance in this field (Andrade-Pizarro et al., 2015; Andrade et al., 2014; Azeredo et al., 2009; Silva-Vera et al., 2018; Wang et al., 2017; Zhao et al., 2019). In this context, Fukuzumi et al. (2009) produced TEMPO-oxidized CNF films from softwood cellulose, which were transparent (90% transmittance at 600 nm), durable (Young's modulus 6.9 ± 1.4 GPa, tensile strengths 233 ± 44 MPa), and demonstrated an extremely low coefficient of thermal expansion (2.7 ppm K^{-1}), and a high oxygen barrier (1 mL m^{-2} day^{-1} Pa^{-1}) when cast on PLA films. High barrier properties have also been reported by Aulin et al. (2010), recording oxygen permeabilities of 9 and 0.6 mL m^{-2} day^{-1} Pa^{-1}, for CNF films 2.54 and 3.19 μm thick, respectively, prepared from a commercial softwood pulp. Zhu et al. (2017) demonstrated the importance of delignification and pressing processes, whereby the resulting highly aligned microstructure of the CNF yielded foldable and flexible anisotropic films, with optical transmittance of nearly 90 % across the visible spectrum, and tensile strength of up to 350 MPa. Furthermore, many researchers have demonstrated the great improvement of films generated by the bulk addition of CNF to diverse base biopolymers. Azeredo et al. (2009) prepared mango-puree-based edible films, whereby the

addition of 36 wt% CNF led to a more than 114% increase in tensile strength, more than 1522% in Young's modulus, and a 37% decrease in water vapor permeability. Several research groups have also demonstrated similar results for chitosan films reinforced with CNFs (Azeredo et al., 2010; Fernandes et al., 2010; Yu et al., 2017; Wu et al., 2014). In general, the incorporation of CNFs has been shown to lead to increased water vapor/gas barrier capacities and enhanced mechanical properties (without significantly affecting film colour/transparency/other optical properties) in a wide variety of biopolymer films (Andrade-Pizarro et al., 2015; Jaramillo et al., 2020; Savadekar et al., 2012; Savadekar & Mhaske, 2012; Svagan et al., 2009; Trovatti et al., 2012; Wang et al., 2017), demonstrating the versatility of CNFs as a packaging material and the need for the sustainable production of high quality CNFs at scale.

Despite the recent breakthroughs in the industrial production of CNFs, several major drawbacks still exist. The energy-intensive fibrillation of cellulosic starting materials into individualized fibrils is one of the main challenges for the economically feasible commercial utilization of CNFs (Bharimalla et al., 2015). Although several well-established pre-treatment methods exist for increasing the ease of fibrillation (e.g. enzymatic or bleaching processes), these are time and often material-intensive procedures which come at an economic cost and often an environmental impact (Arvidsson et al., 2015; Abdul Khalil et al., 2014; Berglund et al., 2020; Delgado-Aguilar et al., 2015; Dufresne, 2017; Serra et al. 2017). As fibrillation itself (via refining, homogenization or grinding) is a relatively efficient and scalable production technique for CNF isolation (Nechyporchuk et al., 2016), developing quicker one-pot

pretreatment methods is extremely desirable. Another major issue concerning commercial production of CNFs is the identification of suitable cellulosic feedstocks that are readily available and ideally based on materials which would otherwise have no commercial relevance (i.e.: waste materials). Currently, the world's leading commercial producers of CNFs generally use wood pulp as a raw material due to its large-scale availability and quality control (Nechyporchuk et al., 2016; Rajinipriya et al., 2018). However, wood pulp has several other well-established commercial uses, and therefore other solutions such as the exploitation of food-processing waste and by-products represents an intriguing alternative (Alemdar & Sain, 2008). Additionally, the hierarchical lignocellulosic cell wall structures found in agricultural and food wastes have a much more porous, less dense structure with a lower lignin content than those found in wood, representing the potential for more efficient fibrillation with less energy demand (Nechyporchuk et al., 2016; Varanasi et al., 2018).

With around 40 million tons of carrots produced worldwide in 2018 (FAO, 2018), carrot pomace left over from juice extraction (accounting for up to 30-50% of the initial carrot mass) (Nguyễn, 2015), represents an attractive alternative as a starting material for CNFs production. This food processing residue, which is often regarded as a waste or even as a manufacturing cost (Siqueira et al., 2016; Sogut & Cakmak, 2020), contains ~ 81 wt % cellulose (on a dry basis) (Siqueira et al., 2016), and therefore represents an inexpensive, sustainable, and renewable source of cellulose fibres. In fact, pristine carrot pomace has already been investigated as a raw material for CNFs production (Berglund et al., 2016; Guimarães et al., 2016; Siqueira et al., 2016; Varanasi et al.,

2018). Initial findings demonstrate that the energy required to manufacture CNFs from carrot is significantly less than from wood fibers (Berglund et al., 2016; Varanasi et al., 2018). Furthermore, carrot CNFs had similar or superior quality to those made from wood sources (Siqueira et al., 2016; Varanasi et al., 2018). However, detailed investigation into the effects of pre-treatment and on the condition of the carrots used on the resulting CNFs properties is lacking. Therefore, herein CNFs was isolated from both fresh and stale carrot pomace, in each case evaluating the effectiveness of a one-pot bleaching pre-treatment on the overall quality of CNFs produced. CNFs suspensions and films made thereof were investigated, with particular emphasis on the fiber morphology and film optical, mechanical, and barrier properties. Finally, carrot CNFs suspensions were utilized as a stand-alone spray coating to lengthen the shelf-life of bananas, serving as a model food system.

5.2 Materials and Methods

5.2.1 Materials

Carrots were supplied from Stegro AG (Basadingen, Switzerland) and used as received. Sodium hydroxide (NaOH, Sigma Aldrich, Buchs, Switzerland), acetic acid (VWR International, Dietikon, Switzerland), and sodium chlorite ($NaClO_2$, 80% powder, VWR Internation, Dietikon, Switzerland) were all used as received. Distilled water was used for all experiments.

5.2.2 CNFs Production from Carrot Pomace

CNF were produced from both fresh (as received) and stale (after 3 weeks of storage) carrots. In both cases, carrots were directly juiced using a standard kitchen juicer, and the carrot pomace was collected. The pomace was then dispersed at 2 wt % in 8 L of water and loaded into a glass 10 L reactor with a heating jacket (LaboTechSystems LTS AG, Reinach, Switzerland). The carrot pomace suspension was washed at 80 °C for 2 h under gentle agitation, and subsequently discharged and vacuum-filtered using a fine metal mesh. Optionally, the washed carrot suspension was then subjected to a bleaching treatment as follows: 9 L of a 1:1:1 volume mixture of acetate buffer (81 g NaOH and 225 mL acetic acid in 2.775 L water), sodium chlorite (63.75 g $NaClO_2$ in 3 L water), and water (3 L) was loaded into a glass 10 L reactor. 500 g of washed and filtered carrot pomace was then added to achieve a final concentration of ~ 2 wt %. The carrot suspension was then bleached at 90 °C for 2 h under gentle agitation, and subsequently discharged, vacuum-filtered, and thoroughly washed with distilled water.

The treated carrot pomace was then dispersed at 1 wt % in water for fibrillation, whereby suspensions were first thoroughly mixed for 15 min using a high shear mixer (10,000 rpm, Ultra-turrax, IKA GmbH & Co, Staufen, Germany). Suspensions were then sequentially passed 10x through a two-chamber microfluidizer (M110Y, Microfluidics Corporation, Newton, Massachusetts) operating at 800 bar. For the first 5 passes, 400 µm and 200 µm grinders were used in series to facilitate the CNF fibrillation. In the case of bleached carrot pomace, 200 µm and 100 µm grinders were used in series for the final 5 passes.

However, due to noticeable clogging in the microfluidizer for non-bleached carrot pomace, 200 µm and 200 µm grinders were used in series for the next 4 passes, with 200 µm and 100 µm grinders used in series solely for the final (10^{th}) pass. Carrot CNF suspensions were then stored in a refrigerator prior to characterization/use. Samples are denoted as: FCNF (CNFs from fresh, non-bleached carrot pomace), SCNF (CNFs from stale, non-bleached carrot pomace), FBCNF (CNFs from fresh, bleached carrot pomace) and SBCNF (CNFs from stale, bleached carrot pomace). This process, including representative images of fresh and stale carrots, is depicted schematically in **Figure 5.1**.

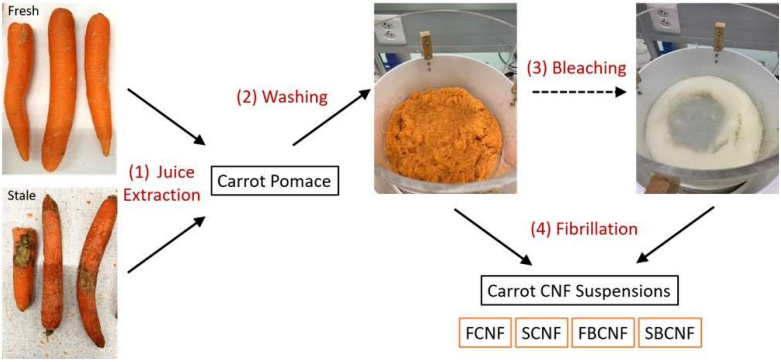

Figure 5.1. Schematic representation of CNFs isolation from carrot pomace.

5.2.3 Characterization of CNF Suspensions

Fiber morphology of CNF suspensions was characterized by scanning electron microscopy (SEM, Fei Nova NanoSEM

230) and optical microscopy (Leica DFC420 microscope). Rheological measurements were performed at 25 °C (Anton Paar MCR302 rheometer) using a double-gap cylinder geometry (Standard Measuring System DG26.7/T200/SS). CNF specific surface area was calculated by the Brunauer-Emmett-Teller (BET) method on a Micromeritics 3 Flex (Micromeritics, USA) device, whereby freeze-dried samples were degassed at 75 °C for 18 h under vacuum prior to the measurements. Cellulose degree of polymerization was determined viscometrically according to the Staudinger-Mark-Houwink equation (Gruber & Gruber, 1981), whereby the necessary limiting viscosity number was determined according to ISO 5351:2004 (ISO, 2004). Measurements were performed in triplicate for each sample. Residual chemical analysis was performed as previously described (Lorenz et al., 2016). Briefly, freeze dried CNF samples were hydrolyzed using H_2SO_4 in a 2-step process. Borate-high performance anionic exchange chromatography (HPAEC) was used to facilitate separation. Cellulose is taken to be the determined glucose content, and hemi-cellulose is taken to be the sum of the remaining hydrolyzed sugars (xylose, mannose, galactose, arabinose, rhamnose). Non-hydrolyzed residual material is assumed to be mostly lignin with some denatured protein residues.

5.2.4 Preparation and Characterization of CNF Films

Carrot CNFs films were formed by vacuum filtration of ~ 0.5 wt % suspensions using a Buchner funnel and 0.65 µm filters (Durapore DVPP membrane filter, Merck Millipore Ltd.). Note that all films were formed from the same volume of

CNF suspension, ensuring a similar concentration of ~ 40 g/m^2 for each film. The wet films were subsequently hot pressed at 90 ˚C and 20 bar for 30 min. Dried films were stored at room temperature until further use/characterization; as required, they were cut to size using a laser cutter (Nova24 60W, Thunderlasers). Film morphology and optical properties were evaluated via SEM (as above) and UV/Vis (UV3600 UV–vis NIR Spectrophotometer, Shimadzu). Tensile testing was performed using a micromechanical testing device equipped with a 5N load cell, as described previously (Burgert et al., 2003). Samples were strained at 1 µm/s (determined by video extensiometry) until breakage to generate stress-strain curves. The Young's modulus was calculated from the initial linear portion of the curves, tensile strength was determined as the maximum stress achieved during testing, and toughness was calculated by numerically approximating the area under the stress-strain curve. Samples were tested in at least quintuplicate, with results presented as the average ± standard deviation. Disintegrability of CNFs films when exposed to simulated composting conditions was evaluated according to the standardized testing procedure described in ISO 20200:2015 (ISO, 2015). A specific quantity of a commercial ripe compost (Radivit®, W. Neudorff GmbH KG, Emmerthal, Germany) was mixed together with the synthetic biowaste, prepared with certain amount of sawdust, rabbit-feed, corn starch, saccharose, cornseed oil and urea. The water content of the solid substrate was around 50 wt% and the aerobic conditions were guaranteed by mixing it softly. Pieces (25mm × 25mm) of test films were placed in a fine-mesh (1.6 mm) bags of inert material, then buried at 4 – 6 cm depth in perforated boxes containing the prepared solid matrix, and incubated at

58 ± 2 °C. The pieces of films (still inside the bags) were recovered at different time points, carefully cleaned from the solid wastes, and photographed to monitor the progress of the composting reaction. The degree of disintegration was determined after a composting cycle (77 days), normalizing the dry mass of the non-disintegrated residues recovered from sieving (2 mm) to the initial dry mass of the test sample.

5.2.5 Spray Coating of CNF Suspensions onto Vegetable Surfaces

0.5 wt% carrot CNFs suspensions were sprayed onto the surface of locally purchased bananas using an atomizing sprayer (Ultra airbrush, Harder & Steenbeck Gmbh &Co. KG), equipped with a 0.2 mm nozzle. The bananas were then allowed to dry at room temperature for 5 min; this process was repeated two more times to ensure that the bananas were completely and uniformly coated. Bananas were weighed and visually observed daily for 14 days to determine the effects of the carrot CNF spray coating. Spray coating morphology on the banana peel surface was evaluated by SEM and optical profilometry (DektakXT Stylus Profiler, Bruker AXS GmbH, Karlsruhe, Germany).

5.3 Results and Discussion

CNFs were produced by mechanical homogenization of fresh and stale carrot pomace fibers, which were subjected to an optional bleaching pre-treatment. Prior to homogenization, both fresh and stale fibers had a similar morphology, with orange pigment and residual non-cellulosic moieties still

clearly visible by optical microscopy (Supporting Information, **Figure S 5.1**). In comparison, the bleached CNFs appeared white in colour, with significantly less non-cellulosic moieties apparent via optical microscopy (**Figure 5.2**). Regardless, in all four cases high quality fibers were able to be produced after 10 passes through the homogenizer, albeit with significantly decreased average flow rate through the microfluidizer for the non-bleached carrot pomace (~ 0.31 kg/h vs 0.42 kg/h), attributed to the presence of residual non-cellulosic moieties such as lignin. This decreased flow rate corresponds to an increased energy demand of ~ 33% for the homogenization of non-bleached carrot pomace as compared to bleached carrot pomace. This increasingly efficient fibrillation of bleached carrot pomace into CNF can be attributed to the increased accessibility of cellulosic fibers within the carrot cell wall. The effect of bleaching as a pre-treatment for preparation of CNF is already well-understood, primarily aiding in the dissolution of non-cellulosic moieties such as lignin and hemicellulose (Balea et al., 2017). Morphological changes within the carrot pomace fibers during fibrillation were also observed via SEM (**Figure 5.3**). Prior to fibrillation, the native cell wall structure is visible in all samples, regardless of pre-treatment. After 10 passes with the microfluidizer, all carrot pomace fibers were successfully broken down into nano-sized fibrils with a classic networked structure and high aspect ratio. Note that thicker fibril bundles (>100 nm) along with some relatively non-fibrillated material could still be seen in all cases, attributed to the relatively low power of the bench-scale microfluidizer used in this work. Albeit carrot pomace fibers which had been exposed to the bleaching pre-treatment appeared to be slightly less aggregated, which is expected as

the presence of relatively non-fibrillated material/fibril aggregates is commonly observed in CNFs with a high content of hemicellulose/lignin (Chen et al., 2018; Ewulonu et al., 2019). Carbohydrate analysis of the carrot CNFs was performed to determine the effects of both carrot condition and bleaching pre-treatment on the chemical composition of resulting CNFs fibers. As seen in **Table 5.1**, the main effect of bleaching is, as expected, the substantial removal of lignin (residuals) from both fresh and stale carrot pomace.

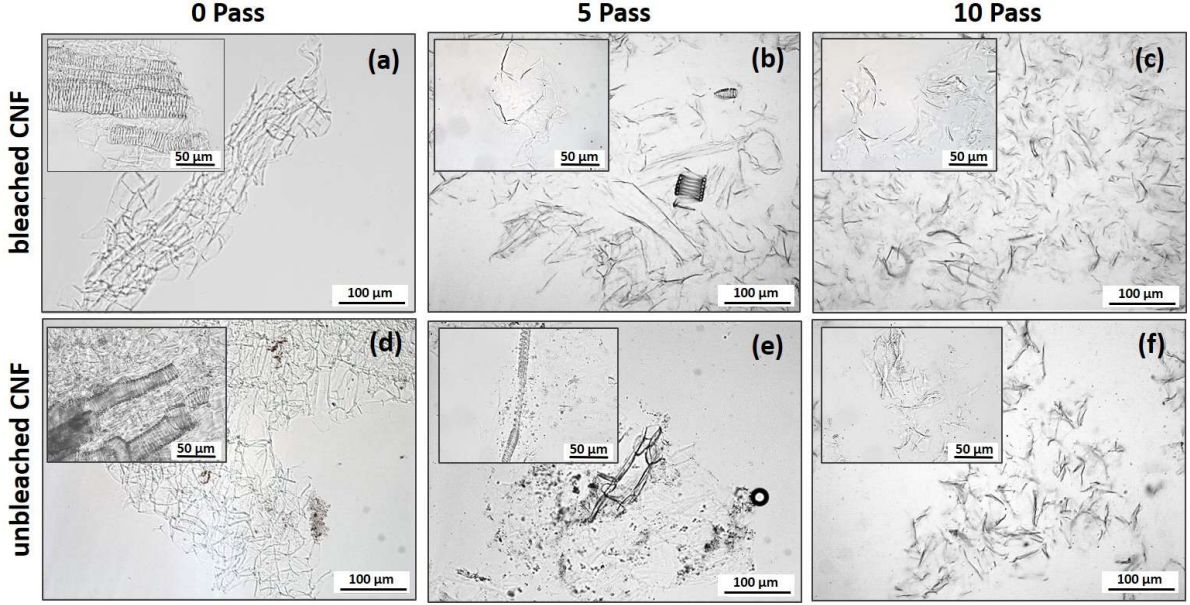

Figure 5.2. Optical micrographs of (stale) bleached and unbleached carrot residues showing structural changes that occurred during fibrillation.int

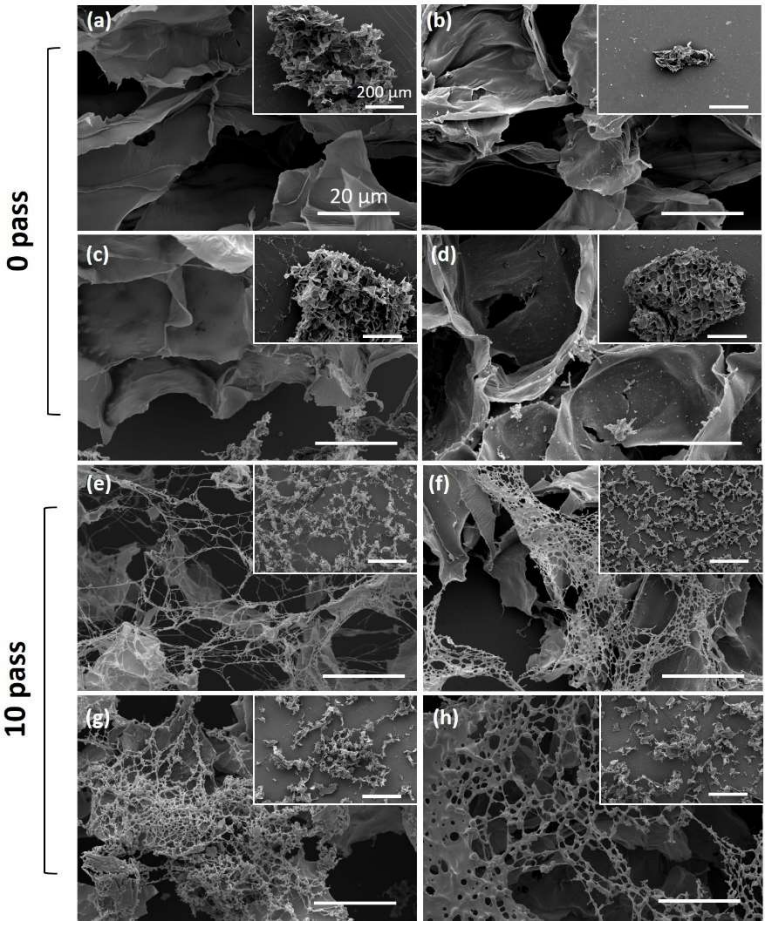

Figure 5.3. SEM images of CNFs from carrot pomace before (0 passes) and after microfluidization (10 passes): (**a**, **e**) FBCNF – fresh bleached carrot pomace; (**b**, **f**) SBCNF – stale bleached carrot pomace; (**c**, **g**) FCNF – fresh carrot pomace; (**d**, **h**) SCNF – stale carrot pomace. All scale bars are 20 µm (insets 200 µm).

Table 5.1. Physico-chemical characterization of CNFs suspensions from carrot pomace.

Sample	Specific Surface Area (m^2/g)	Degree of Polymerization	Carbohydrate Content (%)		
			Cellulose	Hemicellulose	Lignin
FCNF	314 ± 3	855.0 ± 4.2	77.1	16.3	6.6
SCNF	330 ± 3	748.5 ± 1.4	71.1	21.6	7.3
FBCNF	275 ± 7	1222 ± 7.8	59.3	40.5	0.2
SBCNF	357 ± 5	915.5 ± 7.8	64.2	35.7	0.1

Bleaching also apparently reduced the relative percentage of cellulose present in the CNFs fibers (taken as the overall glucose concentration, Supporting Information **Table S 5.1**), attributed primarily to glucose hydrolysis at the elevated temperature used during bleaching. Importantly, as cellulosic content is taken as the sum of glucose in each CNFs suspension, the presence of glucose itself conflates this analysis. The process of boiling carrots is known to significantly solubilize contained glucose, leading to its reduction within the carrot pomace (Myers & Croll, 1921), and thus a reduction in the percent of calculated cellulose within the bleached CNFs suspensions. Furthermore, previous studies on carrots have shown that as a result of wet heat treatment such as pulping/bleaching, mainly low-molecular weight carbohydrates but to some extent also dietary fibre leach into the processing water, causing losses of dry matter (Nyman et al., 2005; Rodríguez-Sevilla et al., 1999; Soria et al., 2009; Yaqoob et al., 2011). Although a limited amount of hemicellulose and lignin has shown to be beneficial in the production of nanofibers (Berglund et al., 2016; Wang et al., 2020), and features such as decreased hornification and higher mechanical strength (Arola et al., 2013; Iwamoto et al., 2008), modification of polarity and hydrophilicity of cellulose (Ewulonu et al., 2019; Herrera et al., 2018; Rojo et al., 2015) have been observed, it has been suggested that both lignin and hemicellulose should be reduced to a certain extent to enable the separation of nanofibrils and ensure the desired outcome (Arola et al., 2013; Berglund et al., 2016; Carrillo et al., 2014; Chen et al., 2019; Ewulonu et al., 2019). However, the large differences in energy consumption and degree of fibrillation, existing

upon pre-treatment conditions, processing methods, chemical composition, and raw materials, make it very difficult to define unique limit contents and non-conflicting results (Albornoz-Palma et al., 2020). The process we conceived in this study allowed the production of residual-lignin cellulose nanofibers, having ~7% lignin content, with a degree of polymerization (DP) comparable to that obtained by pre-delignifying the carrot residues, but with a greater energy consumption being equal mechanical treatment. Remarkably, processing of stale samples, both bleached and unbleached, resulted in a slightly lower DP, which was also related to a higher specific surface area (SSA) of the fibrils. This highlights that structural differences of the cells wall have an important role for the efficient production of cellulose nanofibers. An increase in specific surface area suggests smaller nanofibrils, which are expected to produce films with higher mechanical properties.

0.5 wt % CNFs suspensions were vacuum filtered and hot-pressed to form films. Upon hot pressing, carrot nanofibers formed a dense network due to increased physical entanglement and strong electrostatic interactions. This network tended to have a layered structure, as observed via cross-sectional SEM imaging (**Figure 5.4 a-d**). Films formed from both fresh and stale carrots showed similar properties in terms of both thickness ($\sim 40 \pm 9$ μm) and density ($\sim 1.2 \pm 0.2$ g/cm^3), indicating that the state of the carrot starting material had little effect on the overall film forming ability. Similar observations were made for films from bleached carrot pomace with fresh or stale carrots (thickness $\sim 15 \pm 4$ μm, density $\sim 3.2 \pm 0.3$ g/cm^3). However, film morphology was significantly different between suspensions with bleached and non-bleached carrot pomace; bleached

CNFs films appeared far more compact, reaching a thickness of ~ 1/3 of that of unbleached CNFs films (and correspondingly, a density of ~ 3 x greater). We attribute the considerably lower density of the non-bleached films to the presence of significantly higher residual lignin content, potentially hindering the compaction of cellulose fibers during hot-pressing. Of note, it has previously been demonstrated that lignin can interfere with interfibrillar hydrogen bonding and therefore increases the mesopore diameter of cellulose fibril networks (Albornoz-Palma et al., 2020; Bian et al., 2018; Jiang et al., 2019). In addition, the differences in film thickness and density may also be related to the presence of non-fibrillated material/aggregated fibers (Carrillo et al., 2014), as less aggregated/smaller fibrils should tend to form denser and thinner films (Yook et al., 2020). Here, as previously mentioned, non-bleached CNFs suspensions exhibited larger fibril bundles/aggregates after homogenization, which should hinder the formation of denser films. Importantly, regardless of carrot starting condition or the use of bleaching pre-treating, all films remained stable for over 6 months when stored under ambient conditions. However, when exposed to controlled composting conditions (simulating an intensive aerobic composting process, per ISO 20200) all films were successfully biodegraded within 1 month (Supporting Information, **Figure S 5.2**). Presumably, due to the hydrophilic nature of the CNFs films, moisture from the soil could easily penetrate the networks, thereby weakening the cellulosic chains and making them susceptible to hydrolysis by microorganisms present in the soil. It should be noted that no significant differences in film degradation were evidenced during the composting cycle, suggesting that neither the starting condition of the carrots used, nor the

bleaching pre-treatment significantly affect the susceptibility of CNFs films to biodegradation.

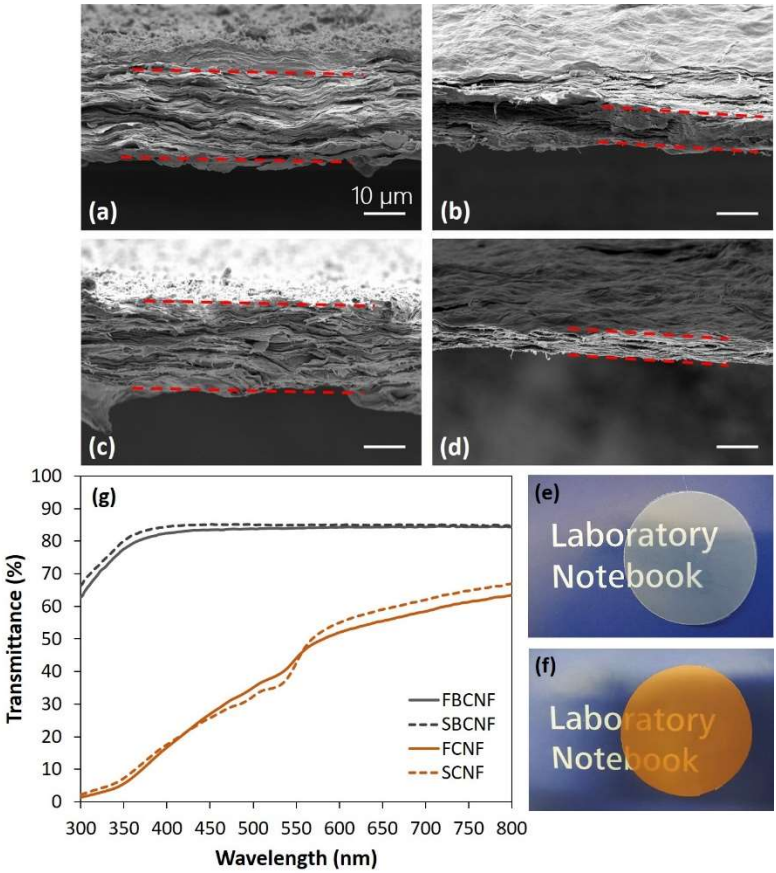

Figure 5.4. Scanning electron micrographs of the cross section of films obtained from: (**a**) FCNF; (**b**) SCNF; (**c**) FBCNF; (**d**) SBCNF. (**g**) Film transparency as measured by UV/Vis, and photographs of (**e**) bleached and (**f**) non-bleached carrot CNFs films.

The optical properties of CNFs films were evaluated via UV/Vis; overall, CNFs films appeared smooth, translucent, and relatively homogenous (**Figure 5.4 e**, **f**), suitable to be used as a see-through packaging or coating material. As with film morphology, no differences were noticed between films prepared from fresh and stale carrot pomace. However, significant differences were apparent between bleached and non-bleached carrot CNFs films, whereby bleached films were highly transparent with no evidence of significant coloration. Non-bleached films were less transparent and appeared orange in colour, as expected due to the presence of residual non-cellulosic components such as lignin and β-carotene (responsible for the orange coloration of carrots). Furthermore, unlike the bleached films, FCNF and SCNF films had a strong absorption in the ultraviolet wavelength range, indicating their ability to act as a UV barrier (Hambardzumyan et al., 2012; Saral Sarojini et al., 2019). This property is useful in preventing decolouration and denaturation of food caused by UV absorption. Differences were also apparent in the opacity/haze of bleached and non-bleached films (**Table 5.2**), decreasing from 19.5 and 16.5 % to 5.3 and 4.5 % as a result of bleaching for fresh and stale samples, respectively. These results are mostly likely related to light absorption of chromophore groups of lignin and other non-cellulosic components (Bian et al., 2018; Carvalho et al., 2019; Chen et al., 2018) as well as to the inherent light scattering of the porous CNFs network (Spence et al., 2011). This makes sense as the thicker (and thus, less dense/more porous) non-bleached carrot CNFs films should scatter more light, and therefore have a lower optical transparency (Carvalho et al., 2019).

The mechanical properties of carrot CNF films were evaluated via tensile testing (**Figure 5.5**) and are summarized in **Table 5.2**.

As with the optical properties, no significant differences could be observed between the fresh and stale films for both bleached and non-bleached samples. However, except for elongation at break, significant improvements in Young's modulus, tensile strength, and toughness were evidenced for bleached carrot CNFs films versus their non-bleached counterparts. Importantly, these three properties are directly related to film thickness; the bleached carrot CNFs can form denser, thinner films (~2.5 x thinner than non-bleached), and therefore show mechanical property improvements on the same order of magnitude (~2.5 x increased versus non-bleached). Critically, elongation at break is an inherent property of the material, unrelated to film thickness; all films demonstrate an elongation at break of ~ 3.5 %, which is comparable to other carrot CNF-based films (Serpa Guerra et al., 2020). Therefore, the use of bleaching as a chemical pre-treatment is critical in allowing the formation of more dense, compact films, leading to enhanced mechanical properties.

Table 5.2. Physical properties of carrot CNF films prepared from fresh and stale carrot pomace with and without bleaching pre-treatment. Results are expressed as average ± standard deviation.

Sample	Optical Properties		Mechanical Properties			
	Transmittance at 600 nm (%)	Opacity (%)	Elongation at Break (%)	Modulus (GPa)	Tensile Strength (MPa)	Toughness (MJ/m^3)
FNFC	51.0 ± 1.4	19.5 ± 0.8	3.7 ± 0.6	2.2 ± 0.3	46 ± 6	1.1 ± 0.3
SNFC	56.5 ± 2.1	16.5 ± 1.1	3.3 ± 0.2	2.2 ± 0.1	45 ± 3	0.9 ± 0.1
FBNFC	83.3 ± 1.4	5.3 ± 0.5	3.4 ± 0.5	4.8 ± 0.3	109 ± 17	2.3 ± 0.7
SBNFC	85.8 ± 1.0	4.5 ± 0.3	3.4 ± 0.6	5.1 ± 0.2	125 ± 18	2.5 ± 1.0

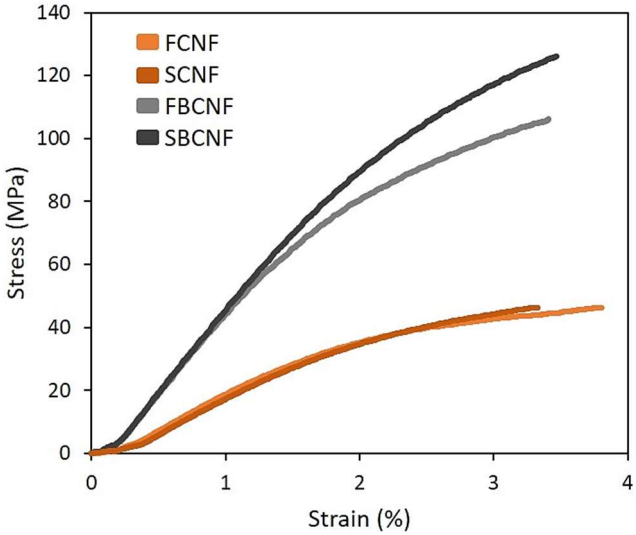

Figure 5.5. Representative stress-strain curves of bleached and unbleached CNF films produced from fresh and stale carrot pomace.

Finally, carrot CNFs suspensions were evaluated as a spray coating (one of the most common industrially relevant techniques to coat foodstuffs (Andrade et al., 2012)) for improving the shelf life of fruits and vegetables. In order to determine feasibility for spraying, the rheological behaviour of CNFs suspensions was analyzed; viscosity as a function of shear rate is shown in **Figure 5.6**, for three different concentrations of carrot CNFs suspensions. Across the concentrations tested (0.25 – 1.0 wt%), all formulations demonstrated a strong shear-thinning behaviour, which is crucial for sprayability. As expected, the viscosity of CNFs suspensions increased with increasing concentration, with little differences apparent between fresh and stale samples. However, bleached CNFs suspensions demonstrated a

markedly higher viscosity than their unbleached counterparts (219 Pa·s and 176 Pa·s vs 82 Pa·s and 109 Pa·s for fresh and stale CNFs at 1.0 wt %, respectively, at 0.001 s^{-1} shear rate), attributed to increased hydrogen bonding/interfibrillar interactions in the bleached (delignified) suspensions (Albornoz-Palma et al., 2020; Chen et al., 2018; Lê et al., 2018).

All tested samples did not show any time dependency (hysteresis) and were all characterized by a rapid viscosity recovery post-shearing (Supporting Information, **Figure S 5.3**). This rapid viscosity recovery and moderately high viscosity at extremely low shear rates (resting viscosity) of film-forming suspensions are both desired to prevent gravity effects after spraying, such as sagging and dripping, which are often critical for the uniformity of a spray coated layer (Peressini et al., 2003). Together, these data suggest that all CNF formulations would be readily sprayable and suitable for coating applications.

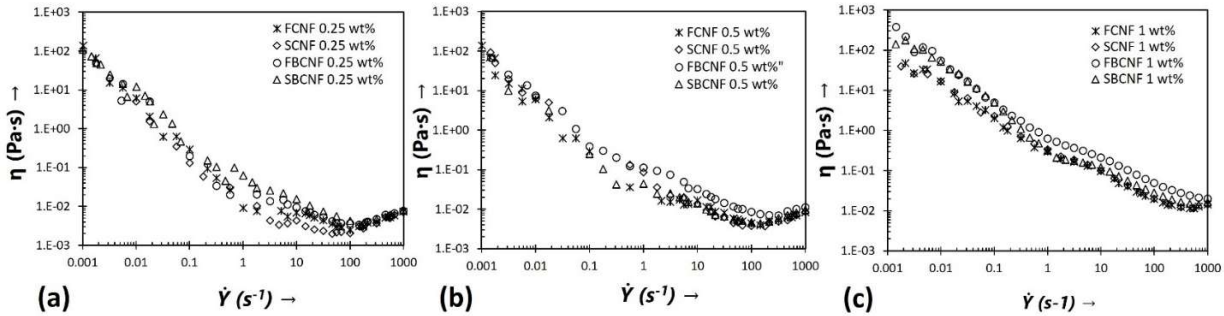

Figure 5.6 Flow curves showing dynamic viscosity (η) versus shear rate ($\dot{\gamma}$) for 0.25 wt% (**a**), 0.5 wt% (**b**) and 1 wt% (**c**) carrot CNF suspensions in water.

The effectiveness of carrot CNFs coatings in preserving fruit freshness was then verified in locally purchased bananas, which served as a model system (**Figure 5.7**). As no significant differences were evidenced for any of the previous experiments between fresh and stale carrots, CNF from stale carrots (bleached and non-bleached) were used for this experiment. Here, 1 mL of 0.5 wt % CNF suspensions was sprayed onto the surface of a banana, which was then allowed to dry for 5 min; this process was repeated 2 more times to ensure a complete and uniform coating was achieved. The visual appearance and weight loss of bananas were then recorded over the next 17 days to assess any effects of the carrot CNFs spray coating. After 14 days post-purchase, the uncoated control bananas, as well as those coated with non-bleached carrot CNFs showed considerable enzymatic browning of the peel (Soradech et al., 2017; Thakur et al., 2019), while the samples coated with bleached carrot CNFs markedly showed a significant delay in browning. Moreover, when the fruits were peeled on day 17, the flesh of bananas coated with the bleached CNFs presented a delayed ripening, firmer appearance, and less bruising in comparison with both the uncoated bananas and those coated with unbleached CNFs (Supporting Information, **Figure S 5.4**). This delayed ripening in bananas coated with bleached CNF is likely due to the film providing enhanced protection against moisture and oxygen, leading to a decline in the respiration rate/production of ethylene of the coated fruit (Jafarizadeh Malmiri et al., 2012; Soradech et al., 2017). This is supported by the improvements in morphology of bleached CNFs films as compared to non-bleached films. In fact, gravimetric analysis revealed that the weight loss (primarily due to water loss/evaporation) of bananas coated with bleached CNFs was

less than that of non-bleached CNFs, and significantly less than that of uncoated bananas (**Figure 5.8**). 17 days post-purchase, the uncoated bananas lost 25% of their initial weight, while weight losses of 18% and 21% were recorded for bananas coated with bleached and non-bleached CNF, respectively. Previous research has demonstrated that coating fruits with a semipermeable film has generally retarded ripening by modifying the levels of endogenous CO_2, O_2 and ethylene (Kittur et al., 2001; Thakur et al., 2019). Several studies have demonstrated that high CO_2 concentrations reduced respiration rates and prevented or delayed responses to ethylene (Banks, 1984; Jafarizadeh Malmiri et al., 2012; Kittur et al., 2001).

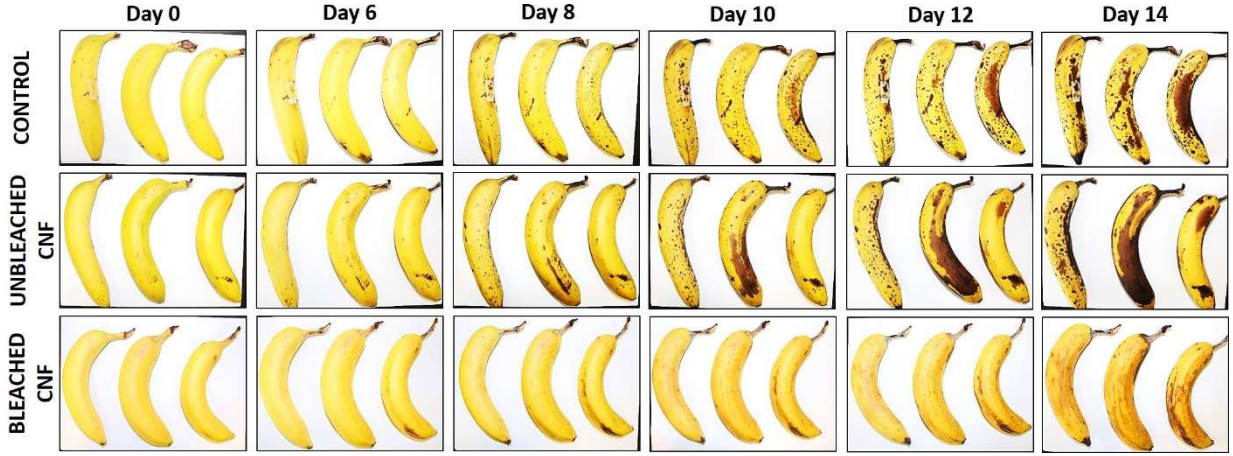

Figure 5.7. Effect of bleached and non-bleached carrot CNF spray coating on the visual appearance of bananas over time. Bananas were stored under ambient conditions (21 °C and 60% RH) and compared against non-coated controls.

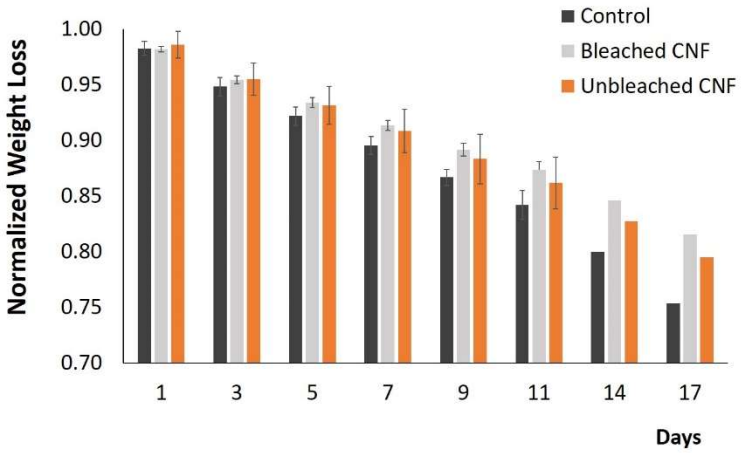

Figure 5.8 Normalized weight loss of bananas which were uncoated (control) or coated with either unbleached or bleached carrot CNFs.

Finally, topographical analysis was performed using optical profilometry (**Figure 5.9**) and SEM (Supporting Information, **Figure S 5.5**) on uncoated and coated banana peels. By optical profilometry, uncoated bananas had an average RMS roughness of 63 µm; this number increased slightly to 76 µm with the non-bleached CNFs coating, suggesting that this coating is rather heterogenous/patchy. Conversely, for the bleached CNFs coating, the RMS roughness decreased to 37 µm, implying that the coating was much more uniform across the entire surface of the banana peel.

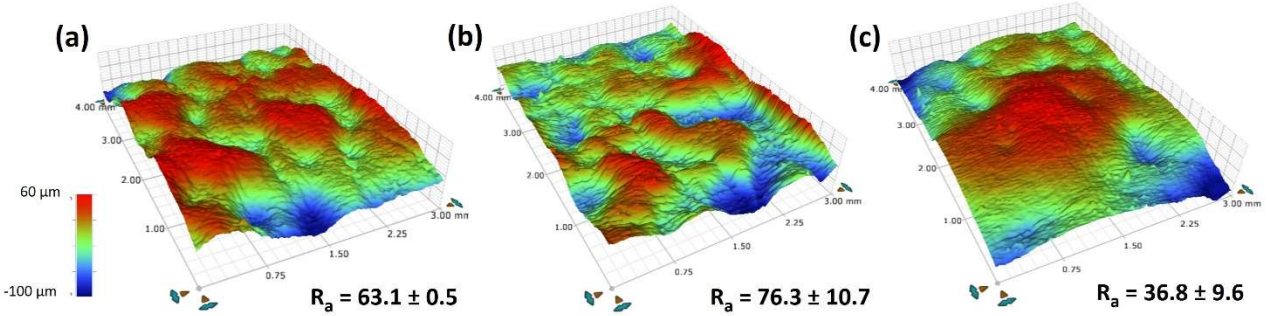

Figure 5.9 3D-mapping by optical profilometer of 3 × 4 mm specimens of banana peels which were either uncoated (control) or coated with non-bleached or bleached carrot CNF. Values represent the average RMS roughness of each specimen.

Similar results were observed via SEM, where individualized epidermal cells are clearly visible on the surface of uncoated bananas as well as those coated with non-bleached CNFs suspensions. This is less evident for the bleached CNFs coating, where a more continuous morphology is observed, suggesting that this coating could be suitable for other food packaging applications.

5.4 Conclusion

In conclusion, high quality CNFs were prepared from carrots for use as a spray coating for food packaging applications. In general, the state of the carrots – fresh (directly as received), or stale (3 weeks of storage) – did not significantly affect the properties of the CNFs suspensions, nor of the films formed from these suspensions. Conversely, the use of a bleaching pre-treatment had a significant impact on the properties of the produced carrot CNFs. Bleaching was found to successfully remove lignin and other residuals from the carrot pomace suspension, leading to a significant decrease in the energy input required for fibrillation, while CNF surface area and degree of polymerization remained largely unaffected. Following, films formed from bleached CNFs had a higher optical transparency due to the removal of lignin and other non-cellulosic components such as β-carotene responsible for the natural coloration of carrots. Bleached CNFs films were also much denser, attributed to increased hydrogen bonding and interfibrillar interactions between individual cellulose fibrils, leading to improved tensile strength, Young's modulus, and toughness as compared to non-bleached CNFs films. Finally, when applied as a spray to coat the surface of bananas, the bleached CNFs suspension was able to

significantly delay enzymatic browning on banana peels by up to 7 days, representing a significant achievement in the field of sustainable materials for food packaging.

5.5 Supporting Information

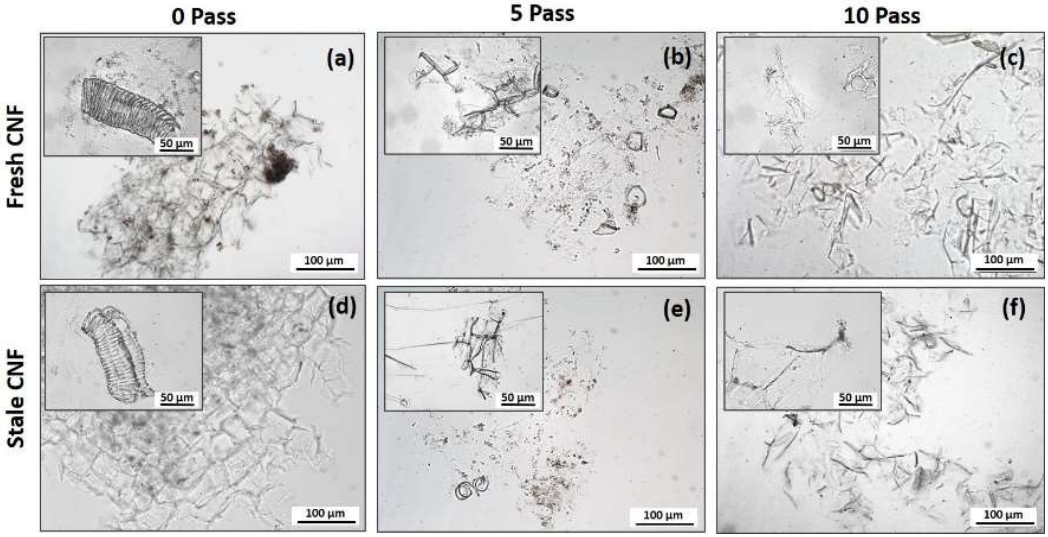

Figure S 5.1 Optical micrographs of fresh and stale (non-bleached) carrot residues after subsequent passes through the microfluidizer.

Table S 5.1. Carbohydrate analysis of carrot CNF fibers, showing relative compositions (%) of hydrolyzed sugars present in each sample.

Sample		Residuals Carbohydrates					
		Glucose	**Xylose**	**Mannose**	**Galactose**	**Arabinose**	**Rhamnose**
FCNF	6.6	77.1	4.1	4.7	3.1	2.5	1.9
SCNF	7.3	71.1	3.9	4.2	5.2	5.6	2.7
FBCNF	0.2	59.3	2.4	3.0	21.4	10.8	3.0
SBCNF	0.1	64.2	3.9	3.3	13.5	10.3	4.7

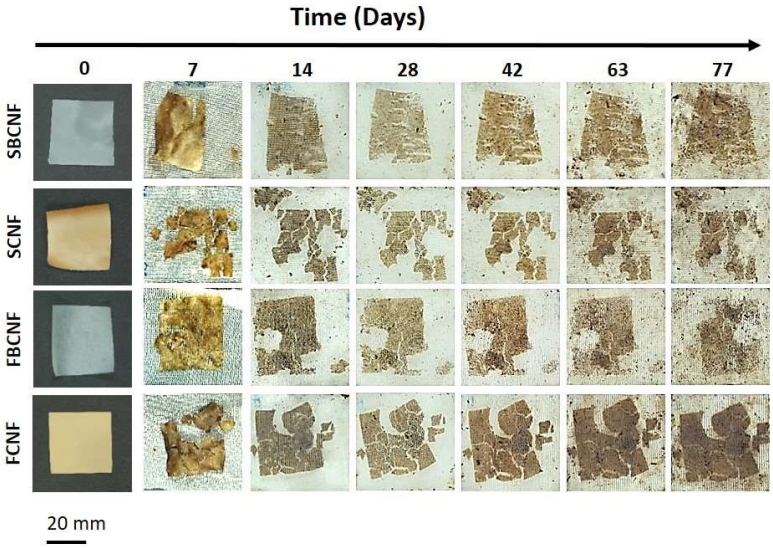

Figure S 5.2 Visual appearance of CNF films over time, upon exposure to controlled composting conditions (according to ISO 20200). Note that the dark colour present in all images after day 14 is due to staining of the mesh holders from soil used for composting – the films became largely embedded within the mesh holders over time.

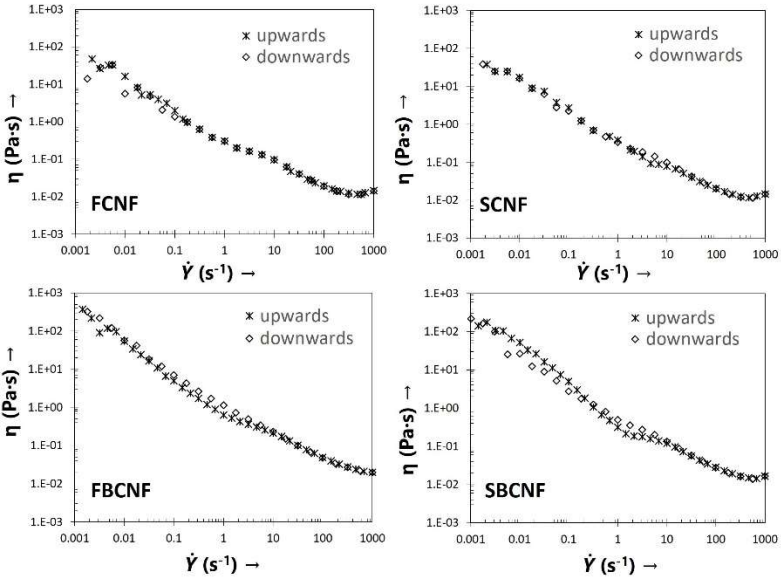

Figure S 5.3 Flow curve of 1 wt% CNFs suspensions, measured from low shear rate to high shear rate (upwards) and back (downwards).

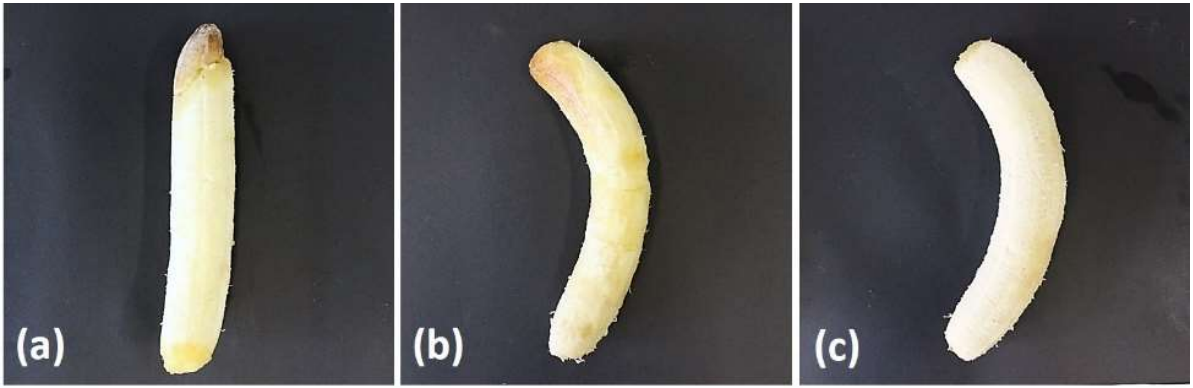

Figure S 5.4 Pictures of peeled bananas 17 days post-purchase, demonstrating the ripening of bananas which were uncoated (**a**), or coated with either non-bleached (**b**) or bleached (**c**) carrot CNFs.

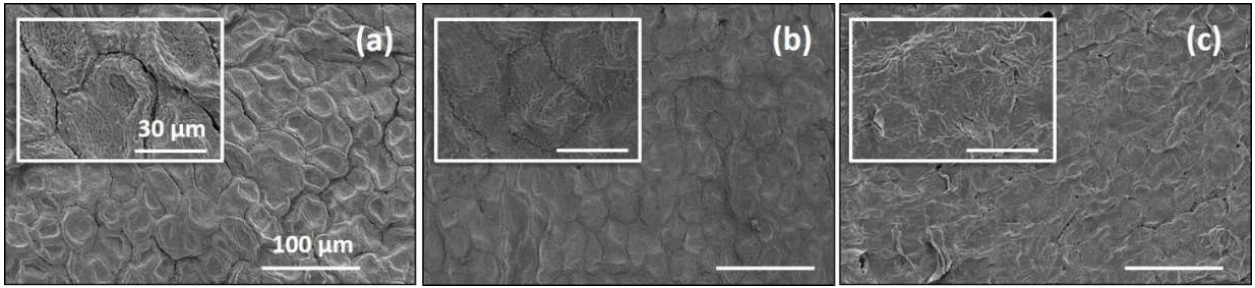

Figure S 5.5 SEM images of the surface of (**a**) uncoated banana peels and banana peels spray coated with (**b**) non-bleached or (**c**) bleached carrot CNFs. All scale bars are 100 µm (insets 30 µm).

References

Abdul Khalil, H. P. S., Davoudpour, Y., Islam, M. N., Mustapha, A., Sudesh, K., Dungani, R., & Jawaid, M. (2014). Production and modification of nanofibrillated cellulose using various mechanical processes: A review. *Carbohydrate Polymers*, *99*(0), 649-665.

Albornoz-Palma, G., Ching, D., Valerio, O., Mendonça, R. T., & Pereira, M. (2020). Effect of lignin and hemicellulose on the properties of lignocellulose nanofibril suspensions. *Cellulose*.

Alemdar, A., & Sain, M. (2008). Isolation and characterization of nanofibers from agricultural residues – Wheat straw and soy hulls. *Bioresource Technology*, *99*(6), 1664-1671.

Andrade-Pizarro, R. D., Skurtys, O., & Osorio-Lira, F. (2015). Effect of cellulose nanofibers concentration on mechanical, optical, and barrier properties of gelatin-based edible films. *Dyna*, *82*(191), 219-226.

Andrade, R., Skurtys, O., Osorio, F., Zuluaga, R., Gañán, P., & Castro, C. (2014). Wettability of gelatin coating formulations containing cellulose nanofibers on banana and eggplant epicarps. *LWT-Food Science and Technology*, *58*(1), 158-165.

Andrade, R. D., Skurtys, O., & Osorio, F. A. (2012). Atomizing Spray Systems for Application of Edible Coatings. *Comprehensive Reviews in Food Science and Food Safety*, *11*(3), 323-337.

Arola, S., Malho, J. M., Laaksonen, P., Lille, M., & Linder, M. B. (2013). The role of hemicellulose in nanofibrillated cellulose networks [10.1039/C2SM26932E]. *Soft Matter*, *9*(4), 1319-1326.

Arvidsson, R., Nguyen, D., & Svanström, M. (2015). Life cycle assessment of cellulose nanofibrils production by mechanical treatment and two different pretreatment

processes. *Environmental Science & Technology*, *49*(11), 6881-6890.

Aulin, C., Gallstedt, M., Lindstrom, T. (2010). Oxygen and oil barrier properties of microfibrillated cellulose films and coatings. *Cellulose*, *17*(3), 559-574.

Azeredo, H. M. C., Mattoso, L. H. C., Avena-Bustillos, R. J., Filho, G. C., Munford, M. L., Wood, D., & McHugh, T. H. (2010). Nanocellulose Reinforced Chitosan Composite Films as Affected by Nanofiller Loading and Plasticizer Content. *Journal of Food Science*, *75*(1), N1-N7.

Azeredo, H. M. C., Mattoso, L. H. C., Wood, D., Williams, T. G., Avena-Bustillos, R. J., & McHugh, T. H. (2009). Nanocomposite Edible Films from Mango Puree Reinforced with Cellulose Nanofibers. *Journal of Food Science*, *74*(5), N31-N35.

Balea, A., Merayo, N., De La Fuente, E., Negro, C., & Blanco, Á. (2017). Assessing the influence of refining, bleaching and TEMPO-mediated oxidation on the production of more sustainable cellulose nanofibers and their application as paper additives. *Industrial Crops and Products*, *97*, 374-387.

Banks, N. H. (1984). Studies of the banana fruit surface in relation to the effects of TAL Pro-long coating on gaseous exchange. *Scientia Horticulturae*, *24*(3), 279-286.

Berglund, L., Breedveld, L., & Oksman, K. (2020). Toward eco-efficient production of natural nanofibers from industrial residue: Eco-design and quality assessment. *Journal of Cleaner Production*, *255*, 120274.

Berglund, L., Noël, M., Aitomäki, Y., Öman, T., & Oksman, K. (2016). Production potential of cellulose nanofibers from industrial residues: Efficiency and nanofiber characteristics. *Industrial Crops and Products*, *92*, 84-92.

Bharimalla, A. K., Deshmukh, S. P., Patil, P. G., & Vigneshwaran, N. (2015). Energy Efficient Manufacturing of

Nanocellulose by Chemo- and Bio-Mechanical Processes: A Review. *World Journal of Nano Science and Engineering*, *5*(4), 204-212, Article 62296.

Bian, H., Gao, Y., Wang, R., Liu, Z., Wu, W., & Dai, H. (2018). Contribution of lignin to the surface structure and physical performance of cellulose nanofibrils film. *Cellulose*, *25*(2), 1309-1318.

Burgert, I., Frühmann, K., Keckes, J., Fratzl, P., & Stanzl-Tschegg, S. (2003). Microtensile Testing of Wood Fibers Combined with Video Extensometry for Efficient Strain Detection. *Holzforschung, v.57, 661-664 (2003)*, *57*.

Carrillo, C. A., Laine, J., & Rojas, O. J. (2014). Microemulsion Systems for Fiber Deconstruction into Cellulose Nanofibrils. *ACS Applied Materials & Interfaces*, *6*(24), 22622-22627.

Carvalho, D. M. d., Moser, C., Lindström, M. E., & Sevastyanova, O. (2019). Impact of the chemical composition of cellulosic materials on the nanofibrillation process and nanopaper properties. *Industrial Crops and Products*, *127*, 203-211.

Chen, H., Wang, X., Bozell, J. J., Feng, X., Huang, J., Li, Q., Ragauskas, A. J., Wang, S., & Mei, C. (2019). Effect of solvent fractionation pretreatment on energy consumption of cellulose nanofabrication from switchgrass. *Journal of Materials Science*, *54*(10), 8010-8022.

Chen, Y., Fan, D., Han, Y., Lyu, S., Lu, Y., li, G., Jiang, F., & Wang, S. (2018). Effect of high residual lignin on the properties of cellulose nanofibrils/films. *Cellulose*, *25*.

Chinga Carrasco, G. (2011). Cellulose fibres, nanofibrils and microfibrils: The morphological sequence of MFC components from a plant physiology and fibre technology point of view. *Nanoscale Research Letters*, *6*, 417.

De France, K. J., Hoare, T., & Cranston, E. D. (2017). Review of Hydrogels and Aerogels Containing Nanocellulose. *Chemistry of Materials*, *29*(11), 4609-4631.

Delgado-Aguilar, M., González Tovar, I., Tarrés Farrés, Q., Alcalà Vilavella, M., Pèlach Serra, M. À., & Mutjé Pujol, P. (2015). Approaching a low-cost production of cellulose nanofibers for papermaking applications. *BioResources*, *10*(3), 5435-5355.

Dufresne, A. (2017). *Nanocellulose: From Nature to High Performance Tailored Materials* (2 ed.). Walter de Gruyter GmbH & Co KG.

Ewulonu, C. M., Liu, X., Wu, M., & Yong, H. (2019). Lignin-Containing Cellulose Nanomaterials: A Promising New Nanomaterial for Numerous Applications. *Journal of Bioresources and Bioproducts*, *4*(1), 3-10.

FAO. (2018). *FAO Global Statistical Yearbook, FAO Regional Statistical Yearbooks.*

Fernandes, S. C. M., Freire, C. S. R., Silvestre, A. J. D., Pascoal Neto, C., Gandini, A., Berglund, L. A., & Salmén, L. (2010). Transparent chitosan films reinforced with a high content of nanofibrillated cellulose. *Carbohydrate Polymers*, *81*(2), 394-401.

Ferrer, A., Pal, L., & Hubbe, M. (2017). Nanocellulose in packaging: Advances in barrier layer technologies. *Industrial Crops and Products*, *95*, 574-582.

Fukuzumi, H., Saito, T., Iwata, T., Kumamoto, Y., & Isogai, A. (2009). Transparent and High Gas Barrier Films of Cellulose Nanofibers Prepared by TEMPO-Mediated Oxidation. *Biomacromolecules*, *10*(1), 162-165.

Garcia, M. P. M., Gómez-Guillén, M. C., López-Caballero, M. E., & Barbosa-Cánovas, G. V. (2016). *Edible Films and Coatings: Fundamentals and Applications*. CRC Press.

Gómez H, C., Serpa, A., Velásquez-Cock, J., Gañán, P., Castro, C., Vélez, L., & Zuluaga, R. (2016). Vegetable nanocellulose

in food science: A review. *Food Hydrocolloids*, *57*, 178-186.

Gruber, E., & Gruber, R. (1981). Viscosimetric determination of the degree of polymerization of cellulose. *Das Papier*, *35*(4), 133-141.

Guimarães, I. C., dos Reis, K. C., Menezes, E. G. T., Rodrigues, A. C., da Silva, T. F., de Oliveira, I. R. N., & Vilas Boas, E. V. d. B. (2016). Cellulose microfibrillated suspension of carrots obtained by mechanical defibrillation and their application in edible starch films. *Industrial Crops and Products*, *89*, 285-294.

Hambardzumyan, A., Foulon, L., Chabbert, B., & Aguié-Béghin, V. (2012). Natural Organic UV-Absorbent Coatings Based on Cellulose and Lignin: Designed Effects on Spectroscopic Properties. *Biomacromolecules*, *13*(12), 4081-4088.

Herrera, M., Thitiwutthisakul, K., Yang, X., Rujitanaroj, P.-o., Rojas, R., & Berglund, L. (2018). Preparation and evaluation of high-lignin content cellulose nanofibrils from eucalyptus pulp. *Cellulose*, *25*(5), 3121-3133.

Hsieh, M.-C., Koga, H., Suganuma, K., & Nogi, M. (2017). Hazy Transparent Cellulose Nanopaper. *Scientific Reports*, *7*(1), 41590.

Hubbe, M. A., Ferrer, A., Tyagi, P., Yin, Y., Salas, C., Pal, L., & Rojas, O. J. (2017). *Nanocellulose in Thin Films, Coatings, and Plies for Packaging Applications: A Review* (Vol. 12) [Barrier properties; Water vapor transmission; Food shelf life; Oxygen transmission; Packages; Cellulose nanomaterials].

International Organization for Standardization - ISO. (2004). *Pulps - Determination of limiting viscosity number in cupri-ethylenediamine (CED) solution* (ISO 5351:2004).

International Organization for Standardization - ISO. (2015). *Plastics — Determination of the degree of disintegration*

of plastic materials under simulated composting conditions in a laboratory-scale test (ISO 20200:2015).

Iwamoto, S., Abe, K., & Yano, H. (2008). The Effect of Hemicelluloses on Wood Pulp Nanofibrillation and Nanofiber Network Characteristics. *Biomacromolecules*, *9*(3), 1022-1026.

Jafarizadeh Malmiri, H., Osman, A., Tan, C. P., & Abdul Rahman, R. (2012). Effects of Edible Surface Coatings (Sodium Carboxymethyl Cellulose, Sodium Caseinate and Glycerol) on Storage Quality of Berangan Banana (Musa Sapientum CV. Berangan) Using Response Surface Methodology. *Journal of Food Processing and Preservation*, *36*(3), 252-261.

Jaramillo, C., Quintero, C., Gomez, C., Zuluaga, R., & López-Córdoba, A. (2020). Alginate-Edible Coatings for Application on Wild Andean Blueberries (Vaccinium meridionale Swartz): Effect of the Addition of Nanofibrils Isolated from Cocoa By-Products. *Polymers*, *12*, 824.

Jiang, Y., Liu, X., Yang, Q., Song, X., Qin, C., Wang, S., & Li, K. (2019). Effects of residual lignin on composition, structure and properties of mechanically defibrillated cellulose fibrils and films. *Cellulose*, *26*(3), 1577-1593.

Khan, A., Huq, T., Khan, R. A., Riedl, B., & Lacroix, M. (2014). Nanocellulose-Based Composites and Bioactive Agents for Food Packaging. *Critical Reviews in Food Science and Nutrition*, *54*(2), 163-174.

Kittur, F., Saroja, N., Habibunnisa, & Tharanathan, R. (2001). Polysaccharide-based composite coating formulations for shelf-life extension of fresh banana and mango. *European Food Research and Technology*, *213*(4), 306-311.

Lê, H. Q., Dimic-Misic, K., Johansson, L.-S., Maloney, T., & Sixta, H. (2018). Effect of lignin on the morphology and rheological properties of nanofibrillated cellulose

produced from γ-valerolactone/water fractionation process. *Cellulose*, *25*(1), 179-194.
Li, F., Mascheroni, E., & Piergiovanni, L. (2015). The Potential of NanoCellulose in the Packaging Field: A Review. *Packaging Technology and Science*, *28*(6), 475-508.
Li, S., & Lee, P. S. (2017). Development and applications of transparent conductive nanocellulose paper. *Science and Technology of Advanced Materials*, *18*(1), 620-633.
Lorenz, D., Erasmy, N., Akil, Y., & Saake, B. (2016). A new method for the quantification of monosaccharides, uronic acids and oligosaccharides in partially hydrolyzed xylans by HPAEC-UV/VIS. *Carbohydrate Polymers*, *140*, 181-187.
Myers, V. C., & Croll, H. M. (1921). The determination of carbohydrates in vegetable foods. *Journal of Biological Chemistry*, *46*(3), 537-551.
Nechyporchuk, O., Belgacem, M. N., & Bras, J. (2016). Production of cellulose nanofibrils: A review of recent advances. *Industrial Crops and Products*, *93*, 2-25.
Nguyễn, H. (2015). Carrot processing- Handbook of Vegetable Preservation and Processing, Second Edition. In *Handbook of Vegetable Preservation and Processing* (pp. 30). CRC press.
Nyman, M., Svanberg, S. J., Andersson, R., & Nilsson, T. (2005). Effects of cultivar, root weight, storage and boiling on carbohydrate content in carrots (Daucus carota L). *Journal of the Science of Food and Agriculture*, *85*, 441-449.
Pauer, E., Wohner, B., Heinrich, V., & Tacker, M. (2019). Assessing the Environmental Sustainability of Food Packaging: An Extended Life Cycle Assessment including Packaging-Related Food Losses and Waste and Circularity Assessment. *Sustainability*, *11*(3), 925.
Peressini, D., Bravin, B., Lapasin, R., Rizzotti, C., & Sensidoni, A. (2003). Starch–methylcellulose based edible films:

rheological properties of film-forming dispersions. *Journal of Food Engineering*, *59*(1), 25-32.

Rajinipriya, M., Nagalakshmaiah, M., Robert, M., & Elkoun, S. (2018). Importance of Agricultural and Industrial Waste in the Field of Nanocellulose and Recent Industrial Developments of Wood Based Nanocellulose: A Review. *ACS Sustainable Chemistry & Engineering*, *6*(3), 2807-2828.

Rodríguez-Sevilla, M. D., Villanueva-Suárez, M. J., & Redondo-Cuenca, A. (1999). Effects of processing conditions on soluble sugars content of carrot, beetroot and turnip. *Food Chemistry*, *66*(1), 81-85.

Rojo, E., Peresin, M. S., Sampson, W. W., Hoeger, I. C., Vartiainen, J., Laine, J., & Rojas, O. J. (2015). Comprehensive elucidation of the effect of residual lignin on the physical, barrier, mechanical and surface properties of nanocellulose films. *Green Chemistry*, *17*(3), 1853-1866.

Saral Sarojini, K., Indumathi, M. P., & Rajarajeswari, G. R. (2019). Mahua oil-based polyurethane/chitosan/nano ZnO composite films for biodegradable food packaging applications. *International Journal of Biological Macromolecules*, *124*, 163-174.

Savadekar, N. R., Karande, V. S., Vigneshwaran, N., Bharimalla, A. K., & Mhaske, S. T. (2012). Preparation of nano cellulose fibers and its application in kappa-carrageenan based film. *International Journal of Biological Macromolecules*, *51*, 1008-1013.

Savadekar, N. R., & Mhaske, S. T. (2012). Synthesis of nano cellulose fibers and effect on thermoplastics starch based films. *Carbohydrate Polymers*, *89*(1), 146-151.

Serpa Guerra, A. M., Gómez Hoyos, C., Velásquez-Cock, J. A., Vélez Penagos, L., Gañán Rojo, P., Vélez Acosta, L., Pereira, M. A., & Zuluaga, R. (2020). Effect of ultra-fine

friction grinding on the physical and chemical properties of curcuma (Curcuma longa L.) suspensions. *Journal of Food Science*, *85*(1), 132-142.

Serra, A., González, I., Oliver-Ortega, H., Tarrès, Q., Delgado-Aguilar, M., & Mutjé, P. (2017). Reducing the amount of catalyst in TEMPO-oxidized cellulose nanofibers: Effect on properties and cost. *Polymers*, *9*(11), 557.

Silva-Vera, W., Zamorano-Riquelme, M., Rocco-Orellana, C., Vega-Viveros, R., Gimenez-Castillo, B., Silva-Weiss, A., & Osorio-Lira, F. (2018). Study of spray system applications of edible coating suspensions based on hydrocolloids containing cellulose nanofibers on grape surface (Vitis vinifera L.). *Food and Bioprocess Technology*, *11*(8), 1575-1585.

Siqueira, G., Oksman, K., Tadokoro, S. K., & Mathew, A. P. (2016). Re-dispersible carrot nanofibers with high mechanical properties and reinforcing capacity for use in composite materials. *Composites Science and Technology*, *123*, 49-56.

Sogut, E., & Cakmak, H. (2020). Utilization of carrot (Daucus carota L.) fiber as a filler for chitosan based films. *Food Hydrocolloids*, *106*, 105861.

Soradech, S., Nunthanid, J., Limmatvapirat, S., & Luangtana-anan, M. (2017). Utilization of shellac and gelatin composite film for coating to extend the shelf life of banana. *Food Control*, *73*, 1310-1317.

Soria, A., Sanz, M., & Villamiel, M. (2009). Determination of minor carbohydrates in carrot (Daucus carota L.) by GC–MS. *Food Chemistry*, *114*, 758-762.

Spence, K. L., Venditti, R. A., Rojas, O. J., Habibi, Y., & Pawlak, J. J. (2011). A comparative study of energy consumption and physical properties of microfibrillated cellulose produced by different processing methods. *Cellulose*, *18*(4), 1097-1111.

Svagan, A. J., Hedenqvist, M. S., & Berglund, L. (2009). Reduced water vapour sorption in cellulose nanocomposites with starch matrix. *Composites Science and Technology*, *69*(3), 500-506.

Thakur, R., Pristijono, P., Bowyer, M., Singh, S. P., Scarlett, C. J., Stathopoulos, C. E., & Vuong, Q. V. (2019). A starch edible surface coating delays banana fruit ripening. *LWT*, *100*, 341-347.

Thomas, S., Mishra, R. K., & Asiri, A. M. (2019). *Sustainable Polymer Composites and Nanocomposites*. Springer International Publishing.

Trovatti, E., Fernandes, S. C. M., Rubatat, L., Perez, D. d. S., Freire, C. S. R., Silvestre, A. J. D., & Neto, C. P. (2012). Pullulan–nanofibrillated cellulose composite films with improved thermal and mechanical properties. *Composites Science and Technology*, *72*(13), 1556-1561.

Varanasi, S., Henzel, L., Sharman, S., Batchelor, W., & Garnier, G. (2018). Producing nanofibres from carrots with a chemical-free process. *Carbohydrate Polymers*, *184*, 307-314.

Wang, W., Liu, Y., Jia, H., Liu, Y., Zhang, H., He, Z., & Ni, Y. (2017). Effects of cellulose nanofibers filling and palmitic acid emulsions coating on the physical properties of fish gelatin films. *Food Biophysics*, *12*(1), 23-32.

Wang, X., Chen, H., Feng, X., Zhang, Q., Labbé, N., Kim, K., Huang, J., Ragauskas, A. J., Wang, S., & Zhang, Y. (2020). Isolation and characterization of lignocellulosic nanofibers from four kinds of organosolv-fractionated lignocellulosic materials. *Wood Science and Technology*, *54*(3), 503-517.

Wu, T., Farnood, R., O'Kelly, K., & Chen, B. (2014). Mechanical behavior of transparent nanofibrillar cellulose–chitosan nanocomposite films in dry and wet conditions. *Journal of the Mechanical Behavior of Biomedical Materials*, *32*, 279-286.

Yaqoob, N., Stack, K., Ur Rehman, I., Cheema, K., Hameed, S., & Mateen, B. (2011). Distribution of a-cellulose, hemicellulose and acid insoluble lignin during total chlorine free bleaching of AS/AQ wheat straw pulp. *Asian Journal of Chemistry*, *23*, 3050.

Yook, S., Park, H., Park, H., Lee, S.-Y., Kwon, J., & Youn, H. J. (2020). Barrier coatings with various types of cellulose nanofibrils and their barrier properties. *Cellulose*, *27*(8), 4509-4523.

Yu, Z., Alsammarraie, F. K., Nayigiziki, F. X., Wang, W., Vardhanabhuti, B., Mustapha, A., & Lin, M. (2017). Effect and mechanism of cellulose nanofibrils on the active functions of biopolymer-based nanocomposite films. *Food Research International*, *99*, 166-172.

Zhao, Y., Simonsen, J., Cavender, G., Jung, J., & Fuchigami, L. H. (2019). *Nano-Cellulose Coatings to Prevent Damage in Foodstuffs* (Washington DC, Patent No. US 10,334,863). U.S. Patent and Trademark Office.

Zhu, M., Wang, Y., Zhu, S., Xu, L., Jia, C., Dai, J., Song, J., Yao, Y., Wang, Y., Li, Y., Henderson, D., Luo, W., Li, H., Minus, M. L., Li, T., & Hu, L. (2017). Anisotropic, Transparent Films with Aligned Cellulose Nanofibers. *Advanced Materials*, *29*(21), 1606284

6 Are cellulose nanocrystals “alien particles” to human experience?

Luciano Piergiovanni[1*], Ghislain Fotie[1], Luana Amoroso[2], Begum Akgun[1], Sara Limbo[1].

1. *DeFENS, Department of Food, Environmental and Nutritional Sciences—PackLAB Università degli Studi di Milano, Via Celoria 2, 20133 Milano, Italy.*
2. *Department of Agricultural, Food and Environment (Di3A), Università degli Studi di Catania, Via Santa Sofia 100, 95123 Catania, Italy.*

This chapter is published in *Packaging Technology and Science*, *2019*, *32*(12), 637-640.

Abstract

A wide family of cellulose-based additives are authorized worldwide as fillers and thickening agents in foods, pills, and tablets, and microcrystalline cellulose (MCC) is, among these, the most important one. Since MCC manufacturing is similar to the main production route of cellulose nanocrystals (CNCs), it is reasonable to wonder whether the MCC would contain CNCs as minor components. In this Short Communication, we provide first results about the occurrence of CNCs in MCC, observed by dynamic light scattering and transmission electron microscopy after serial filtrations of MCC suspensions. The incidence of cellulose nanoparticles has been proved in several different trials in our ongoing works on diverse MCC samples, and the nanoparticles isolated showed shape and dimensions similar to those commonly produced by acidic hydrolysis at

laboratory level. Therefore, the presence of CNCs in many products is considered as a certainty. The foods and the pharmaceuticals we have been consuming so far do indeed contain traces of CNCs to such an extent that this wide presence in consumed products should be taken into account when considering possible limitations of the use of these nanoparticles in food contact materials manufacture.

Keywords: cellulose nanocrystals (CNCs); food contact materials (FCM); microcrystalline cellulose (MCC).

6.1 Introduction

A general, strong prejudice on the use of nanomaterials in food contact materials (FCM) persists all around the world and the European legislation, since 2011, established that in the manufacture of FCM, "substances in nano-form should be used only if explicitly authorized," even ignoring for these applications the functional barrier concept (Commission, 2011). It is worth reminding that according to EU Recommendation 2011/696, nanomaterial means a natural, incidental, or manufactured material containing particles, in an unbound state or as an aggregate or as an agglomerate and where, for 50 % or more of the particles in the number size distribution, one or more external dimensions is in the size range 1 nm -100 nm (European Commission, 2011).
Even though a precautionary policy may be understandable when considering novel substances or inorganic/metallic species, these limitations definitely affect the possible development of innovative, more sustainable, and high-performance packaging materials that include cellulose nanoparticles. On the other side, fundamental and applied

research has already demonstrated the great potential of cellulose nanoparticles, both cellulose nanocrystals (CNCs) and microfibrillated cellulose (MFC), in the improvement of fundamental properties of FCM (Dufresne, 2017; Hubbe et al., 2017). In particular, CNCs have been shown to be very interesting barrier coatings, capable of further reducing the gas permeability than synthetic polymers (e.g., ethylene vinyl alcohol (EVOH)) to a much thinner thickness (Fotie et al., 2017; Li et al., 2013). In addition, no studies to date have demonstrated any dangerousness of the CNCs (Li et al., 2015; Seabra et al., 2018), and recent results suggested that cellulose nanoparticles might potentially be used as useful antimicrobial packaging materials as well as regulators of lipid absorption; in particular, used as food additives or supplements, they might provide a safe and nonchemical means of reducing fat absorption, thus allowing weight loss (DeLoid et al., 2018; Silva et al., 2019).

CNCs are nanoparticles whose shape and dimensions are largely influenced by the type of cellulosic sources and processes used for their fragmentation. However, they are generally reported as rod-like particles, with length of 100 to 200 nm and width of 5 to 10 nm (Li et al., 2015). Such dimensions are practically excluded from any diffusional migration phenomena. It has been demonstrated, in fact, that measurable migration may occur only for nanoparticles up to approximately 3.5 nm in diameter. For 10-nm-diameter particles, an apparent diffusion coefficient (D) of $1.1E^{-35}$ cm^2 s^{-1} was theoretically calculated in a Low-Density Polyethylene (LDPE) host matrix. Such extremely low D results in almost null mobility of the migrants and undeterminable risk of migration (Bott et al., 2014). In this context, the only real risk is that cutting, breaking, or similar

mechanical stresses of the packaging materials containing CNCs can lead to a release of nanocellulose in the food.
In foods and in pharmaceutical products (pills and tablets), the presence of cellulose is very common because a wide group of cellulose-based additives is authorized worldwide as thickening, filler, and functional agents. Recently, European Food Safety Authority (EFSA) has re-evaluated 10 different chemically modified and unmodified celluloses as food additives, concluding that there was no need for a numerical admitted daily intake (ADI) and that there would be no safety concern about the reported uses (Younes et al., 2018). Among all these additives, microcrystalline cellulose (MCC) is certainly the most important. MCC is a cellulose-based, powder-like product, known since the 1950s, whose global annual production is currently around 120,000 tonnes (Battista & Smith, 1962; Vanhatalo, 2017). In general, wood and cotton powder are common sources for the production of MCC, although other biomasses have been proposed.
for its production (Kharismi & Suryadi, 2018). In any cases, MCC manufacturing is quite similar to the main route for CNCs production and generally consists of a chemical acidic hydrolysis, possibly followed by ultrasonication.
Therefore, it is reasonable to wonder whether the MCC would contain CNCs as minor components. The aim of this short communication is reporting first results obtained seeking for the presence of CNCs in different types of MCC, focusing also on the needs for more extended and deeper investigation in this field.

6.2 Materials and Methods

Two different types of cellulose microcrystalline were used: MCC for column chromatography, Merck KGaA, Darmstadt, Germany, and MCC, USP (United State Pharmacopeia) approved, Blackburn Distribution, Nelson, UK. Ultrapure Milli-Q water, 0.22 μm filtered, 18.2 MΩcm, 3 ppb TOC (Millipore, Merck KGaA, Darmstadt, Germany), was used in all the steps of suspensions preparation and filtration.
To check the possible CNCs presence in MCC, seven water suspensions of the two MCCs, in the concentrations ranging from 0% to 9% (m/v), were submitted to a serial filtrations protocol. Paper filters with nominal cut-off 8-12, 5-8, and 1 μm (Sartorius Stedim, Varedo, Italy) and polyvinylidene fluoride (PVDF) hydrophilic membranes filters (Durapore Millipore, Merck KGaA, Darmstadt, Germany) with nominal cut-off 0.22 μm were used in the serial filtrations. The last filtered supernatants were analysed by dynamic light scattering (DLS) for equivalent hydrodynamic diameters, polydispersity, and light scattering intensities using a Litesizer 500, Anton Paar, Graz, Austria; the DLS measurements were performed at 25.0 ± 0.1°C, with a 35 mW laser diode light (λ = 658 nm) and collecting the scattered light at 90° (side scattering angle). The last supernatants, possibly containing particles with expected dimensions lower than 0.22 μm, were freeze-dried for transmission electron microscopy (TEM) observations (LEO 912AB, Zeiss, Oberkochen, Germany) at an accelerating voltage of 80 kV, in order to characterize the morphology and the dimensions of the isolated particles.

6.3 Results and Discussion

Whatever the MCC concentrations in the different water suspensions filtered, it was always detected, by DLS measurements, equivalent hydrodynamic diameters around 100 to 150 nm in the supernatants obtained after the last filtration under the 0.22 μm cut-off, as it is shown in **Figure 6.1**, with a relatively low level of polydispersity around 20%. In order to confirm the presence of nanoparticles in MCC only, i.e., excluding the presence in the water or due to the procedure used, the filtered Milli-Q water (MCC concentration 0%) was also tested. The diameters recorded in this case are not reliable values for many reasons: the cumulant fit error is very high (poor fitting of the correlation function), the number of runs needed to get a result is also very high and the mean intensity recorded was very low.

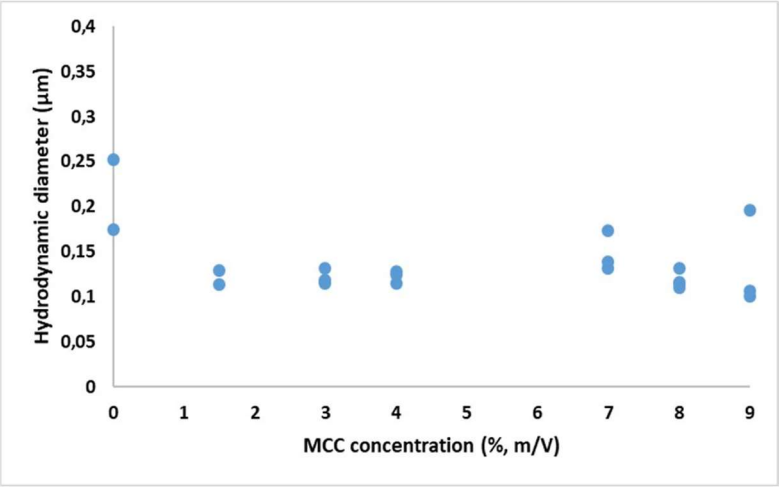

Figure 6.1 Particle size, equivalent hydrodynamic diameters, measured by dynamic light scattering (DLS) for different microcrystalline cellulose (MCC) concentrations, after the serial filtration protocol (n = 3).

Moreover, the presence of nanoparticles appeared roughly proportional to the initial MCC concentration as it is shown by the increasing scattering intensity (DLS, kcounts/s), at least in the range shown in **Figure 6.2**.

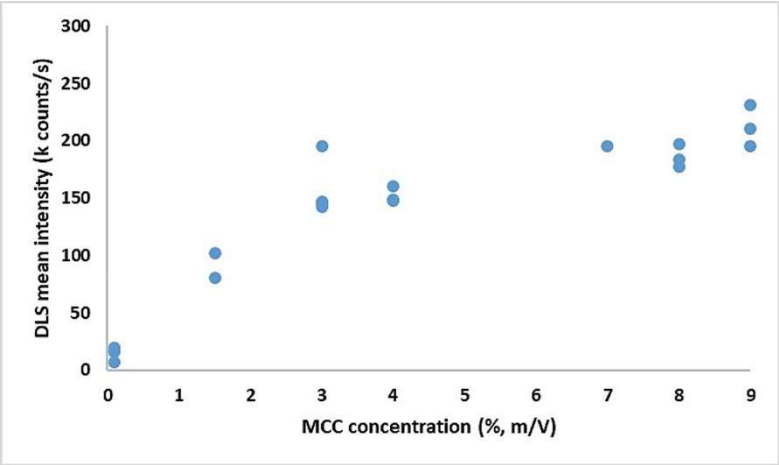

Figure 6.2 Scattering intensity from dynamic light scattering (DLS) measurements for different microcrystalline cellulose (MCC) concentrations, after the serial filtration protocol (n = 3).

TEM observations, carried out on the freeze-dried supernatants from the last filtration (0.22-µm cut-off), confirmed both the presence of CNCs in MCC and the dimensions estimated by DLS. Also, the typical spindle shape of the CNCs was revealed through TEM observations; the dimensions estimated from **Figure 6.3** are approximately 150 to 250 nm in length and 20 to 50 nm in width; dimensions and aspect ratio are consistent with those, commonly measured on CNCs obtained by acidic hydrolysis.

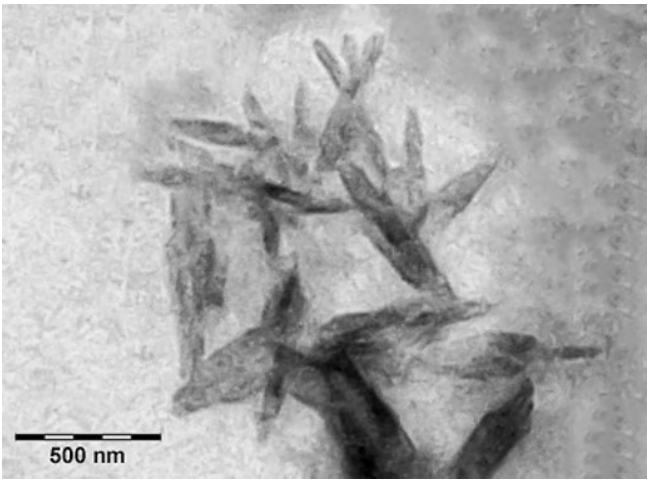

Figure 6.3 A representative 500-nm scale transmission electron microscopy (TEM) image of primary size and morphology of cellulose nanocrystals (CNCs) revealed after serial filtration of microcrystalline cellulose (MCC) suspension.

The freeze-dried material obtained through the serial filtration has been also analysed by Fourier-transform infrared (FTIR) spectroscopy with a Perkin Elmer instrument (Spectrum 100), equipped with attenuated total reflectance (ATR) accessory, and the results (data not shown) confirmed the cellulosic nature of the isolated. First results, to be confirmed, revealed a concentration in the order of parts per million (ppm) of CNCs in the MCC samples tested.

Works are currently in progress in order to verify the possibility that additional amounts of nanocrystals might be produced from MCC by pH, time, and temperature values, typical of gastric digestion. Moreover, a further fundamental undergoing research programme is to find out an accurate procedure to estimate the CNCs amount in different media.

In fact, it is worth reminding that a reliable procedure to assess quantitatively the CNCs is an essential prerequisite for planning migration tests of possible FCM that contain, as fillers or coatings, CNCs.

6.4 Conclusion

In conclusion, it should be considered the presence of CNCs in many foods and pharmaceutical products as a certainty; the foods we have been consuming so far contain traces of CNCs, to such an extent that this wide presence in consumed products should be taken into account when considering possible limitations of the use of these nanoparticles in FCM manufacture.
A thorough investigation is in progress in order to set up a reliable procedure able to quantify the concentration of the cellulose nanoparticles by means of a combination of electron microscopy, imaging techniques, and other appropriate methodologies based on DLS. The physicochemical characterization of such organic nanocrystals in terms of shape, dimensions, and especially concentration and stability in different media represents a fundamental and challenging stage of the scientific assessment of the risk for the application of nanotechnologies in food and feed chain.

References

Battista, O., & Smith, P. (1962). Microcrystalline cellulose. *Industrial and Engineering Chemistry*, *54*(9), 20-29.

Bott, J., Störmer, A., & Franz, R. (2014). A model Study into the Migration Potential of Nanoparticles from Plastics Nanocomposites for Food Contact. *Food Packaging and Shelf Life*, *2*(2), 73-80.

Commission, E. (2011). Commission Regulation (EU) No 10/2011 of 14 January 2011 on plastic materials and articles intended to come into contact with food. (OJ L 12). Brussels, Belgium: *Official Journal of the European Union*, 1–89

DeLoid, G. M., Sohal, I. S., Lorente, L. R., Molina, R. M., Pyrgiotakis, G., Stevanovic, A., Zhang, R., McClements, D. J., Geitner, N. K., & Bousfield, D. W. (2018). Reducing intestinal digestion and absorption of fat using a nature-derived biopolymer: interference of triglyceride hydrolysis by nanocellulose. *ACS Nano*, *12*(7), 6469-6479.

Dufresne, A. (2017). *Nanocellulose: From Nature to High Performance Tailored Materials* (2 ed.). Walter de Gruyter GmbH & Co KG.

European Commission. (2011). Commission Recommendation of 18 October 2011 on the definition of nanomaterial Text with EEA relevance. (2011/696/EU). Brussels, Belgium: *Official Journal of the European Union*, 38-40.

Fotie, G., Rampazzo, R., Ortenzi, M., Checchia, S., Fessas, D., & Piergiovanni, L. (2017). The Effect of Moisture on Cellulose Nanocrystals Intended as a High Gas Barrier Coating on Flexible Packaging Materials. *Polymers*, *9*(9), 415.

Hubbe, M. A., Ferrer, A., Tyagi, P., Yin, Y., Salas, C., Pal, L., & Rojas, O. J. (2017). Nanocellulose in thin films, coatings,

and plies for packaging applications: A review. *BioResources*, *12*(1), 2143-2233.

Kharismi, R. R. A. Y., & Suryadi, H. (2018). Preparation and characterization of microcrystalline cellulose produced from Betung Bamboo (Dendrocalamus asper) through acid hydrolysis. *Journal of Young Pharmacists*, *10*(2), S79.

Li, F., Biagioni, P., Bollani, M., Maccagnan, A., & Piergiovanni, L. (2013). Multi-functional coating of cellulose nanocrystals for flexible packaging applications. *Cellulose*, *20* (5), 2491-2504.

Li, F., Mascheroni, E., & Piergiovanni, L. (2015). The Potential of NanoCellulose in the Packaging Field: A Review. *Packaging Technology and Science*, *28*(6), 475-508.

Seabra, A. B., Bernardes, J. S., Fávaro, W. J., Paula, A. J., & Durán, N. (2018). Cellulose nanocrystals as carriers in medicine and their toxicities: A review. *Carbohydrate Polymers*, *181*, 514-527.

Silva, F., Gracia, N., McDonagh, B., Domingues, F., Nerín, C., & Chinga Carrasco, G. (2019). Antimicrobial activity of biocomposite films containing cellulose nanofibrils and ethyl lauroyl arginate. *Journal of Materials Science*, *54*.

Vanhatalo, K. (2017). *A new manufacturing process for microcrystalline cellulose (MCC).* [Aalto University publication series, Doctoral Dissertations 152/2017., Aalto University]. Finland.

Younes, M., Aggett, P., Aguilar, F., Crebelli, R., Di Domenico, A., Dusemund, B., Filipič, M., Jose Frutos, M., Galtier, P., Gott, D., Gundert-Remy, U., Georg Kuhnle, G., Lambré, C., Leblanc, J.-C., Lillegaard, I. T., Moldeus, P., Mortensen, A., Oskarsson, A., Stankovic, I., Tobback, P., Waalkens-Berendsen, I., Wright, M., Tard, A., Tasiopoulou, S., & Woutersen, R. A. (2018). Re-evaluation of celluloses E 460(i), E 460(ii), E 461, E 462,

E 463, E 464, E 465, E 466, E 468 and E 469 as food additives. *EFSA Journal*, *16*(1).

7 Concluding Remarks and Future Perspectives

At a time when the world is battling with environmental challenges and many companies are looking to find biocompatible solutions for their products and business, nanocellulose has climbed to the top of the list of the most promising bio-based materials.

In light of the results discussed in this dissertation, cellulose nanomaterials, generated from residues of agricultural and industrial activities, which ideally would otherwise have no commercial relevance and with low values for energy recovery, can be regarded as promising materials to replace synthetic polymers, reduce global dependence on fossil sources, and provide simplified waste disposal. The use of residues affords significant advantages in bridging the gap between nanocellulose research and its market uptake of the food packaging, and the ensuing peculiarities make these nanomaterials very attractive for a broad range of applications in this field.

In terms of expected impacts, the integration of the production of nanocellulose from bio-waste within the process generating the waste itself opens interesting likelihood for its exploitation. This would put in contact companies involved in the development of packaging materials and those interested in the supply of biomass, in an attempt to promote mutual competitive advantages in an industrial symbiosis perspective.

Potentially, this research may constitute an embryonic but fundamental phase for the technological transfer of acquired knowledge on the production and application of CNMs at the

pilot plant level, revealing the structural differences of cellulose nanomaterials from different sources and different preparation processes, and their impact on the performance of films made thereof.

Therefore, further research in this field is strongly encouraged to face the issues linked to the scaling-up, and to better understand the role of diverse structures and properties in the function and application of nanocellulose for different purpose. Further research should also promote sustainable-by-design approaches and contribute to the framework of EU nano-safety and regulatory strategies and standardisation. New nanomaterials from different sources need also to be validated in terms of the economic and environmental sustainability (through Life Cycle Assessment and Life Cycle Cost), and compared with other well-established solutions. But certainly, the key point that is leading this technologic milestone is related with the great efforts being carried out by governments and public institutions to pursue the global strategy based on favouring the sustainable growth, driven by socio-economic interests and expectation, and arising from climate change problems.